UNIVERSIDADE TECNOLÓGICA FEDERAL DO PARANÁ
PROGRAMA DE PÓS-GRADUAÇÃO EM ENGENHARIA MECÂNICA E DE MATERIAIS – PPGEM

GABRIEL MERHY DE OLIVEIRA

MODELAGEM MATEMÁTICA DE FENÔMENOS TRANSITÓRIOS EM FLUIDOS NÃO NEWTONIANOS

TESE

CURITIBA
2018

GABRIEL MERHY DE OLIVEIRA

MODELAGEM MATEMÁTICA DE FENÔMENOS TRANSITÓRIOS EM FLUIDOS NÃO NEWTONIANOS

Tese apresentada ao Programa de Pós-Graduação em Engenharia Mecânica e de Materiais da Universidade Tecnológica Federal do Paraná, Campus Curitiba, como requisito parcial para obtenção do título de Doutor em Engenharia – Área de Concentração: Engenharia Térmica.

Orientador: Prof. Cezar O. R. Negrão, PhD.

Coorientador: Prof. Admilson T. Franco, Dr.

CURITIBA

2018

Dados Internacionais de Catalogação na Publicação

O48m 2018

Oliveira, Gabriel Merhy de
Modelagem matemática de fenômenos transitórios em fluidos não newtonianos / Gabriel Merhy de Oliveira. -- 2018.
94 f.: il.; 2018.

Disponível também via World Wide Web
Texto em português com resumo em inglês
Tese (Doutorado) - Universidade Tecnológica Federal do Paraná. Programa de Pós-graduação em Engenharia Mecânica e de Materiais. Área de Concentração: Engenharia Térmica, Curitiba, 2018
Bibliografia: p. 87-90

1. Fluidos - Escoamento. 2. Pressão - Propagação. 3. Modelos matemáticos. 4. Tixotropia. 5. Poços de petróleo - Perfuração. 6. Transitórios (Dinâmica). 7. Engenharia térmica. 8. Engenharia mecânica – Teses. I. Negrão, Cezar Otaviano Ribeiro, orient. II. Franco, Admilson Teixeira, coorient. III. Universidade Tecnológica Federal do Paraná - Programa de Pós-graduação em Engenharia Mecânica e de Materiais, inst. IV. Título.

CDD: Ed. 22 -- 620.1

Biblioteca Ecoville da UTFPR, Câmpus Curitiba
Lucia Ferreira Littiere – CRB 9/1271

Ministério da Educação
Universidade Tecnológica Federal do Paraná
Diretoria de Pesquisa e Pós-Graduação

TERMO DE APROVAÇÃO DE TESE Nº 18

A Tese de Doutorado intitulada: **Modelagem Matemática de Fenômenos Transitórios em Fluidos Não Newtonianos**, defendida em sessão pública pelo Candidato **Gabriel Merhy de Oliveira**, no dia 28 de setembro de 2018, foi julgada para a obtenção do título de Doutor em Engenharia, área de concentração: Engenharia Térmica, e aprovada em sua forma final, pelo Programa de Pós-Graduação em Engenharia Mecânica e de Materiais – PPGEM.

BANCA EXAMINADORA:

Prof. Ph.D. Cezar Otaviano Ribeiro Negrão - Presidente - UTFPR

Prof. Dr. Moisés Alves Marcelino Neto – UTFPR

Prof. Dr. Silvio Luiz de Mello Junqueira – UTFPR

Prof. Ph.D. Marcelo Risso Errera – UFPR

Profª Drª Viviana Cocco Mariani - PUC-PR

A via original deste documento encontra-se arquivada na Secretaria do Programa, contendo a assinatura da Coordenação após a entrega da versão corrigida do trabalho.

Curitiba, _____de _____de 20___.

Carimbo e assinatura do Coordenador do Programa

_____

Dedico este trabalho à minha amiga, companheira e amada esposa Paula, por sempre estar ao meu lado, me confortando e apoiando com seu amor, carinho e compreensão. Aos meus maravilhosos pais, Vilmar e Carla, que sempre me incentivaram, acreditaram e não mediram esforços para fazer o melhor para seus filhos. E, em especial, em memória do meu digníssimo avô, Carlos Alberto Merhy, que mesmo nos momentos de dificuldade, luta e de dor nunca deixou de encarar a vida com alegria. Vô, sua alegria de viver e sua postura correta sempre serão motivos de orgulho para mim.

AGRADECIMENTOS

A Deus, por sua benção, proteção e por dar-me forças e saúde para superar este desafio. A Nossa Senhora do Perpétuo Socorro por sua misericordiosa interseção sempre acalmando, serenando e me tranquilizando nos momentos de grande dificuldade. Somente através de muita fé consegui encontrar forças para acreditar que o melhor está por vir e não desistir no meio desta jornada.

A minha esposa Paula, por todo amor, carinho, companheirismo, paciência, afeto e apoio durante toda esta luta. Mesmo diante de toda a distância física entre nós, no dia a dia, você conseguiu estar sempre presente me dando segurança e confiança para seguir em frente.

Aos meus pais, Vilmar e Carla, a minha irmã, Raisa, pelo amor, carinho, compreensão, dedicação, paciência e apoio durante toda minha vida.

Aos meus orientadores Professores Cezar Otaviano Ribeiro Negrão e Admilson Teixeira Franco, pelos ensinamentos transmitidos, pelo incentivo constante, pela oportunidade, orientação, confiança, amizade, dedicação, disposição e suporte contínuo, tanto no âmbito acadêmico como no pessoal, ao longo desses mais de 12 anos desde minha iniciação científica. Muito obrigado pela paciência que tiveram comigo neste período tumultuado. Não sei como expressar minha gratidão por tudo que vocês fizeram para eu acreditar no potencial do meu trabalho e tornar possível a finalização desta etapa tão importante em minha vida.

Aos professores da banca examinadora, pela atenção e contribuições dedicadas a esta tese.

Aos amigos, pelos momentos de descontração, amizade e solidariedade muitas vezes prestada.

Aos colegas do Centro de Pesquisas em Reologia e Fluidos Não Newtonianos (CERNN), pelo companheirismo e apoio na solução de diversos problemas. Aos mestrandos/doutorandos/pesquisadores Fernando Kroetz, Holmes, Jonathan, Rodrigo Seiji, e Tainan pela dedicação e empenho em suas pesquisas, em âmbito numérico e experimental, na área de fenômenos transientes. Sem as discussões que tivemos não teria adquirido grande parte do conhecimento utilizado para elaboração desta tese.

Aos engenheiros pesquisadores e grandes amigos: Alan Lugarini, Fernando De Lai, Diogo Andrade, Nezia de Rosso, Rubens Fernandes, Tainan Gabardo e Vinicius Polleto, por todos os momentos que passamos juntos, pelas profundas discussões técnicas e filosóficas e

pelo esforço extra dedicado por cada um de vocês com o projeto Petrobras, muitas vezes realizando atividades que a mim competiam. Sem a parceria, colaboração e ajuda de vocês esta tese com certeza não seria finalizada. Muito Obrigado.

Aos membros do Centro de Pesquisas da PETROBRAS (CENPES), ao Consultor Sênior André Leibsohn Martins, e em especial ao Engenheiro Rodrigo Azevedo Silva, que colaboraram fornecendo informações e dados experimentais para a validação do modelo e entendimento do problema.

À Universidade Tecnológica Federal do Paraná (UTFPR), ao Programa de Pós-Graduação em Mecânica e de Materiais (PPGEM) e ao Centro de Pesquisa em Reologia e Fluidos Não Newtonianos (CERNN), por toda estrutura proporcionada para o desenvolvimento desta tese.

À Agência Nacional do Petróleo – ANP – à Financiadora de Estudos e Projetos – FINEP – por meio do Programa de Recursos Humanos para o Setor Petróleo, Gás Natural e Biocombustíveis - PRH-ANP/MCT – (PRH10/UTFPR), ao Prêmio PETROBRAS de Tecnologia, em conjunto com CNPq (Conselho Nacional de Desenvolvimento Científico e Tecnológico) por terem incentivado e apoiado a realização da pesquisa durante a minha graduação e mestrado. Sem estes incentivos nestas etapas, certamente não teria seguido para o doutorado.

Por fim, a todos aqueles que de alguma forma, direta ou indiretamente, me apoiaram neste projeto.

RESUMO

OLIVEIRA, Gabriel Merhy. **Modelagem Matemática de Fenômenos Transitórios em Fluidos Não Newtonianos.** 2018. 94 f. Tese (Doutorado) - Universidade Tecnológica Federal do Paraná. Programa de Pós-graduação em Engenharia Mecânica e de Materiais, Curitiba, 2018.

No presente trabalho é apresentado um modelo matemático desenvolvido com o objetivo de prever a propagação de pressão em problemas transitórios compressíveis de fluidos não newtonianos. Os problemas físicos explorados são: i) fechamento abrupto de válvulas; ii) transmissão de pressão em fluidos de perfuração de poços de petróleo e; iii) reinício de escoamento de petróleo gelificado em tubulações. O escoamento do fluido é considerado unidimensional, fracamente compressível e isotérmico. O modelo baseia-se nas equações de balanço da massa e de quantidade de movimento que são resolvidas iterativamente através do método das características. A compressibilidade do fluido é considerada através da utilização de uma equação de estado que relaciona a massa específica com a pressão. Para representar o comportamento do fluido são utilizados dois modelos constitutivos: viscoplástico e tixotrópico. A distribuição de tensão de cisalhamento é considerada linear na direção radial, sendo que para o fluido viscoplástico utiliza-se o fator de atrito para escoamento plenamente desenvolvido enquanto que para o fluido tixotrópico integra-se o perfil de velocidades radial. Estes modelos foram apresentados em três publicações: "*Mathematical model for viscoplastic fluid hammer*"; "*Modeling and validation of pressure propagation in drilling fluids pumped into a closed well*" e; "*The effect of compressibility on flow start-up of waxy crude oils*". As principais conclusões dos trabalhos são: i) a pressão não se transmite completamente em fluidos viscoplásticos, o que contrasta com fluidos newtonianos; ii) a propagação de pressão depende da condição de contorno; da dissipação viscosa e da tensão limite de escoamento em casos de fluidos viscoplásticos; iii) a quebra da estrutura gelificada de fluidos tixotrópicos depende da relação entre os tempos de propagação de pressão e do característico de quebra do gel.

Palavras-chave: Escoamento Fracamente Compressível e Transitório. Propagação de Pressão. Modelo Matemático. Método das Características. Fluido Tixotrópico

ABSTRACT

OLIVEIRA, Gabriel Merhy. **Mathematical Modeling of Transient Phenomena in Non Newtonian Fluids.** 2018. 94 f. Thesis - Federal University of Technology – Paraná. Postgraduate Program in Mechanical and Materials Engineering, Curitiba, 2018.

In the current work a mathematical model is presented in order to predict pressure propagation in transient compressible non-Newtonian flow problems. The physical problems dealt are: i) fluid hammer problem; ii) pressure transmission in well drilling fluids and; iii) flow start-up of waxy crude oils in pipelines. The flow is considered one-dimensional, weakly compressible and isothermal. The model is based on the mass balance and momentum balance equations that are solved iteratively by the method of characteristics. The fluid compressibility is considered by employing a equation of state that correlates fluid density and pressure. Two constitutive models were used to represent the fluid behavior: viscoplastic and thixotropic. The shear stress distribution across the pipeline section is considered linear in the radial direction so that the friction factor approach is used for the viscoplastic fluid and the velocity profile is integrated across the pipeline section for the thixotropic fluid. These models were presented into three publications: “Mathematical model for viscoplastic fluid hammer”; “Modeling and validation of pressure propagation in drilling fluids pumped into a closed well” and; “The effect of compressibility on flow start-up of waxy crude oils”. The main conclusions are: i) pressure is not fully transmitted in viscoplastic fluids; ii) pressure propagation depends on pipeline boundary condition and; gel breaking of thixotropic fluids depends on the ratio of the pressure wave propagation time and the breaking characteristic time.

Keywords: Weakly Compressible Unsteady Flow. Pressure Propagation. Numerical Model. Method of Characteristics. Thixotropic Fluid.

LISTA DE FIGURAS

NOMENCLATURA

Artigo: ***Mathematical model for viscoplastic fluid hammer***

B	Número de Bingham	$[-]$
c	Velocidade de propagação da onda de pressão	$[m\,s^{-1}]$
C^+ , C^-	Linhas características	$[-]$
d	Diâmetro da tubulação	$[m]$
f	Fator de atrito de Fanning	$[-]$
g	Aceleração da gravidade	$[m\,s^{-2}]$
h	Altura do reservatório	$[m]$
l	Comprimento da tubulação	$[m]$
M_R	Número de Mach de referência	$[-]$
N	Número de células do domínio	$[-]$
p	Pressão dimensional	$[Pa]$
P	Pressão adimensional	$[-]$
Re	Número de Reynolds	$[-]$
t	Tempo dimensional	$[s]$
T	Tempo adimensional	$[-]$
v	Velocidade média do escoamento	$[m\,s^{-1}]$
V	Velocidade média do escoamento adimensional	$[-]$
z	Posição axial ao longo da tubulação	$[m]$
Z	Posição axial na forma adimensional	$[-]$

Símbolos

α	Compressibilidade isotérmica do fluido	$[Pa^{-1}]$
$\dot{\gamma}$	Taxa de cisalhamento	$[s^{-1}]$
γ	Condutância do fluido de Bingham	$[-]$
ΔT	Intervalo de tempo adimensional	$[-]$
ΔZ	Comprimento adimensional de cada célula	$[-]$
δ	Razão de aspecto da tubulação	$[-]$
η	Viscosidade plástica do fluido de Bingham	$[Pa\,s]$
θ	Temperatura	$[K]$
λ	Parâmetro característico do problema	$[-]$
ρ	Massa específica do fluido	$[kg\,m^{-3}]$

τ	Tensão de cisalhamento	$[\,Pa\,]$
τ_w	Tensão de cisalhamento na parede da tubulação	$[\,Pa\,]$
τ_y	Tensão limite de escoamento do fluido de Bingham	$[\,Pa\,]$

Subscritos

R	Relativo ao parâmetro de referência
0	Referente a condição inicial

Artigo: ***Modeling and validation of pressure propagation in drilling fluids pumped into a closed well***

A	Área da seção transversal	$[\,m^2\,]$
B	Número de Bingham	$[-]$
B_R	Número de Bingham de referência	$[-]$
C^+, C^-	Linhas características	$[-]$
c	Velocidade de propagação da onda de pressão	$[\,m\,s^{-1}\,]$
d_h	Diâmetro hidráulico da tubulação	$[\,m\,]$
d	Diâmetro interno da tubulação da coluna	$[\,m\,]$
d_1	Diâmetro interno do espaço anular	$[\,m\,]$
d_2	Diâmetro externo do espaço anular	$[\,m\,]$
f	Fator de atrito de Fanning	$[\,-\,]$
F_+, F_-	Coeficientes das Eqs. (4.17) e (4.18)	$[\,Pa\,]$
g	Aceleração da gravidade	$[\,m\,s^{-2}\,]$
G_+, G_-	Coeficientes das Eqs. (4.19) e (4.20)	$[\,Pa\,s\,m^{-3}\,]$
l	Comprimento da tubulação	$[\,m\,]$
M	Número de Mach	$[-]$
N	Número de células do domínio	$[-]$
p	Pressão dimensional	$[\,Pa\,]$
P	Pressão adimensional	$[-]$
q	Vazão volumétrica dimensional	$[\,m^3 s^{-1}\,]$
Q	Vazão volumétrica adimensional	$[-]$
R_+, R_-	Coeficientes das Eqs. (4.21) e (4.22)	$[\,Pa\,s\,m^{-3}\,]$
Re	Número de Reynolds	$[-]$
t	Tempo dimensional	$[\,s\,]$
T	Tempo adimensional	$[-]$

v	Velocidade média do escoamento	$[\,m\,s^{-1}\,]$
V	Velocidade média do escoamento adimensional	$[\,-\,]$
z	Posição axial ao longo da tubulação	$[\,m\,]$
Z	Posição axial na forma adimensional	$[\,-\,]$

Símbolos

α	Compressibilidade isotérmica do fluido	$[\,Pa^{-1}\,]$
β	Parâmetro adimensional do problema (Eq. (4.32))	$[\,-\,]$
γ	Condutância do fluido de Bingham	$[\,-\,]$
Δt	Intervalo de tempo	$[\,s\,]$
Δz	Comprimento de cada célula do domínio	$[\,m\,]$
δ	Razão de aspecto da tubulação	$[\,-\,]$
ζ	Parâmetro geométrico (Eq. (4.7))	$[\,-\,]$
η	Viscosidade plástica do fluido de Bingham	$[\,Pa\,s\,]$
θ	Temperatura	$[\,K\,]$
λ	Parâmetro adimensional do problema (Eq. (4.28))	$[\,-\,]$
ρ	Massa específica do fluido	$[\,kg\,m^{-3}\,]$
τ	Tensão de cisalhamento	$[\,Pa\,]$
τ_w	Tensão de cisalhamento média na parede da tubulação	$[\,Pa\,]$
τ_y	Tensão limite de escoamento do fluido de Bingham	$[\,Pa\,]$

Subscritos

A	Relativo ao espaço anular
lam	Escoamento em regime laminar
i	Posição axial na malha
in	Relativo a entrada
P	Relativo ao interior do tubo
set	Valor de referência
t	Relativo ao instante de tempo atual
$turb$	Escoamento em regime turbulento
z	Relativo a posição axial

Artigo: ***The effect of compressibility on flow start-up of waxy crude oils***

a,b,m	Constantes adimensionais do modelo tixotrópico	$[-]$
c	Velocidade de propagação da onda de pressão	$[ms^{-1}]$
C^+ , C^-	Linhas características	$[-]$
d	Diâmetro interno da tubulação	$[m]$
e , f	Coeficientes da Eq. (5.31)	$[-]$
F_+ , F_-	Coeficientes das Eqs. (5.27) e (5.28)	$[-]$
G_s	Módulo de elasticidade da microestrutura	$[Pa]$
G_0	Módulo de elasticidade do material totalmente estruturado	$[Pa]$
K	Índice de consistência	$[Pa\,s^n]$
l	Comprimento da tubulação	$[m]$
M	Número de Mach	$[-]$
n	Índice de lei de potência	$[-]$
N_r	Número de células do domínio na direção radial	$[-]$
N_z	Número de células do domínio na direção axial	$[-]$
p	Pressão dimensional	$[Pa]$
p_0	Valor final da pressão imposta na entrada	$[Pa]$
Q_0	Valor final da vazão imposta na entrada	$[m^3s^{-1}]$
r	Posição radial ao longo da tubulação	$[m]$
Re	Número de Reynolds	$[-]$
t	Tempo dimensional	$[s]$
T	Temperatura	$[K]$
t_{eq}	Tempo característico da mudança da microestrutura	$[s]$
t_r	Tempo de rampa	$[s]$
v	Componente da velocidade na direção axial $v(r,z,t)$	$[ms^{-1}]$
V	Velocidade média do escoamento na direção axial $V(z,t)$	$[ms^{-1}]$
$\overline{V}$	Velocidade média na direção axial via integração (Eq. (5.33))	$[ms^{-1}]$
z	Posição axial ao longo da tubulação	$[m]$

Símbolos

α	Compressibilidade isotérmica do fluido	$[Pa^{-1}]$
$\dot{\gamma}$	Taxa de cisalhamento	$[s^{-1}]$
$\ddot{\gamma}$	Variação temporal da taxa de cisalhamento	$[s^{-2}]$
$\dot{\gamma}_{yd}$	Taxa de cisalhamento de transição de τ_y entre τ_{yd}	$[s^{-1}]$
$\dot{\gamma}_{eq}$	Taxa de cisalhamento de equilíbrio	$[s^{-1}]$

Δt	Intervalo de tempo	$[\,s\,]$
Δz	Comprimento de cada célula do domínio	$[\,m\,]$
δ	Razão de aspecto da tubulação	$[-]$
η_v	Viscosidade equivalente	$[\,Pa\,s\,]$
η_0	Viscosidade do estado completamente estruturado	$[\,Pa\,s\,]$
η_∞	Viscosidade do estado completamente desestruturado	$[\,Pa\,s\,]$
η_{eq}	Viscosidade de equilíbrio	$[\,Pa\,s\,]$
θ_1	Tempo de relaxação	$\left[s\right]$
θ_2	Tempo de retardo	$\left[s\right]$
λ	Parâmetro estrutural	$[-]$
λ_0	Parâmetro estrutural do estado completamente estruturado	$\left[-\right]$
λ_{eq}	Parâmetro estrutural de equilíbrio	$\left[-\right]$
ρ	Massa específica do fluido	$[\,kg\,m^{-3}\,]$
τ	Tensão de cisalhamento	$[\,Pa\,]$
$\dot{\tau}$	Variação temporal da tensão de cisalhamento	$[\,Pa\,s^{-1}\,]$
τ_y	Tensão limite de escoamento estático	$[\,Pa\,]$
τ_{yd}	Tensão limite de escoamento dinâmico	$[\,Pa\,]$
τ_w	Tensão de cisalhamento média na parede da tubulação	$[\,Pa\,]$
ϕ	Parâmetro adimensional do problema	$[-]$

Subscritos

eq	Relativo a condição de equilíbrio
i	Posição na malha axial
in	Relativo a entrada
j	Posição na malha radial

Sobrescritos

$*$	Variável ou Parâmetro na forma adimensional
k	Relativo ao instante de tempo durante o processo iterativo

SUMÁRIO

1 INTRODUÇÃO

Operar instalações hidráulicas sempre em condições de regime permanente é impossível. Exemplos de situações transitórias são: atuações de válvulas, pressurização de tubulações e paradas e reinício de escoamento de fluidos. Compreender como ocorrem estes fenômenos e saber estimar previamente as pressões geradas e o intervalo de tempo necessário até a estabilização é fundamental para todos que trabalham com sistemas hidráulicos.

Muitos estudos, tanto numéricos quanto experimentais, têm sido realizados com o objetivo de conhecer melhor o comportamento dos sistemas submetidos às mais adversas condições transientes.

Neste cenário, apesar da grande quantidade de estudos já realizados com fluidos newtonianos, muito pouco se conhece sobre o comportamento de fluidos não newtonianos (mesmo os com comportamento reológico simples) e muito menos ainda é estudado sobre fluidos tixotrópicos em escoamentos transitórios.

Visando explorar parte desta lacuna, a presente tese de doutorado traz três artigos publicados em periódicos qualificados explorando as seguintes situações transitórias em tubulações: i) fechamento abrupto de válvulas; ii) transmissão de pressão em fluidos de perfuração de poços de petróleo e; iii) reinício de escoamento de petróleo gelificado. Além dos artigos, também se discorre brevemente sobre outras atividades realizadas na área de fenômenos transitórios que revelam ainda mais as contribuições e o ineditismo do estudo na área de fluidos não newtonianos.

1.1 Objetivo Geral

Define-se como objetivo geral da tese a modelagem matemática e numérica da propagação de pressão em fluidos não newtonianos durante eventos transitórios.

1.2 Objetivos Específicos

Com o objetivo principal deste trabalho traçado e diante das lacunas observadas na literatura, utiliza-se o modelo matemático desenvolvido para explorar três situações transitórias típicas em operações hidráulicas. Neste cenário, apontam-se como objetivos específicos da presente tese:

i. Avaliar o efeito da viscoplasticidade durante o súbito fechamento de válvulas;
ii. Verificar a transmissão de pressão em operações realizadas em poços de petróleo;
iii. Analisar o efeito da compressibilidade no reinício da circulação de fluidos gelificados em tubulações.

1.3 Estrutura do Trabalho

Para cumprir com os objetivos estabelecidos utiliza-se da forma de coletânea de artigos para a apresentação da tese. Assim, divide-se esta tese em seis capítulos. No primeiro capítulo introdutório faz-se a abordagem do tema, apresenta-se e contextualiza-se o problema e os objetivos são traçados. No Capítulo 2 apresenta-se a metodologia geral empregada no modelo matemático desenvolvido para avaliar a propagação da pressão durante escoamentos transientes e sintetizam-se os diferenciais explorados em cada artigo apresentado na coletânea. Os capítulos 3, 4 e 5 reproduzem os três artigos publicados na versão enviada para os periódicos especializados. O sexto capítulo traz as conclusões gerais sobre o tema explorado e temas para trabalhos futuros.

No Apêndice A discute-se brevemente sobre o programa computacional gerado como parte das atividades realizadas durante o doutorado. No Apêndice B comenta-se sobre o Prêmio ANP de Inovação Tecnológica 2016 no qual parte do trabalho desenvolvido nos últimos anos em conjunto com outras universidades e empresas consagrou-se vencedor. Outros trabalhos publicados na área de estudos de fenômenos transitórios realizados durante o doutorado são listados no Apêndice C.

2 SÍNTESE DA COLETÂNEA DE ARTIGOS CIENTÍFICOS

A coletânea de artigos que é apresentada na sequência desta tese contém três artigos publicados em periódicos qualificados ao longo dos últimos anos: Oliveira et al. (2013), Oliveira et al. (2015) e Oliveira e Negrão (2015). A apresentação destes artigos não está em ordem cronológica de publicação, pois se optou por priorizar uma sequência mais lógica de organização, aumentando a complexidade de estudo com o avanço dos capítulos. No capítulo 3 é estudado o fenômeno transiente causado pelo súbito fechamento de uma válvula. No Capítulo 4 analisa-se a transmissão de pressão ao longo da geometria típica de um poço de petróleo. No último artigo desta coletânea, apresentado no Capítulo 5, avalia-se o efeito da compressibilidade do fluido no processo de quebra da estrutura gelificada durante o reinício do escoamento de um petróleo parafínico que estava em repouso em uma tubulação.

Os presentes artigos estão relacionados pois abordam fenômenos transitórios em fluidos não newtonianos e a metodologia de solução das equações governantes empregadas na modelagem matemática deles é praticamente a mesma, as diferenças básicas entre os artigos estão principalmente nas condições de contorno empregadas, na geometria do problema e nas equações constitutivas para representar o comportamento reológico do fluido.

O escoamento do fluido é considerado unidimensional, fracamente compressível e isotérmico ao longo de toda a geometria. A compressibilidade do fluido é considerada através da utilização de equação de estado que relaciona a massa específica com a pressão. Admite-se que o escoamento é fracamente compressível e a tubulação é perfeitamente rígida. Desta forma, correlaciona-se a velocidade máxima de propagação da onda de pressão com a compressibilidade do fluido.

O modelo geral para resolver o problema transitório baseia-se nas equações de balanço da massa e da quantidade de movimento, que formam o sistema de equações diferenciais parciais hiperbólicas, tendo como incógnitas a pressão, a vazão e a tensão de cisalhamento na parede e como variáveis independentes, a posição e o tempo. Para resolver o problema, estas equações parciais são convertidas em equações diferenciais totais através do método das características (Wylie et al., 1993). As equações diferenciais ordinárias resultantes são então integradas pelo método das diferenças finitas a partir de uma condição inicial.

Para expressar os efeitos viscosos proporcionados pelo fluido não newtoniano escoando na tubulação, emprega-se o conceito de tensão de cisalhamento média na parede da tubulação. A forma como se considera este termo em cada um dos artigos merece destaque e

será tratada na sequência com a apresentação dos diferenciais observados em cada artigo da coletânea.

2.1 Mathematical Model for Viscoplastic Fluid Hammer (2015)

Publicado em 2015 no *Journal of Fluids Engineering*, o artigo pode ser considerado como o mais simples da presente coletânea, trata do fenômeno transitório tipicamente conhecido como golpe de aríete (Streeter e Wylie, 1974; Ghidaoui et al., 2005; Bergant et al., 2006), aplicado para o caso do escoamento de fluido não newtoniano de Bingham. O problema contempla a avaliação da variação da pressão ao longo da tubulação após o súbito fechamento de válvula localizada na saída da tubulação que está conectada ao reservatório. A condição inicial do problema consiste do escoamento em regime permanente do fluido pela tubulação.

O efeito do comportamento reológico do fluido de Bingham é considerado através da avaliação da tensão de cisalhamento na parede com base na correlação para fator de atrito proposta por Swamee e Aggarwal (2011).

O maior diferencial do trabalho está na abordagem do fluido como viscoplástico, consideração que acaba levando a resultados inovadores, uma vez que pode ser observado em alguns casos, após a parada por completo do escoamento, distribuição não uniforme da pressão ao longo da tubulação. Estudos de casos mostraram gradiente de pressão não uniforme ao longo da tubulação que é dependente da tensão limite de escoamento do fluido, da inércia do escoamento, de parâmetros geométricos da tubulação e também da compressibilidade do fluido.

2.2 Modeling and Validation of Pressure Propagation in Drilling Fluids Pumped into a Closed Well (2013)

O segundo artigo, publicado em 2013 no *Journal of Petroleum Science and Engineering*, explora a propagação da pressão ao longo da geometria típica de um poço de petróleo a fim de avaliar o quanto da pressão é transmitida ao longo do poço. Neste trabalho, os fluidos de perfuração são tratados como não newtoniano de Bingham e os efeitos viscosos são computados através do conceito de fator de atrito. Os resultados do modelo são comparados com alguns valores experimentais para o escoamento de um fluido newtoniano

(água) e dois fluidos de perfuração. Não só a magnitudemas também as frequências de oscilação dos valores medidos e calculados concordam muito bem. Ao contrário do que ocorre para o fluido newtoniano, tanto os valores medidos quanto os calculados de pressão para fluido de Bingham não estabilizam uniformemente ao longo do poço após a pressurização. Nestes casos a pressão prevista e a medida não são completamente transmitidas nos testes.

A principal contribuição do trabalho, além da validação via comparação com resultados experimentais obtidos em poço real de petróleo instrumentado, consiste na identificação de parâmetros operacionais que permitem estabelecer metodologias de pressurização que favorecem a transmissão de pressão em tubulação fechada.

Além disso, em comparação com os trabalhos existentes na literatura, o modelo desenvolvido diferencia-se principalmente por: i) considerar o escoamento através do interior da coluna de perfuração e através do espaço anular formado entre a coluna de perfuração e a parede do poço; ii) empregar o método das características para converter as equações diferenciais parciais em totais com fluidos não newtonianos.

2.3 The Effect of Compressibility on Flow Start-up of Waxy Crude Oils (2015)

No terceiro artigo é apresentado o estudo sobre o reinício do escoamento de fluido tixotrópico com características elásticas e viscoplásticas (modelo de Souza Mendes e Thompson (2013)). O artigo foi publicado em 2015 no *Journal of Non-Newtonian Fluid Mechanics,* periódico de maior difusão na área de fluidos não newtonianos.

Assim como os outros dois artigos apresentados, o modelo é formado pelas equações de conservação da massa e do balanço da quantidade de movimento. O escoamento é considerado isotérmico, laminar e fracamente compressível. A solução das equações é obtida através do método das características. A principal diferença em relação aos modelos apresentados nos artigos anteriores é a consideração da tixotropia do material através de equação constitutiva de natureza elastoviscoplástica. Para resolver a equação admite-se que a tensão de cisalhamento varia de forma linear ao longo do raio da tubulação.

Em relação aos trabalhos similares encontrados na literatura, o presente artigo destaca-se principalmente por abordar de forma diferente a modelagem do escoamento em oleodutos uma vez que considera que o tempo para o reinício do escoamento e a magnitude

das pressões durante a quebra da estrutura gelificada dependem tanto do tempo de resposta do material como da sua compressibilidade.

No artigo são explorados os efeitos de dois tipos de condições de contorno para avaliar o reinício, sendo: i) de pressão prescrita e, ii) de vazão volumétrica prescrita na entrada da tubulação. A primeira condição tem por objetivo estimar o tempo necessário enquanto a segunda, a máxima pressão durante o reinício do escoamento. Considerando o material como elastoviscoplástico o efeito da elasticidade do material também é investigado.

3 MATHEMATICAL MODEL FOR VISCOPLASTIC FLUID HAMMER

Gabriel M. Oliveira, Admilson T. Franco, Cezar O. R. Negrão

Journal of Fluids Engineering, 2015; 138(1):011301-011301

The current work presents a mathematical model to simulate "viscoplastic fluid hammer" – overpressure caused by sudden viscoplastic fluid deceleration in pipelines. The flow is considered one-dimensional, isothermal, laminar and weakly compressible and the fluid is assumed to behave as a Bingham plastic. The model is based on the mass and momentum balance equations and solved by the method of characteristics. The results show that the overpressures taking place in viscoplastic fluids are smaller than those occurring in Newtonian fluids and also that two pressure gradients – one negative and one positive – are possibly noted after pressure stabilization. The pressure stabilizes non-uniformly on the pipeline because viscoplastic fluids present yield stresses. Overpressure magnitudes depend not only on the ratio of pressure wave inertia to viscous effect but also on the Bingham number. The pipeline designer should take into account the viscoplastic fluid behavior reported in this paper when engineering a new pipeline system.

Keywords: Viscoplastic Fluid Transients. Yield Stress, Pressure Wave, Mathematical Model

3.1 Introduction

Sudden valve closures in hydraulic systems can produce overpressure and shock waves, usually called water hammer (Streeter and Wylie, 1974), which may damage the overall system. The pressure peaks caused by valve closure should be predicted during pipeline design in order to provide reliability and safety to the system. However, not only water is transported in pipeline system but also several other non-Newtonian fluids, such as slurries, sewage, pastes and suspensions (Mitsoulis, 2007). Many of these fluids, called viscoplastic, flow only if the applied shear exceeds the fluid yield stress and their flow must also be appropriately controlled to prevent damage caused by sudden valve closure. The pressure surge caused by step changes of flows of such fluids is herein named "viscoplastic fluid hammer". Despite nowadays valve operations being designed to actuate slowly enough

to avoid high overpressures, viscoplastic fluid hammer is still a problem of concern, as will be discussed in the current text.

In hydraulics of Newtonian fluids, many studies have been conducted to model and to understand the water hammer phenomenon, as cited by the excellent reviews of Streeter and Wylie (1974), Ghidaoui et al. (2005) and Bergant et al. (2006). Brunone et al. (2000), for instance, measured velocity profiles in pipelines of transient flows produced by fast valve closures. Brunone et al. (2004) presented an interesting experimental and numerical study about the energy dissipation phenomenon that occurs in laminar transient flows.

Many software applications available for designing pipeline systems include water hammer analysis (Ghidaoui et al., 2005). However, studies of viscoplastic fluid hammer have not been found in the literature and very few software applications allow the evaluation of non-Newtonian fluid flows. The existing studies usually deal with the Power-Law fluid model. Wahba (2013), for instance, investigated the Non-Newtonian fluid-hammer taking place in Power-Law fluids and discussed the shear-thickening and shear-thinning effects of the fluid. The well-established criteria to predict water hammer in Newtonian fluids, nevertheless, may not be appropriate to design pipelines working with viscoplastic fluids.

Viscoplastic fluids behave differently from Newtonian fluids as they present a yield stress and consequently their viscosity is shear rate dependent (Bird et al., 1987). Oliveira et al. (2012b), for instance, reported that the pressure of a viscoplastic fluid compressed within a horizontal closed pipe stabilizes non-uniformly. Although several works that deal with transient flows of non-Newtonian fluids in pipelines have already been performed (Cawkwell and Charles, 1987; Sestak et al., 1987; Chang et al., 1999; Davidson et al., 2004; Vinay et al., 2006; Vinay et al., 2007; Wachs et al., 2009; Oliveira et al., 2010; Negrão et al., 2011), none has investigated the viscoplastic fluid hammer phenomenon.

Considering the lack of literature in the subject and in order to contribute to a better understanding of the problem, this work presents a mathematical model to predict pressure propagation in a viscoplastic fluid after a sudden valve closure at the outlet of a horizontal pipe connected to a fluid reservoir. The influence of non-dimensionless parameters on the pressure propagation, on pressure peaks and on the final pressure distribution along the pipe is discussed.

3.2 Mathematical Model

The problem to be studied consists of a reservoir connected to a long horizontal pipe with a valve controlling the fluid flow at the outlet, as shown in Figure 3.1. The fluid height in the reservoir, *h*, is kept constant so that the pressure at the pipe inlet has a constant magnitude, $p_R=\rho gh$. In addition, the fluid flow is considered isothermal and one-dimensional, the pipe is assumed completely rigid, i.e., pipe wall does not deform during compression, and the valve is closed instantaneously.

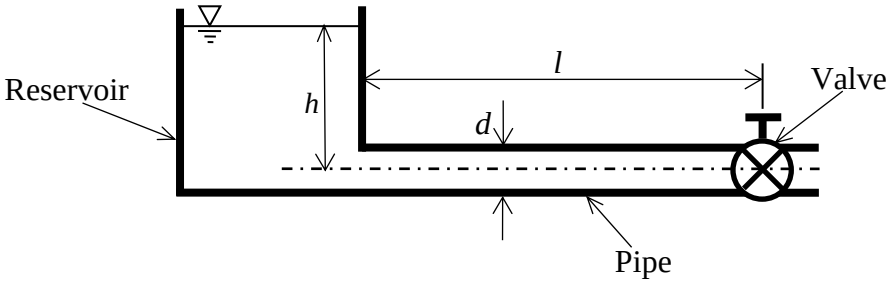

Figure 3.1 – Illustration of the physical problem.

By applying the hypotheses above, the mass and momentum balance equations can be written as,

$$\frac{\partial \rho}{\partial t}+\rho\frac{\partial v}{\partial z}+v\frac{\partial \rho}{\partial z}=0 \tag{3.1}$$

$$\rho\frac{\partial v}{\partial t}+\rho v\frac{\partial v}{\partial z}=-\frac{\partial p}{\partial z}-\frac{4}{d}\tau_w \tag{3.2}$$

where v is the average velocity across the pipe section, ρ is the fluid density, p is the pressure, τ_w is the average shear stress at the pipe internal surface, d is the pipe diameter, t is time and z is the axial coordinate. The isothermal compressibility, α, that is assumed constant for the fluid flow, is defined as (Anderson, 1990):

$$\alpha=\frac{1}{\rho}\frac{\partial \rho}{\partial p}\bigg|_{\theta}=\frac{1}{\rho c^2} \tag{3.3}$$

where c is the wave speed and θ is the fluid temperature.

For Bingham fluids, the shear stress is defined as a function of shear rate according to the following:

$$\tau = \tau_y + \eta\dot{\gamma} \qquad |\tau| > \tau_y \tag{3.4}$$

$$\dot{\gamma} = 0 \qquad |\tau| \le \tau_y \tag{3.5}$$

where τ is the shear stress, $\dot{\gamma}$ is the shear rate, τ_y is the fluid yield stress and η is the plastic viscosity (Bird et al., 1987).

A linear cross-section change of shear stress is usually assumed by others (Chang et al., 1999) so as to reduce the complexity caused by the radial stress dependence. As will be discussed in Section 3.3, this assumption is acceptable for the current work and will be accomplished by using the Fanning friction factor, f:

$$\tau_w = \frac{f\rho v^2}{2} \tag{3.6}$$

For laminar Bingham fluid flows, f is obtained from the Buckingham-Reiner´s equation (Swamee and Aggarwal, 2011):

$$f = \frac{16}{Re}\left[1 + \frac{4B}{3} - \frac{1}{3}\left(\frac{8^4 B^4}{(f\,Re)^3}\right)\right] \tag{3.7}$$

where Re ($=\rho v d/\eta$) is the Reynolds number, and B ($=\tau_y\, d/8\eta v$) is the Bingham number. According to Melrose et al. (1958), a fluid conductance for Bingham fluids can be defined as $\gamma = 16/(f\,Re)$, which can be calculated from:

$$\gamma = 1 - \frac{4}{3}\gamma B + \frac{1}{3}(\gamma B)^4 \tag{3.8}$$

where γ varies from 0 (very large Bingham number) to 1 (Newtonian fluid). Fluid conductance is a correction to the classical form of the Newtonian friction factor, $f = 16/(\gamma\, Re)$. When the Bingham number is very large, say greater than 10^6, the conductance can be approximated by $\gamma = 1/B$.

As reported by Wylie et al. (1993), the non-linear advective terms in equations (3.1) and (3.2) can be neglected for weakly compressible flows at low velocities. By substituting Eq. (3.3) into Eq. (3.1) and the shear stress τ_w, evaluated by Eqs. (3.6), (3.7) and (3.8), into Eq. (3.2), the mass and momentum balance equations can be rewritten, respectively, in dimensionless form as:

$$\frac{\partial P}{\partial T} + \lambda \frac{\partial V}{\partial Z} = 0 \tag{3.9}$$

$$\lambda \frac{\partial V}{\partial T} + \frac{\partial P}{\partial Z} + \frac{V}{\gamma} = 0 \tag{3.10}$$

where P, V, Z and T are, respectively, the nondimensional pressure, the average axial velocity, the axial position, and time, which are defined as: $P=p/p_R$, $V=v/v_R$, $Z=z/l$, $T=tc/l$. l is the pipe length, v_R ($=p_R d^2/32\eta l$) is the steady-state average velocity of a Newtonian fluid ($\gamma=1$) and p_R is the pressure difference between the pipe inlet and outlet. v_R is obtained from Eq. (3.2) by considering the valve completely opened. Despite ρcv being usually used for pressure nondimensionalization, the inlet pressure was chosen as a reference not only because the reservoir pressure is more representative of the flow but also because this pressure does not change for the different cases to be studied.

The parameter λ in Eqs. (3.9) and (3.10) is the ratio of wave speed inertia, ρcd, and plastic viscosity of the Bingham fluid, η, multiplied by the pipe aspect ratio:

$$\lambda = \left(\frac{\rho cd}{32\eta} \right) \frac{d}{l} = \frac{\delta}{32} \frac{Re_R}{M_R} \tag{3.11}$$

λ can also be defined as product of the aspect ratio ($\delta = d/l$) and the Reynolds number ($Re_R=\rho v_R d/\eta$) divided by the Mach number, ($M_R=v_R/c$). Wahba (2008), nonetheless, defined λ as the ratio between the excessive pressure force generated by the transient phenomenon (Joukowsky force - ρcvd^2) and the viscous force ($\eta ldv/d$) acting to damp the transient pressure.

The fluid conductance, Eq. (3.8), can be rewritten by using parameters that are based on reference values:

$$\gamma = 1 - \frac{4}{3}\gamma \frac{B_R}{V} + \frac{1}{3}\left(\gamma \frac{B_R}{V} \right)^4 \tag{3.12}$$

where B_R ($=4\tau_y l/p_R d$) is the Bingham number that characterizes the flow viscoplasticity. B_R is equal to the ratio of the yield stress and the wall shear stress in the fully developed steady state flow.

3.2.1 Boundary and Initial Conditions

A constant pressure is defined as the inlet boundary condition:

$$P(Z=0,T)=1 \qquad T \geq 0 \tag{3.13}$$

and a zero velocity at the outlet is assumed for the sudden valve closure:

$$V(Z=1,T)=0 \qquad T \geq 0 \tag{3.14}$$

The steady state flow with the valve completely opened is considered the initial condition. This condition is obtained by making the time derivative of Eq. (3.10) equal to zero which provides the initial fluid velocity, $v_0=\gamma_0 v_R$, where γ_0 is the fluid conductance based on the initial velocity and on the Bingham number. Notably, the larger the Bingham number the smaller the conductance and therefore the smaller the initial velocity. For cases where the pressure difference is not high enough to exceed the yield stress, $B_R \geq 1$, the fluid rests within the pipe.

3.2.2 Method of Solution

The governing equations are solved by the method of characteristics (MOC) that is typically used for solving hyperbolic partial differential equations (see Wylie et al., 1993). The method consists of simplifying partial differential equations to a family of ordinary differential equations, along which the solution can be integrated from an initial condition. In the current case, Eqs. (3.9) and (3.10) are reduced to two total differential equations, which are valid over the characteristic lines $dZ/dT=\pm 1$. Inasmuch as c is constant, plots of dZ/dT provides straight lines on the Z–T plane, such as C^+ and C^- in Figure 3.2. In order to solve numerically the equations, the pipe are divided into N equal reaches, ΔZ, as shown in Figure 3.2, and the time-step is computed according to $\Delta T=\Delta Z$. If P and V are both known at position $i-1$ and $i+1$, the ordinary differential equations can be integrated over the characteristic lines C^+ and C^-, respectively, and therefore, be written in terms of unknown variables P and V at point i. By solving the two resulting algebraic equations, P and V can be obtained at point i as a function of known values at points $i-1$ and $i+1$. As the fluid conductance depends on the value of the instantaneous velocity an iterative procedure is performed using the average velocity calculated for a Newtonian fluid as the first value. This process takes place until the

relative difference between two consecutive values of V is smaller than 0.1%. As soon as convergence has been achieved, the solution evolves to the next time-step and then proceeds until the desired time duration has been covered.

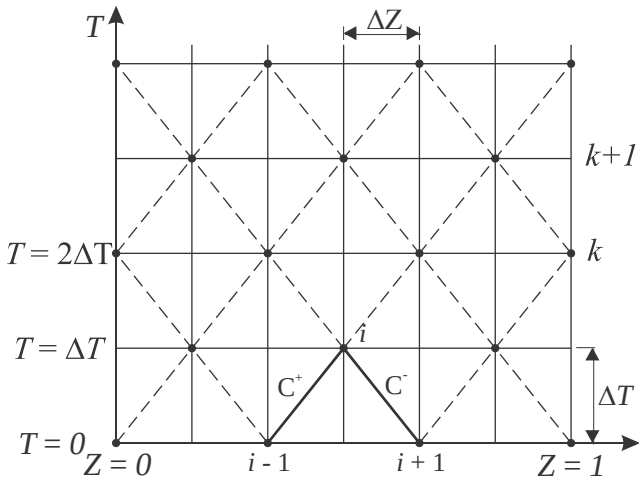

Figure 3.2 – Spatial and temporal grid.

3.3 Results and Discussions

3.3.1 Model Verification and Validation

In order to verify the model validity, the grid size was firstly analyzed. Figure 3.3a and Figure 3.3b show, respectively, the effect of the grid size on the time change of pressure at position Z=0.6 and on the axial pressure distribution at time T=0.4 after the valve closure. The analysis was conducted for λ=1.0 and B_R=0.5 and six different grid sizes: 50, 100, 200, 500, 1000, 2000 points in the axial position. The method of characteristics requires that the dimensionless axial reaches and time-steps being equal, $\Delta T=\Delta Z=1/N$. As shown in Figure 3.3, the results become grid independent for N=1000 in order that $\Delta T=\Delta Z=10^{-3}$. Inasmuch as the solution evolves ever two time-steps the least time-step to be considered is 2×10^{-3}.

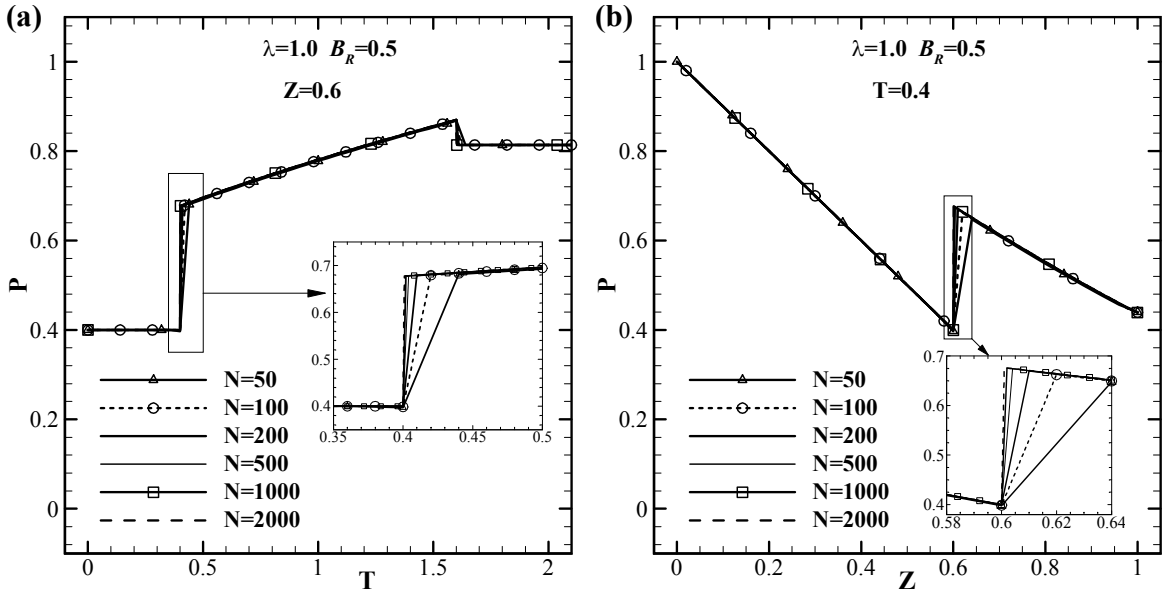

Figure 3.3 – Effect of mesh size for λ=1.0 and B_R=0.5. (a) Time evolution of pressure at Z=0.6 and (b) axial pressure distribution at T=0.4.

Few controlled experimental results to evaluate transient flows of viscoplastic fluids are available in the literature. Oliveira et al. (2013) showed that drilling fluids do not transmit pressure after being pressurized within a closed well and have compared their model results, with good agreement, to experimental data obtained in a drilling rig. Considering that experimental data for viscoplastic fluid hammer were not found in the literature, the current model results were compared with the classical water hammer data of Holmboe and Rouleau (1967). They conducted their experiments in a copper pipe of 1.0 inch diameter filled with high viscosity oil. The pressure responses obtained at the valve and at the pipe midpoint positions are shown in Figure 3.4a and Figure 3.4b, respectively. Different from the nondimensionlization used by Holmboe and Rouleau (1967), the pressure herein was scaled by $\rho c v_0$, so that $(p-p_0)/\rho c v_0=(P-P_0)/\lambda$. For the data displayed in Figure 3.4, λ is equal to 18.6. Despite the model limitations, already pointed out in the literature Bird et al., 1987, the maximum pressure obtained with the model is quite close to the measured value. The differences, however, increase with the sequence of oscillatory cycles. Although the use of a periodic friction factor should approximate the results (Wylie et al., 1993), this is outside the scope of the current work.

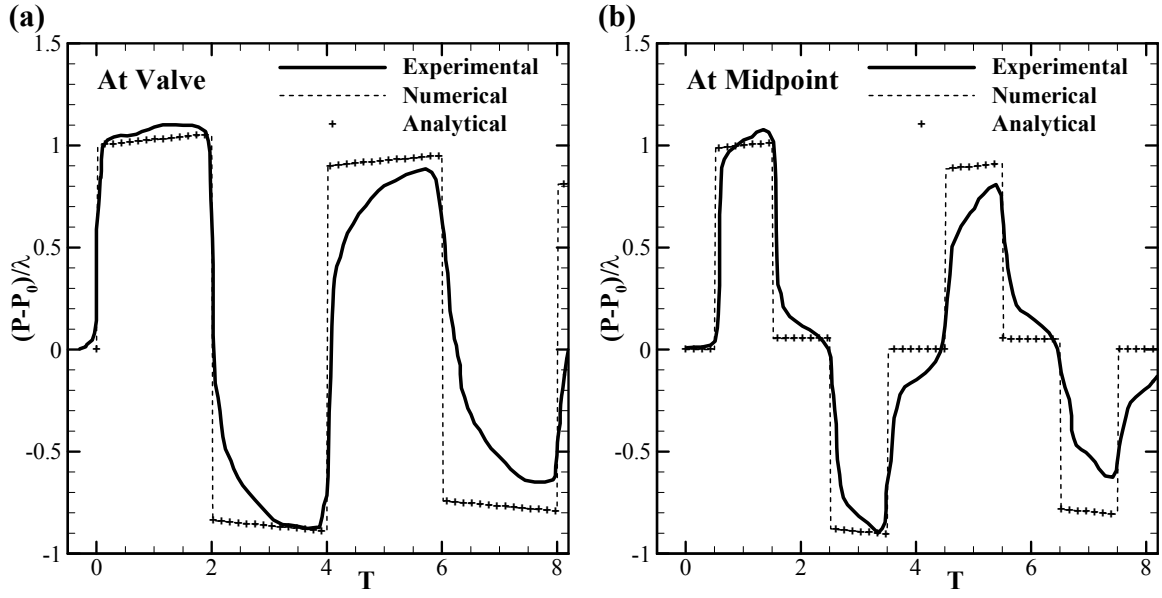

Figure 3.4 – Comparisons of the numerical results with experimental data [24] and with an analytical solution. Time evolution of pressure (a) at the valve position and (b) at pipe midpoint position.

Figure 3.4 also depicts the results of an analytical solution for Eqs. (3.9) and (3.10) solved for Newtonian fluids (γ= 1). This analytical solution, here proposed, is based on the work of Sobey (2004):

$$P(Z,T) = 1 - 2\lambda e^{\frac{-T}{2\lambda}} \sum_{n=1}^{\infty} \left\{ \frac{(-1)^n}{\beta_n^2} \sin \beta_n Z \left[\left(\omega_n - \frac{1}{4\lambda^2 \omega_n} \right) \sin \omega_n T - \frac{\cos \omega_n T}{\lambda} \right] \right\} \tag{3.15}$$

$$V(Z,T) = -2e^{-\frac{T}{2\lambda}} \sum_{n=1}^{\infty} \left[\frac{(-1)^n}{\beta_n} \cos \beta_n Z \left(\cos \omega_n T + \frac{1}{2\lambda \omega_n} \sin \omega_n T \right) \right] \tag{3.16}$$

where, $\beta_n = (2n-1)\pi/2$, $\omega_n{}^2 = \beta_n{}^2 - 1/4\lambda^2$, and n is an integer number. For the results shown in Figure 3.4, 20,000 terms were used in the summation of Eq. (3.15). As noted, the numerical and analytical solution results coincide.

3.3.2 Numerical Results

A model sensitivity analysis is now conducted for different values of λ and B_R. λ was varied from 0.1 to 10.0 and B_R from 0.0 (Newtonian fluid) to 0.75. These limits of λ represent, for instance, a pipe length ranging from 10 to 1000 m for c=1000 m/s, ρ=1000 kg/m^3, d=10mm and η=0.03125 Pa.s. On the other hand, B_R=0.75 means that the inlet

pressure is 33.3 % (1.0/0.75) larger than the minimum pressure required to exceed the fluid yield stress.

When the fluid is flowing in steady-state and the valve is suddenly closed, the pressure at the valve increases instantaneously to the Joukowsky pressure ($\rho c v_0 = \rho c \gamma_0 v_R$) and propagates in direction to the reservoir (Z=0.0) (Wylie et al., 1993). This pressure, with dimensionless magnitude of $\lambda\gamma_0$ ($\rho c \gamma_0 v_R / p_R$), is attenuated during propagation because of viscous dissipation. If the pressure wave reaches the reservoir with sufficient energy, the wave is reflected back to the valve. The pressure reflection at the valve and at the reservoir takes place until the wave is completely dissipated. It is well known that the final pressure for a Newtonian fluid is uniform along the pipe and equal to p_R. On the other hand, the pressure propagates in a Bingham fluid only if the pressure gradient is larger enough to surpass the fluid yield stress and therefore, the final pressure can be non-uniformly distributed along the pipe as observed by Oliveira et al. (2012b).

Figure 3.5 presents the time evolution of pressure fields for Newtonian (B_R=0.0) and Bingham (B_R=0.5) fluids with λ=1.0. Whilst Figure 3.5a and Figure 3.55c show the pressure distribution along the pipe for different times after the valve closure (T=0; 0.2; 0.4; 0.8, 1.0), Figure 3.5b and Figure 3.5d present the pressure distribution after the wave reflection at the reservoir (T=1.2; 1.4; 1.6; 1.8). Note that T=1.0 is the time for the pressure wave to travel one pipe length.

When the valve is closed, the pressure at the valve increases instantaneously to $\lambda\gamma_0$ so that the magnitude for the Newtonian fluid is 1.0 (γ_0=1.0) and for the Bingham fluid is only 35% of this value (γ_0=0.354). With time evolution, the viscous effect dissipates the wave energy reducing the magnitude of the propagating pressure. Whereas the magnitude of pressure at T=0.2 and Z=0.8 for the Newtonian fluid is 1.1 (Figure 3.5a), the pressure obtained for the Bingham fluid at the same time and position is only 0.51 (Figure 3.5c). As the pressure propagates in direction to the valve after reflection at the reservoir at T=1.0, the pressure is reduced upstream and increased downstream of the wave, as shown in Figure 3.5b and Figure 3.5d. The pressure is then reflected continuously until it is completely dissipated. In contrast with Newtonian fluid that presents a uniform final pressure distribution, the pressure for the Bingham fluid is non-uniformly distributed with two gradients along the pipe.

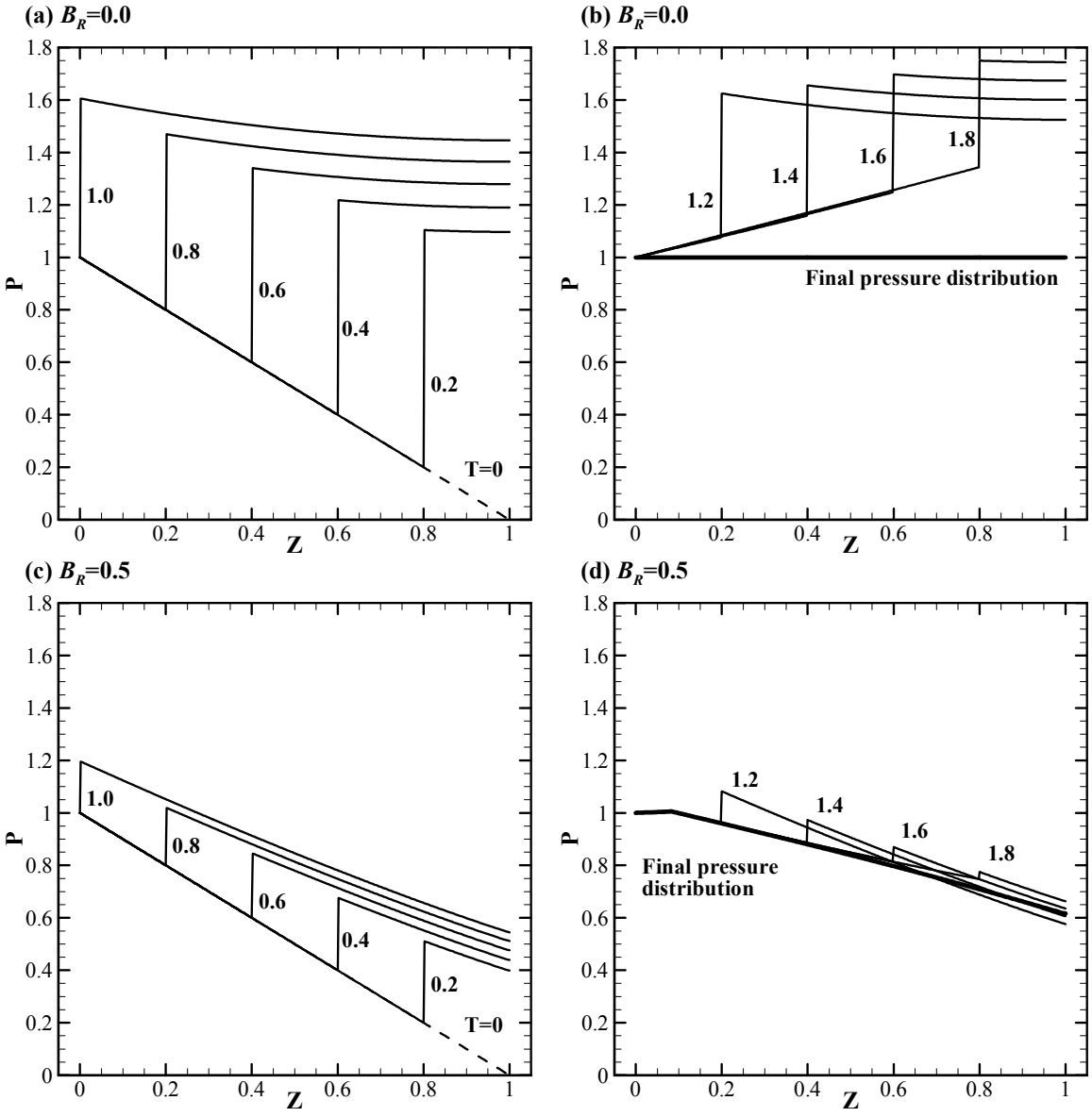

Figure 3.5 – Time evolution of the axial pressure distribution for λ=1.0. (a, b) - B_R=0 and (c, d) - B_R=0.5.

The axial velocity along the pipe for the cases of Figure 3.5 is shown in Figure 3.6. As depicted, the flow decelerates to zero at the valve position and then its velocity is continuously reduced from the valve position to the inlet as the pressure wave propagates. As already mentioned, the initial velocity value for B_R=0.5 is 35 % of that observed for Newtonian fluid. After the reflection at the reservoir at T=1.0, the Newtonian fluid flows to the reservoir (negative velocities) whereas the Bingham fluid stops flowing. The Bingham fluid does not flow back to the reservoir because the axial pressure gradient is not high enough to exceed the fluid yield stress.

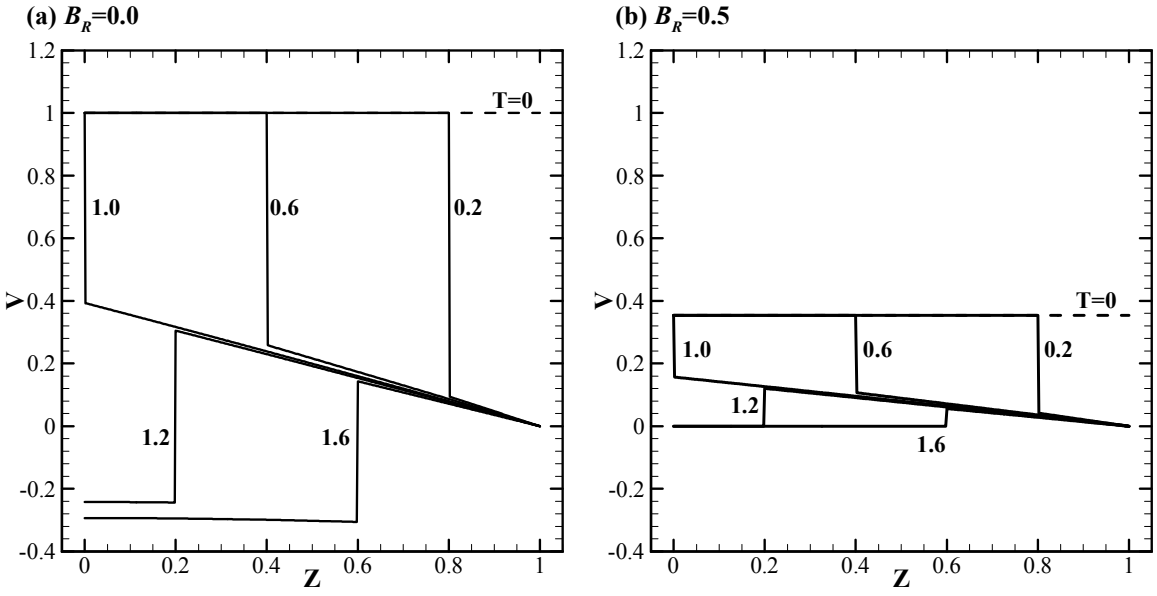

Figure 3.6 – Time evolution of the axial velocity distribution for λ=1.0. (a) B_R=0 and (b) B_R=0.5.

In an addition to Figure 3.6, Figure 3.7 shows the time evolution of pressure (Figure 3.7a) and of the average velocity (Figure 3.7b) at the pipe midpoint position for both fluids. On one hand, the Bingham fluid stops flowing after T=1.5 and the pressure stabilizes around 0.85. On the other hand, the Newtonian fluid motion continues for a longer period and stabilizes at 1.0, as the fluid dissipation is lower.

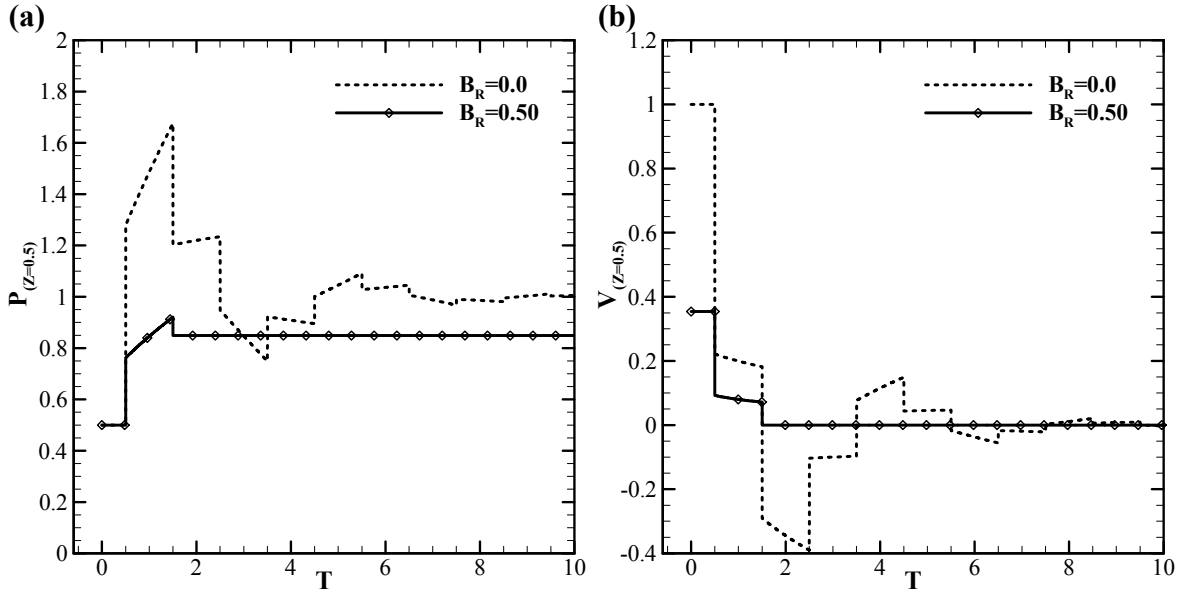

Figure 3.7 – Effect of the Bingham number on the time evolution of (a) pressure and (b) velocity at pipe midpoint position for λ=1.0.

The smaller the λ, the faster the pressure wave dissipation and few oscillations are noted before the complete fluid stop. Figure 3.8a depicts the evolution of pressure fields for λ=0.1 and B_R=0.0 and Figure 3.8b, for λ=0.1 and B_R=0.5, respectively. For this low value of λ, the pressure does not reflect at the pipe end and the final pressure distribution for the Bingham fluid (Figure 3.8b) shows only one gradient. Noticeably, the wave stops propagating as soon as the pressure gradient is not high enough to surpass the fluid yield strength ($\tau_y \pi d/A$) and then, the pressure stabilizes non-uniformly along the pipe. In addition, it was observed that the final pressure gradient is in the order of minus B_R, which in this case is -0.5. This result can be predicted by inspecting Eq. (3.10) and making the velocity derivative with respect to time equal to zero. As the fluid stops moving, the conductance is reduced to a tiny value. In order to make $\gamma \to 0$ in Eq. (3.12), the product $\gamma\left(B_R/V\right)$ must approach 1.0. Consequently, γ tends to V/B_R and the pressure gradient in Eq. (3.10) results in minus B_R independently of the value of λ. However, this result was not observed in the numerical results for larger values of λ because of the several wave reflections at the pipe ends (see Figure 3.5c and Figure 3.5d).

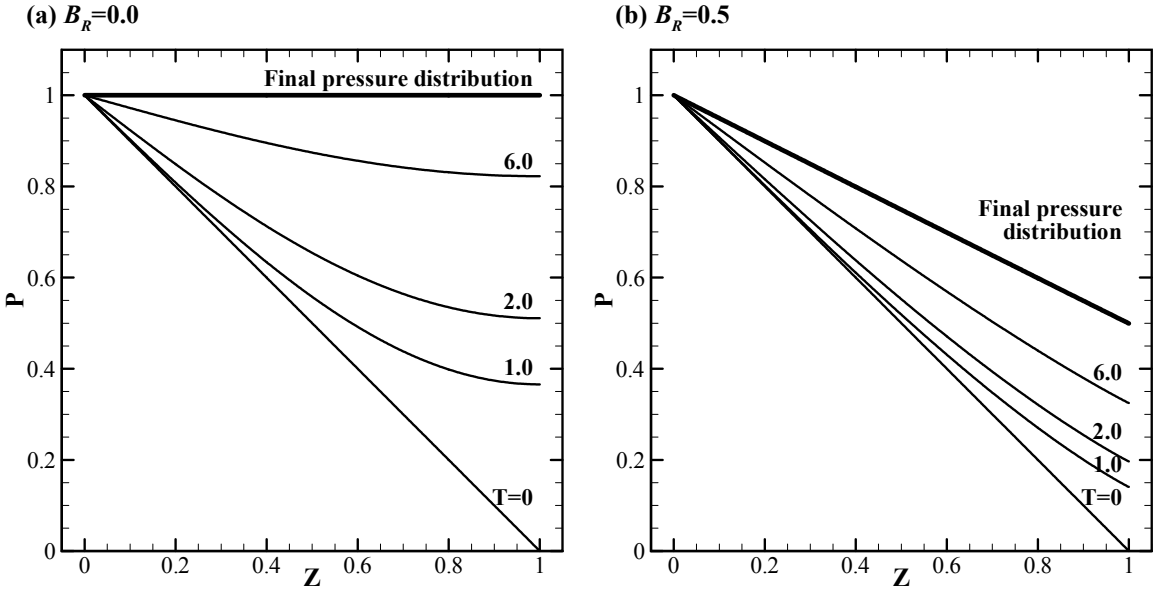

Figure 3.8 – Time evolution of the axial pressure distribution for λ=0.1. (a) B_R=0 and (b) B_R=0.5.

A sensitivity analysis was conducted by varying the Bingham number and λ as both affect pressure wave dissipation. Small values of λ mean the Reynolds and/or the aspect ratio are small in comparison with the Mach number implying highly dissipative cases which rapidly damp oscillations. Figure 3.9 shows how these parameters affect the time evolution of pressure at the valve position after a sudden valve closure. As can be seen, the pressure peaks

increase with the reduction of the Bingham number. Besides, the steady-state pressure stabilizes at the reservoir pressure (P=1.0) for the Newtonian fluid (B_R=0) and reduces with the increase of the Bingham number. An exception is made to the case in which λ=1.0 and B_R=0.25, as the pressure stabilizes 20% above the reservoir pressure. As expected, the higher the λ the more oscillating is the pressure and the larger is the magnitude of the peaks. Notably, the pressure undergoes a sudden rise of $\lambda\gamma_0$ soon after the valve closure. Not only the oscillations and the initial pressure peak increase with λ but also the time to reach steady-state.

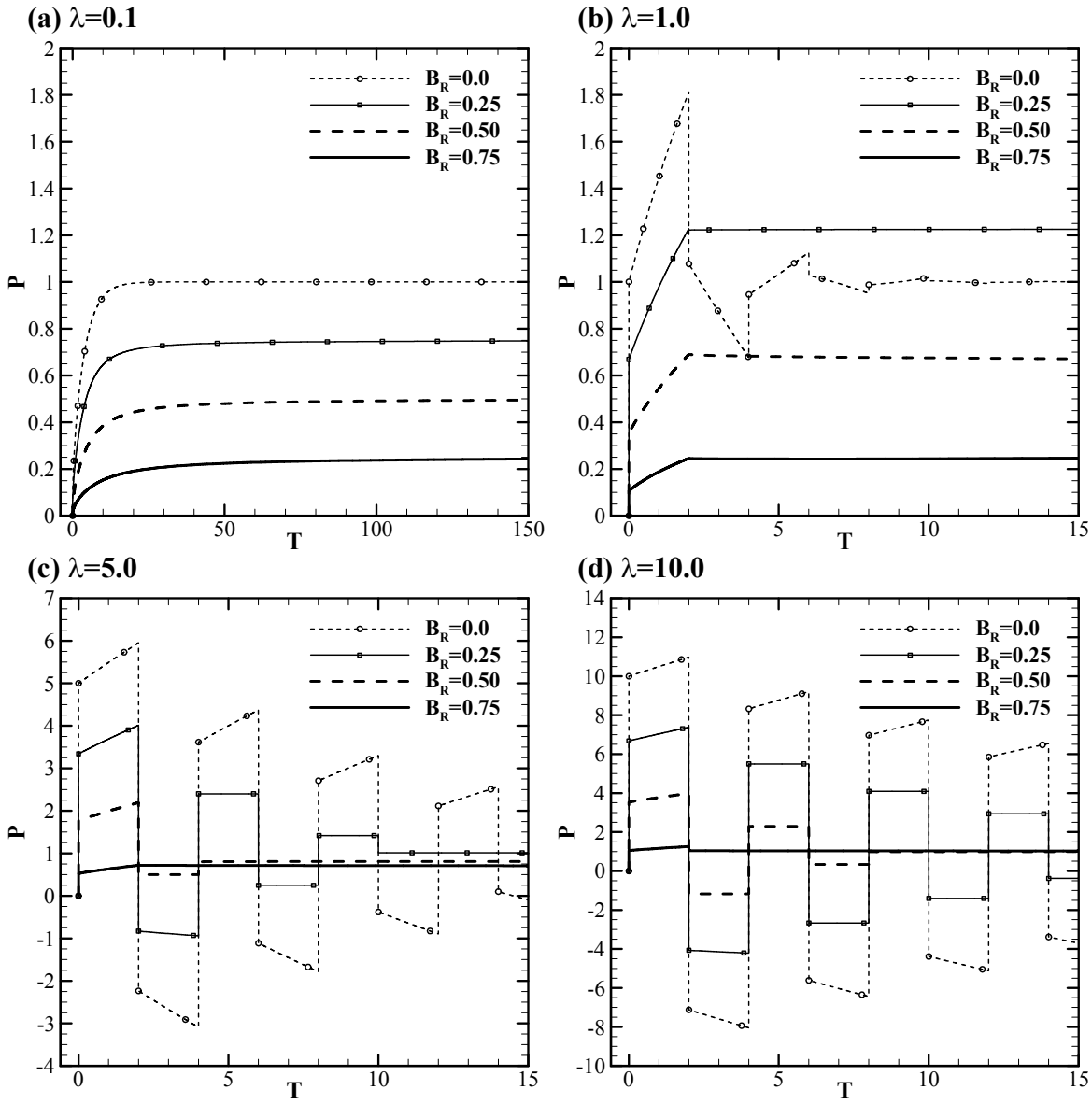

Figure 3.9 – Effect of the Bingham number on the time evolution of pressure at the valve position for (a) λ=0.1, (b) λ=1.0, (c) λ=5.0 and (d) λ=10.0.

Figure 3.9a shows that the pressure does not oscillate and increases gradually toward the steady-state for λ=0.1. For this highly dissipative case, the final pressure approximates to (1-B_R). As the Bingham number augments, the initial pressure decreases because of the reduction of the initial conductance. The problem is still quite dissipating for λ=1.0, as the Newtonian fluid motion is the only oscillating case shown in Figure 3.9b. Figure 3.9d, on the other hand, illustrates that rising λ to10.0 makes the problem quite oscillating. As λ increases reducing viscous dissipation, the maximum pressure that takes place at T=2.0 can be approximated by:

$$P_{\max} = \lambda\gamma_0 + (1 - B_R) \tag{3.17}$$

For λ=5, the maximum pressure evaluated by Eq. (3.17) results in 6.0, 4.1, 2.3 and 0.78, for B_R equal to 0.0, 0.25, 0.5 and 0.75, respectively. It is shown in Figure 3.9c that increasing the Bingham number, the pressure at T=2.0 deviates from the estimated maximum. Whereas the maximum pressure is approximately 6.0 for Newtonian fluid, it is reduced to 92 % of that estimated by Eq. (3.17) for B_R=0.75. For a less dissipative case (λ=10), on the other hand, the maximum pressure values evaluated by Eq. (3.17) (11.0, 7.4, 4.0 and 1.3, for B_R equal to 0.0, 0.25, 0.5 and 0.75, respectively) are very close to the numerical counterparts shown in Figure 3.9d at T=2.0.

Not only the maximum pressure but also the final pressure distribution along the pipe is important for designing purposes. Figure 3.10 and Figure 3.11 depict the effects of λ and B_R in the pressure distribution after stabilization. As already mentioned, the pressure observed for the Bingham fluid is nonuniformly distributed along the pipe after stabilization. Figure 3.10a shows a negative pressure gradient in the pipe for λ=0.1 and adverse pressure gradients for λ=1.0 and λ=10.0. For the higher dissipating case (λ=0.1), the pressure wave produced at the valve position is quickly dissipated without reflection, whereas for λ=1.0, the pressure wave is reflected at the inlet and then stops propagating when the adverse pressure gradient is not high enough to exceed the fluid yield stress. As the λ=10.0 case is the less dissipating one, the pressure wave is reflected several times (see Figure 3.9d) at the pipe ends before pressure stops propagating. On the other hand, the higher the Bingham number the larger the apparent fluid viscosity and consequently, the higher the pressure wave dissipation. Figure 3.10b shows that the final pressure distribution for B_R=0.75 and λ=1.0 is similar to that for λ=0.1 and that the difference between the inlet and outlet pressure is approximately (1-B_R). In contrast, two

pressure gradients along the pipe are seen for λ=10.0. The pressure increases from the inlet to Z≈0.83, reaching a maximum of 1.067, and then decreases.

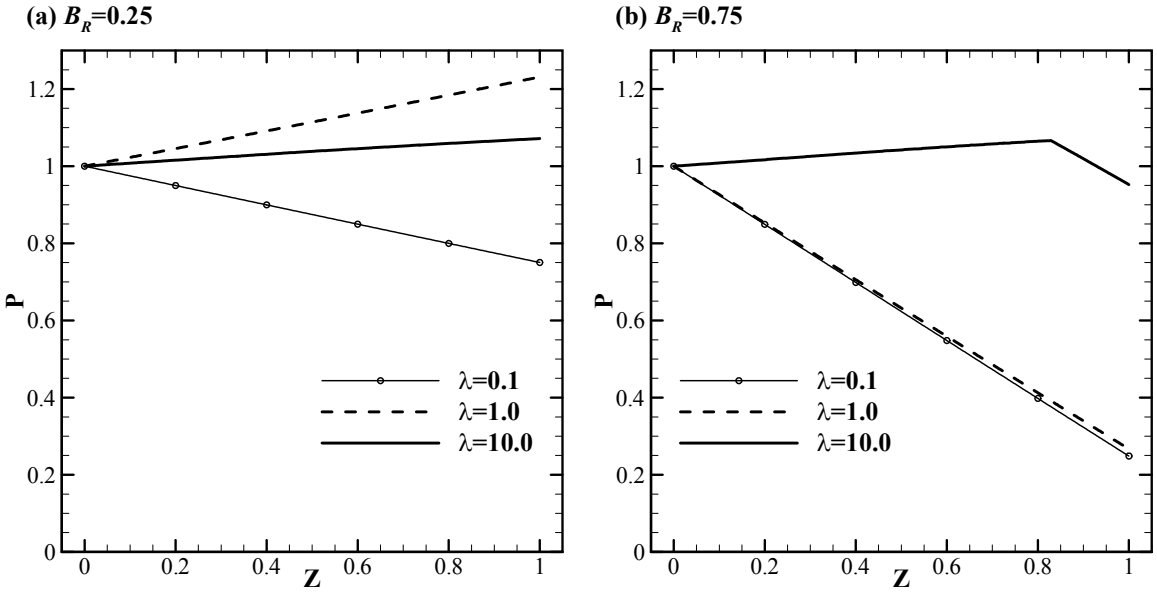

Figure 3.10 – Effect of λ on the final pressure distribution for (a) B_R=0.25 and (b) B_R=0.75.

Figure 3.11 summarizes the effect of the Bingham number on the final pressure distribution for λ=1.0. The larger the Bingham number the smaller is the final pressure at the valve. For B_R=0.5, however, two pressure gradients are again observed with a maximum pressure at Z≈0.08.

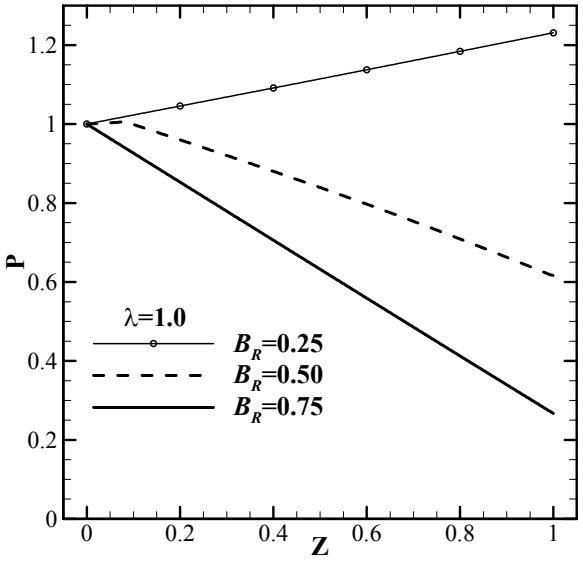

Figure 3.11 – Final pressure distribution as a function of the Bingham number for λ=1.0.

3.4 Conclusions of Paper 1

This paper presents a mathematical model to predict the pressure surge resulting from a step change of viscoplastic fluid flow in pipelines, herein called viscoplastic fluid hammer. The transient model is based on the one-dimensional conservation equations of mass and momentum and also on the Bingham fluid model to represent the viscoplastic fluid behavior. The set of equations are iteratively solved by the Method of Characteristic.

In contrast to water hammer in which the pressure oscillates several times before reaching a uniform value along the pipeline, the pressure for viscoplastic fluids reaches a stable nonuniform axial distribution after oscillations. As soon as the axial pressure gradient is not enough to surpass the fluid yield stress, the pressure reflection stops. The final pressure gradient along the pipe depends on the flow dissipation. Whereas the dimensionless pressure gradient is always negative and proportional to $-B_R$ (Bingham number) for the very high dissipative cases, two pressure gradients are noted throughout the pipe – one positive and one negative – for the less dissipative cases. In the latter, the maximum pressure at the valve position is approximately $\lambda\gamma_0+(1-B_R)$. γ_0 is the Bingham fluid conductance that varies from zero ($B_R \rightarrow \infty$) to one ($B_R = 0$), and λ is the ratio of Joukowsky force and the viscous force. It was noted that the initial dimensionless pressure rise that follows the valve closured is equal to $\lambda\gamma_0$.

Finally, it can be concluded that pipeline designers should not only consider the Reynolds number, the Mach number and the pipe aspect ratio, but also the Bingham number in order to predict pressure peaks and final pressure distributions caused by the viscoplastic fluid hammer.

4 MODELING AND VALIDATION OF PRESSURE PROPAGATION IN DRILLING FLUIDS PUMPED INTO A CLOSED WELL

Gabriel M. Oliveira, Admilson T. Franco, Cezar O. R. Negrão,
André Leibsohn Martins, Rodrigo A. Silva
Journal of Petroleum Science and Engineering 103 (2013) 61–71

This study presents a mathematical model to simulate the pressure propagation that takes place when a drilling fluid is pressurized within a closed pipe-annular geometry. The model assumes that fluid motion is one-dimensional and weakly compressible and the system is considered isothermal. The model comprises the continuity and momentum balance equations, which are iteratively solved by the method of characteristics. The proposed model can be applied to both Newtonian and Bingham fluids. The viscous effect is considered in the model using the friction factor approach. Pressure values obtained from the model are compared to experimental data from Oliveira et al.(2012a) for a Newtonian (water) and two drilling fluids. Not only the magnitudes but also the oscillation frequencies of the measured and computed values show a qualitatively fair agreement for both kinds of fluid. Both measured and computed values show that pressure is not fully transmitted in drilling fluids. Three dimensionless numbers are identified as the model governing parameters. A model sensitivity analysis shows that pressure propagation can be enhanced by combining the governing parameters.

Keywords: Pressure Propagation. Drilling Fluids. Bingham Fluid. Compressible Flow. Transient Simulation.

4.1 Introduction

Due to large well depths, pressure propagation in drilling fluids plays a significant role in drilling operations. For instance, pressure applied at the surface should be transmitted to the bottom of the hole in order to operate hydraulically actuated completion valves. In addition, fluctuations of bottomhole pressure, reflected at the surface, may indicate the undesired influx of formation fluid. Nevertheless, engineers complain that drilling fluids cause a delay in pressure propagated from the bottom to the surface and in some cases the

magnitude of the pressure wave is reduced, undermining the drilling operations. In the first case, an expensive fluid substitution process may be required to guarantee pressure propagation and in the latter, a delay in influx detection may cause safety problems.

In spite of the little attention paid by the literature to the above problem, the pressure propagation that takes place in flow start-ups of viscoplastic materials, such as drilling fluids, represents a situation similar to the one that has been investigated by many authors (Cawkwell and Charles, 1987; Sestak et al., 1987; Chang et al., 1999; Davidson et al., 2004; Vinay et al., 2006; Vinay et al., 2007; Wachs et al., 2009; Oliveira et al., 2010; Negrão et al., 2011; El-Gendy et al., 2012). Most of the works dealt with the development of mathematical models that simulate the restart of either drilling fluids or waxy crude oils. El-Gendy et al. (2012) carried out the only experimental work on the flow start-up of a gelled material, using the PIV technique. Unlike flow start-ups that occur in an open-ended pipe, the pressure propagation to operate a hydraulic actuated valve takes place in a closed ended pipe.

Water hammer, which commonly happens when a valve is suddenly closed at the end of a pipeline system, is another important pressure propagation phenomenon. Despite the fact that this problem has been studied for decades, the reviews of Streeter and Wylie (1974), Ghidaoui et al. (2005) and Bergant et al. (2006) never reported an investigation regarding water hammer in viscoplastic fluids. The most recent works about water hammer (Brunone et al., 1995; Bergant et al., 2006; Wahba, 2008; Duan et al., 2012) have been concerned with the fast damping of pressure peaks that is observed in experiments when compared to 1D model results. Another transient fluid flow involving viscoplastic fluid is the oil flow that takes place in horizontal well-reservoir domains. Owayed and Tiab (2008) modeled this problem as a compressible flow in porous media of a Bingham fluid to evaluate pressure responses.

Oliveira et al. (2012b) have recently studied the pressure wave propagation in a Bingham fluid compressed within a closed ended pipe, numerically. They demonstrated that a pressure applied at one end of the pipe is attenuated at the other end because of the fluid yield stress. If the pressure gradient along the pipe is not high enough to exceed the yield stress the fluid stops moving and the pressure does not propagate anymore. Oliveira et al. (2012b) also concluded that the final pressure profile along the pipe depends on the Bingham number, the relationship between the pipe aspect ratio, and the Reynolds and Mach numbers. In contrast with real applications, where constant flow rates are imposed at the pipe inlets, Oliveira et al. (2012b) carried out simulations with constant pressure instead of constant flow rates as occurs in field operations. They have never corroborated their results with measurements.

The current work proposes a mathematical model to simulate the pressure propagation in drilling fluid pumped throughout a closed well. The model is solved numerically using the method of characteristics. A constant flow rate is assumed as the inlet boundary condition and the model results are compared with pressure values measured in an experimental plant. A sensitivity analysis of the model parameters are thus carried out in order to check how their values affect pressure propagation.

4.2 Mathematical Model

4.2.1 Problem Description

Figure 4.1a depicts a schematic representation of the drilling operation at the wellbore in which a drilling fluid is pumped into the drillpipe and then returns to the wellhead through the annular space. In the current study, the fluid flows into the drillpipe towards the annulus, which is closed to flow. Thus, the fluid accumulates in the drillpipe and annulus. Despite changes, the cross-sectional areas of the drillpipe and annular space are taken to be constant, as shown in Figure 4.1b. According to Figure 4.1c, the drillpipe internal diameter is identified as d and the internal and external diameters of the annular space, as d_1 and d_2, respectively. Notice that the drill bit, which is located at the end of the drillpipe, is not included in the model. Thus, it is assumed that the fluid goes directly from the drillpipe to the annular space. The drillpipe and the case are regarded as non-deformable so that deformation of this structure is not considered in this model. The problem can be simplified by assuming a compressible, isothermal and one-dimensional flow. The shear stress in the walls of the drillpipe and annular space is calculated using the friction factor approach and the drilling fluid is modeled as a Bingham fluid.

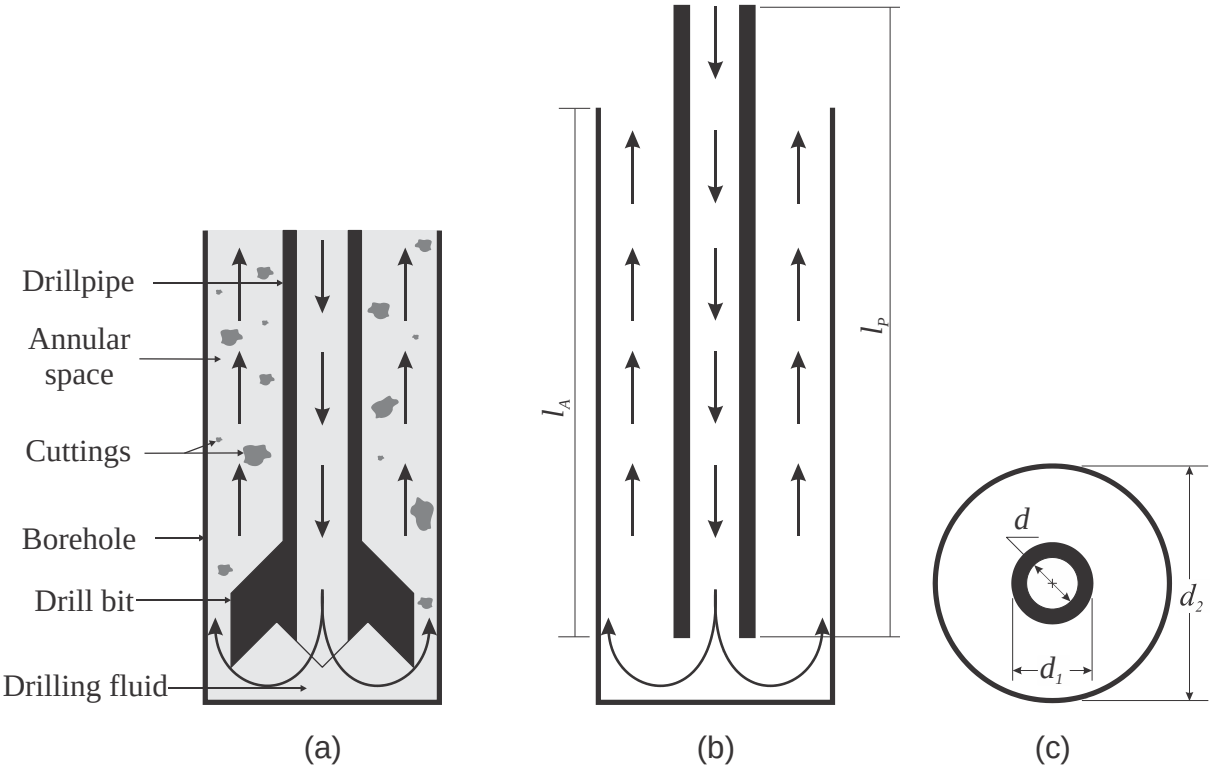

Figure 4.1 – (a) Illustration of the drilling fluid circulation in the wellbore. (b) Longitudinal view and (c) cross section of drillpipe and annular space.

4.2.2 Governing Equations

By applying the above hypotheses, the mass and momentum balance equations can be written for either the drillpipe or annular space as:

$$\frac{\partial \rho}{\partial t} + \rho \frac{\partial v}{\partial z} + v \frac{\partial \rho}{\partial z} = 0 \tag{4.1}$$

$$\rho \frac{\partial v}{\partial t} + \rho v \frac{\partial v}{\partial z} = -\frac{\partial p}{\partial z} - \frac{4}{d_h} \tau_w + \rho g \tag{4.2}$$

where v is the average velocity across the geometry cross section, ρ is the fluid density, p, the pressure, g is the gravity acceleration, τ_w, the average value of the shear stress on the pipe or annular space wall, d_h is the hydraulic diameter of the drillpipe (d) or annular space (d_1-d_2), t, time and z, the axial coordinate. A constant isothermal compressibility is assumed for the fluid, which is defined according to Anderson (1990) as:

$$\alpha = \frac{1}{\rho} \frac{\partial \rho}{\partial p}\bigg|_{\theta} = \frac{1}{\rho c^2} \tag{4.3}$$

where c is the wave speed and θ is the fluid temperature.

Similar to fully developed flows, a linear variation of shear stress is admitted across the pipe sectional area (Oliveira et al., 2012b) and therefore, τ_w can be computed by using the friction factor approach:

$$\tau_w = \frac{f \rho v^2}{2} \tag{4.4}$$

where f is the Fanning friction factor. As discussed by Oliveira et al. (2010), the non-linear terms of the momentum and mass balance equations can be disregarded for weakly compressible flows, such as those that take place in drilling fluids. As the drillpipe and annular space average velocities are different, v is replaced by the ratio of volumetric flow rate, q, and cross sectional area, A, in Eq. (4.1) and (4.2). Finally, Eq. (4.3) is substituted into Eq. (4.1) and τ_w is replaced by Eq. (4.4) in Eq. (4.2), resulting in the following:

$$\frac{\partial p}{\partial t} + \frac{\rho c^2}{A}\frac{\partial q}{\partial z} = 0 \tag{4.5}$$

$$\frac{1}{A}\frac{\partial q}{\partial t} + \frac{1}{\rho}\frac{\partial p}{\partial z} + \frac{2 f q|q|}{A^2 d_h} - g = 0 \tag{4.6}$$

The friction factor depends not only on the fluid's properties but also on the geometry of the domain. For laminar flows of Bingham fluids, the Fanning friction factor for both drillpipe and annular space can be written as (Melrose et al., 1958):

$$f_{lam} = \frac{16\zeta}{\gamma \mathrm{Re}_{z,t}} \tag{4.7}$$

where ζ is geometric parameter which is 1.0 for pipe flows and is a function of d_1/d_2 for annular flows (see White, 2003), γ is the fluid conductance of the Bingham fluid and $Re_{z,t}$ is the Reynolds number that is a function of time and axial position ($Re_{z,t}=\rho v d_h/\eta$) and η is the fluid plastic viscosity. Eqs. (4.8) and (4.9) are the correlations used to calculate the fluid conductance for the pipe and annular space, respectively, which was obtained from Melrose et al.(1958):

$$\gamma_P = 1 - \frac{\gamma_P \mathrm{B}_{z,t}}{6} + \frac{1}{3}\left(\frac{\gamma_P \mathrm{B}_{z,t}}{8}\right)^4 \tag{4.8}$$

$$\gamma_A = 1 - \frac{\gamma_A \mathrm{B}_{z,t}}{8} + \frac{1}{2}\left(\frac{\gamma_A \mathrm{B}_{z,t}}{12}\right)^3 \tag{4.9}$$

where $B_{z,t}$ is the Bingham number ($B_{z,t}=\tau_y d_h/v\eta$) which depends on time and space. τ_y is the fluid yield stress and the subscripts *P* and *A* are the drillpipe and annular space, respectively. Eq. (4.7) can be reduced to the Newtonian friction factor if the conductance is made equal to one.

According to Melrose et al. (1958), the Bingham fluid flow is considered laminar when the product of the Reynolds number and the conductance, γ, is smaller than 2100. Otherwise the flow regime is assumed turbulent. For drilling fluid cases shown in Section 4.5, only laminar flows are investigated. On the other hand, both laminar and turbulent cases are considered for water flows. The turbulent Newtonian flow is admitted to take place when the Reynolds number is larger than 2100 and the turbulent friction factor adopted is the one proposed by Blasius (White, 2003):

$$f_{turb} = 0.079\,\mathrm{Re}_{z,t}^{-0.25}, \quad \mathrm{Re}_{z,t} > 2100 \tag{4.10}$$

4.3 Solution Algorithm

The governing equations are solved by the method of characteristics (MOC) that is typically used for solving hyperbolic partial differential equations (see Wylie et al., 1993). In comparison to the ordinary finite volume method, which is usually employed to solve this kind of equation, the number of grid points that provides accurate results can be considerably smaller. The method consists of simplifying partial differential equations to a family of ordinary differential equations, along which the solution can be integrated from an initial condition. In the current case, Eqs. (4.5) and (4.6) are reduced to two total differential equations, which are valid over the characteristic lines $dz/dt = \pm c$:

$$\left.\begin{aligned} &\frac{dp}{dt}+\frac{\rho c}{A}\frac{dq}{dt}+\frac{2f\rho cq|q|}{A^2 d_h}-\rho cg=0 && (4.11)\\ &\frac{dz}{dt}=+c && (4.12)\end{aligned}\right\} \quad C^+$$

$$\left.\begin{aligned} &-\frac{dp}{dt}+\frac{\rho c}{A}\frac{dq}{dt}+\frac{2f\rho cq|q|}{A^2 d_h}-\rho cg=0 && (4.13)\\ &\frac{dz}{dt}=-c && (4.14)\end{aligned}\right\} \quad C^-$$

Inasmuch as *c* is constant, plots of Eqs. (4.12) and (4.14) provide straight lines on the *z-t* plane, as shown in Figure 4.2. It is worth noting that Eqs. (4.11) and (4.13) are valid only over the appropriate characteristic line.

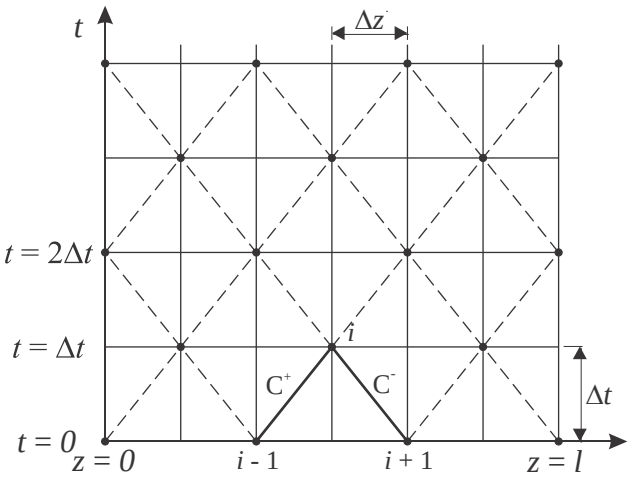

Figure 4.2 – *z-t* grid for solving the governing equation.

Both drillpipe and annular space are divided into *N* equal reaches, *Δz*, as shown in Figure 4.2. In order to satisfy both Eqs. (4.12) and (4.14), the time-step is computed according to $\Delta t=\Delta z/c$. If *p* and *q* are both known at position *i-1*, Eq. (4.11) can be integrated over the characteristic line C^+ and therefore, be written in terms of unknown variables *p* and *q* at point *i*. Integration of Eq. (4.13) along the line C^-, with conditions known at *i+1*, leads to a second equation in terms of the same two unknown variables at *i*. By solving the two resulting algebraic equations, *p* and *q* can be obtained at point *i* as a function of known values at points *i-1* and *i+1*:

$$p_i = \frac{F_+ G_- + F_- G_+}{G_+ + G_-} \tag{4.15}$$

$$q_i = \frac{F_+ - F_-}{G_+ + G_-} \tag{4.16}$$

where,

$$F_+ = p_{i-1} + \left(\frac{\rho c}{A_{i-1}} - \frac{R_+}{\gamma_{i-1}} \right) q_{i-1} + \rho g \Delta z \tag{4.17}$$

$$F_- = p_{i+1} - \left(\frac{\rho c}{A_{i+1}} - \frac{R_-}{\gamma_{i+1}} \right) q_{i+1} - \rho g \Delta z \tag{4.18}$$

$$G_{+} = \frac{\rho c}{A_{i-1}} + \frac{R_{+}}{\gamma_i} \tag{4.19}$$

$$G_{-} = \frac{\rho c}{A_{i+1}} + \frac{R_{-}}{\gamma_i} \tag{4.20}$$

$$R_{+} = \frac{16\zeta_{i-1}\eta\Delta z}{\left(Ad_h^2\right)_{i-1}} \tag{4.21}$$

$$R_{-} = \frac{16\zeta_{i+1}\eta\Delta z}{\left(Ad_h^2\right)_{i+1}} \tag{4.22}$$

Note that the friction factor equation (Eq. (4.7)) is already substituted into Eqs. (4.15) and (4.16) and that p_i and q_i are evaluated as a function of known values at the previous time-step. Solution of the problem begins with the fluid standing still at time zero, so that p and q are known at each computing point i for $t=0$. The solution consists in finding p and q for each grid point along $t=\Delta t$, then proceeding to $t=2\Delta t$, etc., until the desired time duration has been covered.

As these equations were developed for laminar flows, the following correction is necessary for turbulent Newtonian flows (Bingham fluid flow is always laminar for the cases considered here):

$$R' = Rf_{turb} / f_{lam} = Rf_{turb}\,\mathrm{Re}_{z,t}/16\zeta \tag{4.23}$$

where R is either R_+ or R_-. In other words, R_+ or R_- is replaced by R' in the case of turbulent flows. In addition, G_+ and G_- need to be computed iteratively as the conductance, γ and R' depend on the value of the volumetric flow rate. The iterative process takes place until the relative difference between two consecutive values of q is smaller than 0.1%.

In order to have only one grid size for the whole domain, the drillpipe and annular space are divided into N_P and N_A volumes, respectively, and the grid length is computed according to $\Delta z=(l_P+l_A)/(N_A+N_P)$. Figure 4.3 illustrates the grid distribution for both drillpipe and annular space. It is noteworthy that the axial coordinate is defined from top to bottom for the drillpipe and from bottom to top for the annular space. A grid of 328 points was found to provide accurate results; it was then used for all simulations.

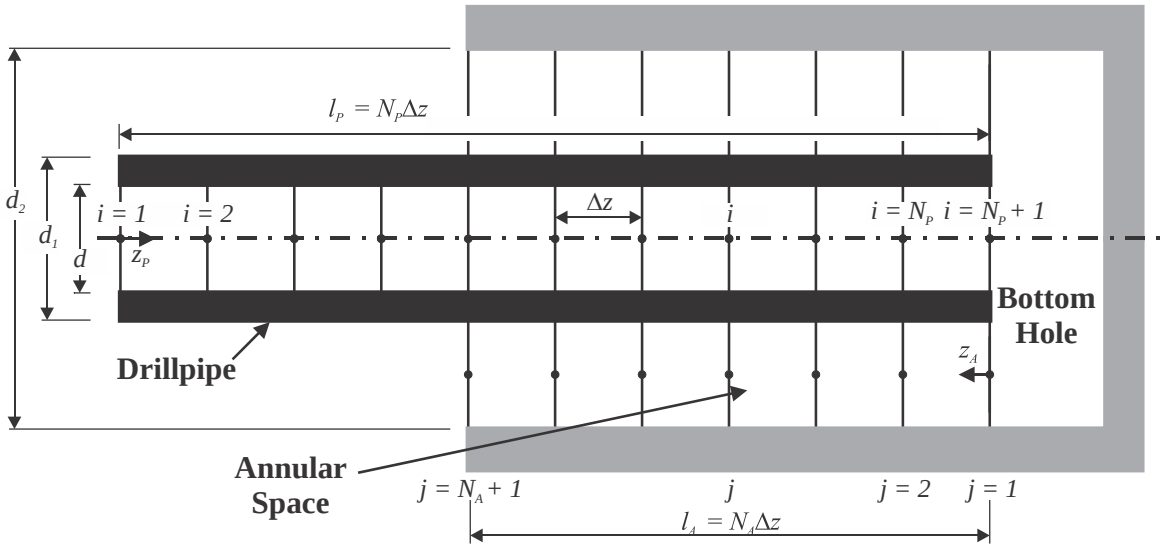

Figure 4.3 – Grid distribution in the drillpipe and annular space.

4.4 Description of the Experimental Rig

The model is validated with experimental data from Oliveira et al. (2012a). These data were obtained in an experimental drilling rig, which consists of a drillpipe with internal and external diameters of 76 mm and 88.9 mm (3.5”), respectively, and a well case with a 157 mm internal diameter, as shown Figure 4.4. Two fiber Bragg grating sensors were placed within the drillpipe and six in the annular space to measure pressure and temperature. In order to simplify analysis the results of only three sensors (S1, S2 and S3), as indicated in Figure 4.4, are used in the comparisons. The first was located within the drillpipe and the last two in the annular space at 29 m (S1), 1192 m (S2) and 14.64 m (S3) below the wellhead, respectively.

The end of the drillpipe was assembled without the drill bit and placed very close to the well bottom. In such cases, the lengths of both the drillpipe and annular space were approximately 1192 m. During the tests, the fluid is pressurized through the drillpipe and the annular space is kept closed. The vertical arrows shown in Figure 4.4 indicate the direction of the fluid motion. The circulation system was connected to the wellhead by a high pressure pipe to control the pump flow rate and maximum pressure at the pump outlet. The wellhead maximum pressure was established according to the fluid weight, as the bottom hole pressure cannot exceed 27.6 MPa (4000 psi). To measure the data, an acquisition system which is compatible with fiber Bragg grating technology was used, with an acquisition rate of 1.0 Hz.

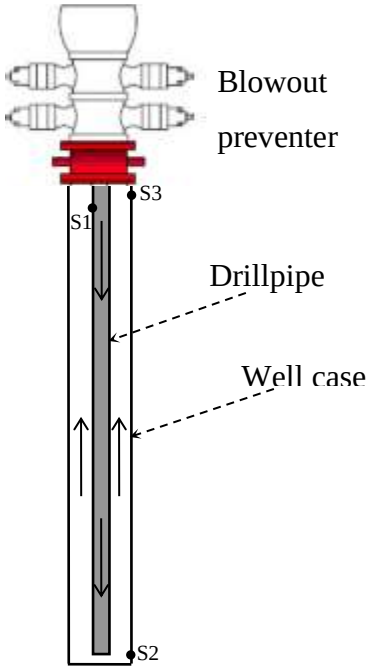

Figure 4.4 – Schematic representation of the experimental rig.

The tests were performed as follows: i) the well was firstly filled with water or drilling fluid; ii) the flow line was then closed to avoid a return of fluid; iii) the fluid was then pumped into the well at a constant flow rate and; iv) when the bottom hole pressure reached 27.6 MPa (4000 psi) (maximum working pressure), the pump was turned off; v) after pressure stabilization, the well was depressurized by opening the choke.

The tests were run for several fluids but only three were used in the comparison: water and two drilling fluids (fluid A and B). Fluid A is lighter and less viscous than fluid B. The rheology properties of fluids A and B were obtained by a Fann 35A viscometer and fit the Bingham model. The wave speeds of the fluids were estimated by rating the distance between two pressure sensors and the time for pressure to be transmitted from the first to the second sensor. The water properties were obtained from the literature (White, 2003). The plastic viscosity (viscosity for water), the yield stress, the wave speed and the density of the fluids are shown in Table 4.1.

Table 4.1 – Fluid properties.

Property	**Water**	**Fluid A**	**Fluid B**
η [Pa.s]	0.001	0.0235	0.0677
τ_y [Pa]	0	2.166	10.88
c [m/s]	1350	1000	1011
ρ [kg/m^3]	1000	1150	1929

4.4.1 Model Setup

As an initial condition, the fluid is considered to stand still within the domain (drillpipe and annular space) and consequently, the volumetric flow rate is zero throughout the domain, $q(z,t=0)=0$. The initial pressure condition is considered to be the hydrostatic one. Since the well is maintained closed during the test, the flow rate is set to zero as the outlet boundary condition, $q(z=l_P+l_A,t)=0$. Inasmuch as the fluid is injected into a closed domain, the pressure within the well increases continuously until a pre-defined pressure value, p_{set}, is reached and the pump is turned off. To achieve this situation, the following boundary condition is established at the inlet:

$$q(z=0,t)=\begin{cases} q_{in} & \text{if} \quad t \le t_{set} \\ 0 & \text{if} \quad t > t_{set} \end{cases} \tag{4.24}$$

where t_{set} is the time for the inlet pressure to reach p_{set}. As the pump flow rate was not precisely measured and the experimental tests were mainly conducted to evaluate pressure propagation after the pump shutdown, the boundary value of the pump flow rate was set to match the calculated and measured pressures at the first sensor (S1).

4.5 Model Validation

Three sets of experimental data were chosen for comparison with the current model results. The first test was carried out with water, whereas the other two were performed with two different drilling fluids (fluids A and B).

4.5.1 Water

For the water case, the pump was turned on with a constant flow rate of 1.122 l/s (0.42 bpm) and was switched off when the pressure at the wellhead was 14.69 MPa (2130 psi). Figure 4.5 and Figure 4.6 show comparisons of the computed and measured values of the pressure in the first (located at the drillpipe inlet – S1) and in the third sensor (placed close to the wellhead – S3), respectively. It is worth of noting that the hydrostatic pressure was subtracted from all values shown in Figs. 4.5–4.8.

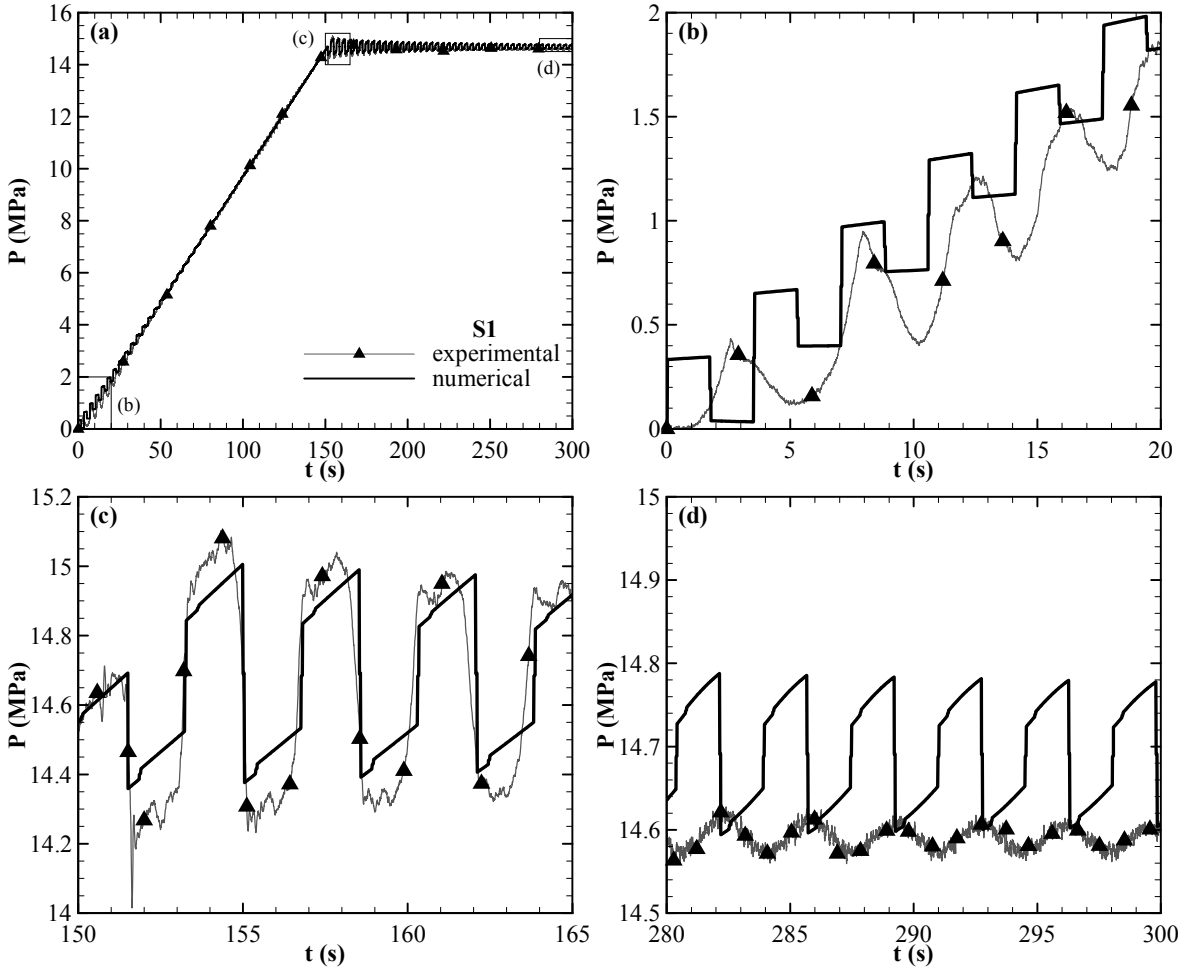

Figure 4.5 – Time evolution of measured and computed values of pressure at position S1 for a water flow rate of 1.122 l/s. (a) From start-up to 300s; (b) From start-up to 20s; (c) From 150s (after the pump shutdown) to 165s; (d) From 280s to 300s.

The comparison during the first 150s (see Figure 4.5b) cannot be taken into account, as the flow rate was imposed to make the measured and computed pressures as close as possible. After the pump had been turned off and the flow rate made equal to zero, a fair match between the measured and computed values can be seen in Figure 4.5c, as they oscillate with a similar frequency and amplitude. It is worth noting that the oscillation is due to pressure reflections at the domain boundaries and that the frequency coincides with the wave speed divided by the length of the domain. However, the experimental and numerical values start to diverge soon after the pump shutdown, as the oscillation of the measured pressure dissipates much faster than the computed counterpart. Despite the large discrepancy, the pressure agreement in Figure 4.6 is still reasonable during the time the pressure is rising and soon after the pump is shutdown. It is worth noting that the measured values again dissipate faster than the calculated ones. According to the literature, the fast dumping of

pressure peaks are attributed to 2D effects that are not considered in the current model (Brunone et al., 1995; Bergant et al., 2001).

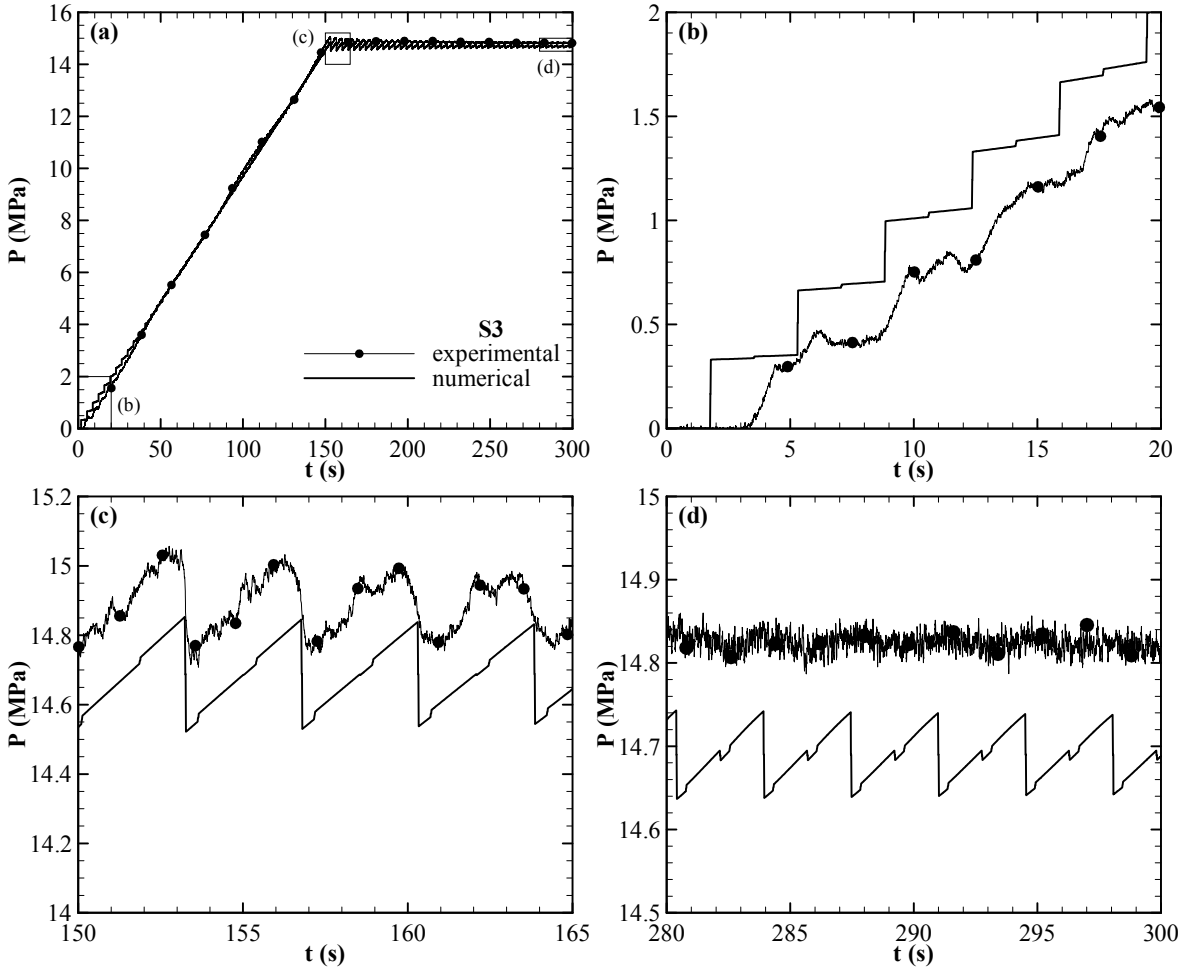

Figure 4.6 – Time evolution of measured and computed values of pressure at position S3 for a water flow rate of 1.122 l/s. (a) From start-up to 300s; (b) From start-up to 20s; (c) From 150s (after the pump shutdown) to 165s; (d) From 280s to 300s.

4.5.2 Drilling Fluids

Similar tests were conducted for two drilling fluids, A and B. For fluid A, the flow rate was set to the constant value of 1.462 l/s (0.55 bpm) until the pressure at the wellhead reached 13.82 MPa (2004 psi) and then the pump was switched off. Figure 4.7 shows the time evolution of measured and computed pressure values for sensors S1, S2 and S3. Similar to the previous case, measured and computed values show good qualitative agreement. However, both measured and computed values do not oscillate as much as the pressures in the water test and this can be attributed to the fluid yield stress. As soon as the pump is turned off, the

pressure starts to reflect back and forth at the boundaries and the pressure gradient begins to reduce within the domain. When the magnitude of the pressure gradient is not high enough to exceed the yield stress, the pressure no longer reflects and then stabilizes. This issue was further discussed in a previous paper (Oliveira et al., 2012b).

Although the measured and computed curves have similar responses, the computed values stabilize slightly faster. Furthermore, the pressure peak observed in the measured values is not seen in the computed counterpart in sensor S3 (see Figure 4.7d). Unlike the Newtonian fluid, whose pressure is uniform along the whole domain after equilibrium is established (if the hydrostatic pressure is subtracted), the Bingham fluid pressure stabilizes at different values for each domain position. One can see that the stable value at the outlet (sensor S3) is larger than the stable inlet value (sensor S1), for both measured and computed curves (see Oliveira et al. (2012b) for further explanations).

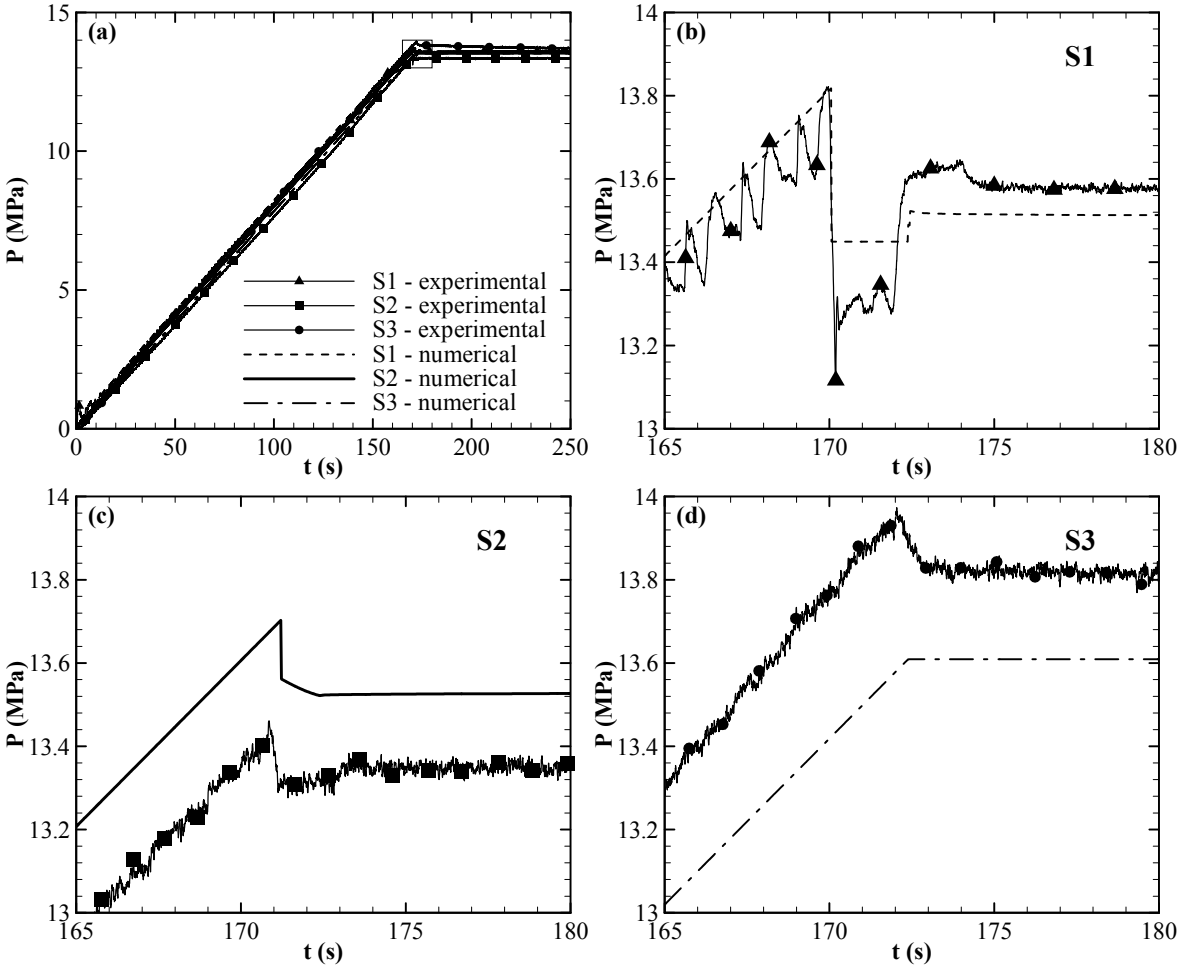

Figure 4.7 – Time evolution of measured and computed values of pressure for fluid A at (a) S1, S2 and S3 positions from the start-up to 250s and at positions (b) S1, (c) S2 and (d) at S3 from 165s to 180s.

In the experiments with fluid B, the flow rate was set to the constant value of 0.952 l/s (0.359 bpm) and the pump was turned off when the wellhead pressure reached 7.6 MPa (1102 psi). Comparisons between the measured and computed values are shown in Figure 4.8. Not only are the measured and computed values again similar, but they also do not oscillate, as noted with the fluid A results. S1 and S2 pressures reduce suddenly after the peak and then stabilize, as shown, respectively, in Figure 4.8b and Figure 4.8c. Despite the deviation of the measured and computed pressures during the pump-up period, their values at S3 position respond similarly, as they both reach a maximum and then become constant. The complete absence of oscillation in this case is due to a higher yield stress of this drilling fluid, which dissipates the pressure wave faster than in the previous case.

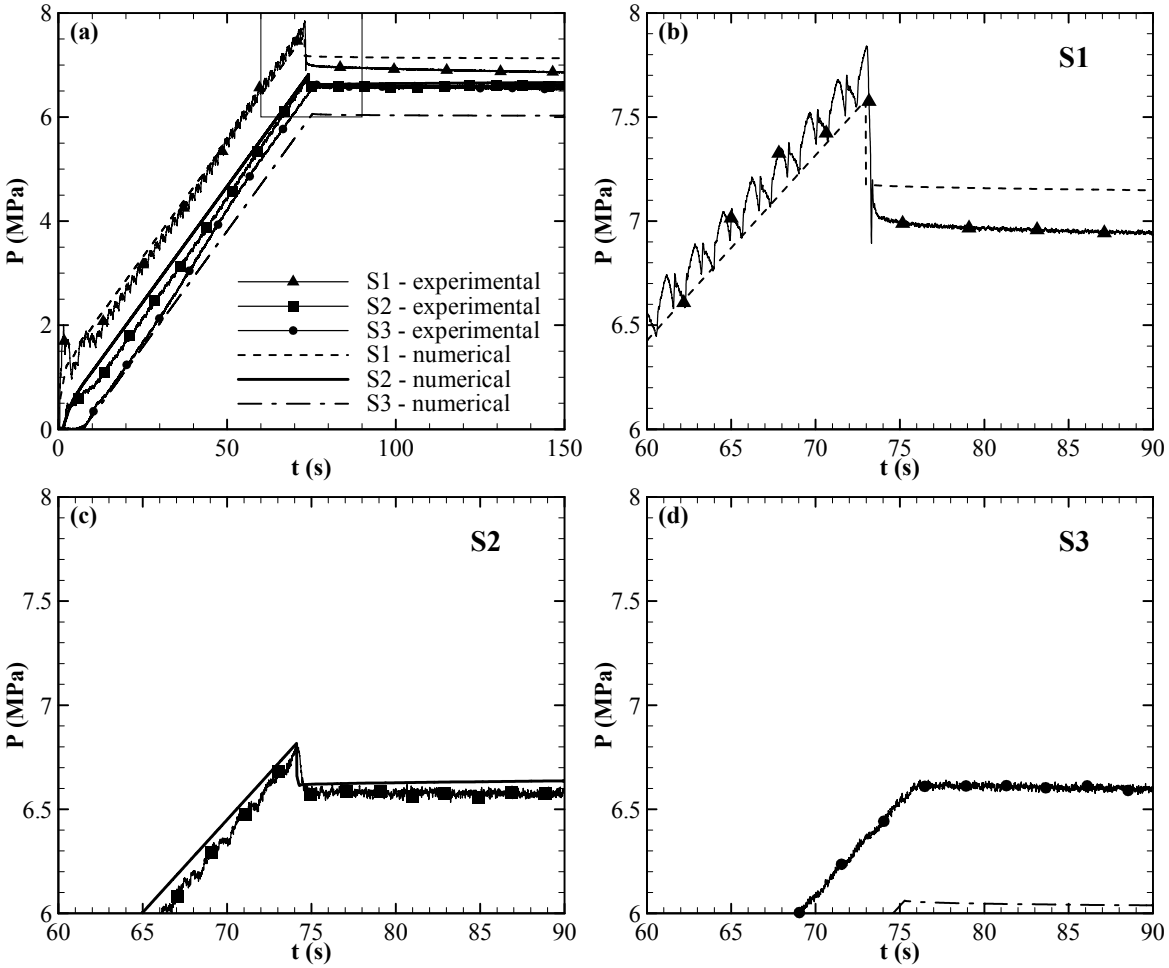

Figure 4.8 – Time evolution of measured and computed values of pressure for fluid B at positions S1, S2 and S3 from the start-up to 150s and at positions (b) S1, (c) S2 and (d) S3 from 60 s to 90s.

4.6 Numerical Results

A sensitivity analysis is now carried out to investigate how some parameters affect the non-propagation of pressure. In order to reduce the number of parameters, the problem was simplified to a laminar flow in a horizontal pipe with constant cross-sectional area. Eqs. (4.5) and (4.6) are thus normalized according to:

$$\frac{\partial P}{\partial T}+\beta\frac{\partial Q}{\partial Z}=0 \tag{4.25}$$

$$\beta\frac{\partial Q}{\partial T}+\frac{\partial P}{\partial Z}+\frac{\beta}{\lambda}\frac{Q}{\gamma}=0 \tag{4.26}$$

where P, Q, Z, and T are the dimensionless pressure, volumetric flow rate, axial position and time, which are defined as $P=p/p_{set}$, $Q=q/q_{in}$, $Z=z/l_P$ and $T=tc/l_P$, respectively. The parameter β and λ are defined, respectively, as:

$$\beta=\frac{\rho c v_{in}}{p_{set}} \tag{4.27}$$

$$\lambda=\frac{1}{32}\left(\frac{\rho c d}{\eta}\right)\frac{d}{l_P}=\frac{\delta}{32}\frac{Re}{M} \tag{4.28}$$

and γ can be rewritten according to the dimensionless variable as:

$$\gamma=1-\frac{8}{6}\gamma\frac{\lambda}{\beta}\frac{B_R}{Q}+\frac{1}{3}\left(\gamma\frac{\lambda}{\beta}\frac{B_R}{Q}\right)^4 \tag{4.29}$$

where $v_{in}=q_{in}/A$. δ is the aspect ratio of the pipe ($=d/l_P$), M ($=v_{in}/c$) is the Mach number, Re is the Reynolds number ($=\rho v_{in} d/\eta$) and B_R ($=4\tau_y l_P/p_{set} d$) is the Bingham number based on p_{set}.

In addition to λ and B_R, defined by Oliveira et al. (2012b) as governing parameters, the current scaling also includes β. This new parameter is necessary because this problem is a constant flow rate case rather than the step-change pressure problem studied by Oliveira et al. (2012b). It is worth mentioning that λ is the product of a Reynolds number based on the pressure wave speed ($=\rho cd/\eta$) and the pipe aspect ratio (d/l_P). Wahba (2008), nonetheless, defined λ as the ratio between the excessive pressure force generated by the transient phenomenon (Joukowsky force - $\rho c v_{in} d^2$) and the viscous force ($\eta l_P d v_{in}/d$) acting to damp the transient pressure. On the other hand, β can be interpreted as the ratio of the Joukowsky force and the pressure force applied at the pump shutdown ($p_{set} d^2$). According to Thorley (2004),

$\rho c v_{in}$ is the pressure increase that a frictionless fluid undergoes when it is suddenly decelerated from v_{in} to zero.

Figure 4.9 shows that the pressure increases almost linearly with a constant pump flow rate. This result can be anticipated by taking a lumped approach for the mass conservation equation:

$$\frac{\partial m}{\partial t} = \rho q_{in} \tag{4.30}$$

Eq. (4.30) states that the rate of change of mass within the pipe, m, is balanced by the pump mass flow rate. By considering the pressure as uniform within the pipe and by using the definition of compressibility, the mass conservation Eq. (4.30) can be alternatively written as,

$$\frac{\partial p}{\partial t} = \frac{\rho q_{in}}{\alpha \forall} \tag{4.31}$$

where $\forall$ is the pipe volume. Eq. (4.31) establishes that the compression rate is a constant value that depends on the pump flow rate, the pipe geometry and on the fluid's properties. Alternatively, in dimensionless form, the compression rate is equal to β:

$$\frac{\partial P}{\partial T} = \beta \tag{4.32}$$

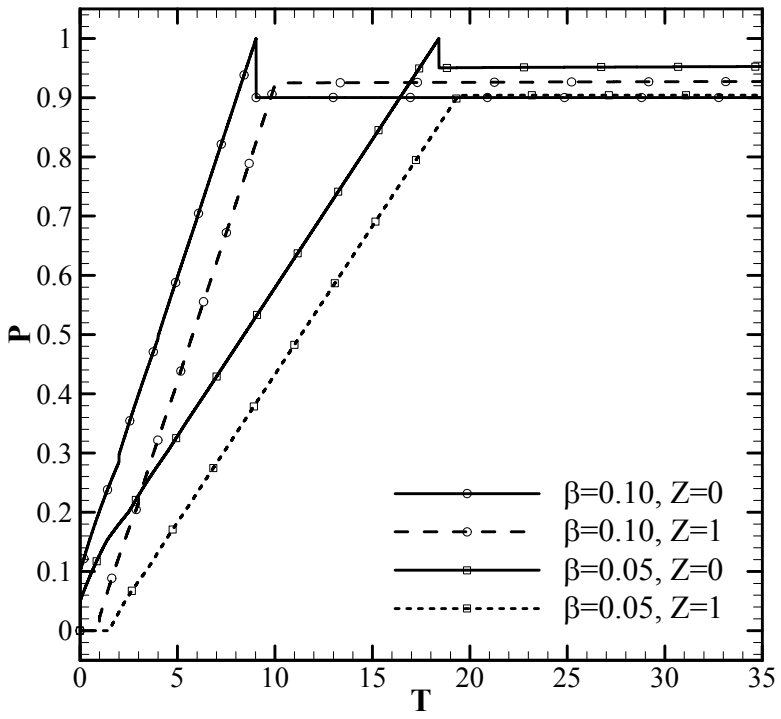

Figure 4.9 – Effect of β on inlet and outlet pressure variations for λ=1 and B_R=0.1.

This is corroborated by the results of Figure 4.9 as the maximum value of inlet pressures ($P=1$) is reached in almost $T=1/\beta$. Figure 4.9 also shows that the larger the β the faster the pressure change, which means that the compression rate increases with the inlet flow rate. As can be seen, the inlet pressure reduces after the pump is turned off and such a reduction increases with β. It is worth noting that the outlet pressure starts rising only after the propagation of the pressure wave from the inlet to the outlet.

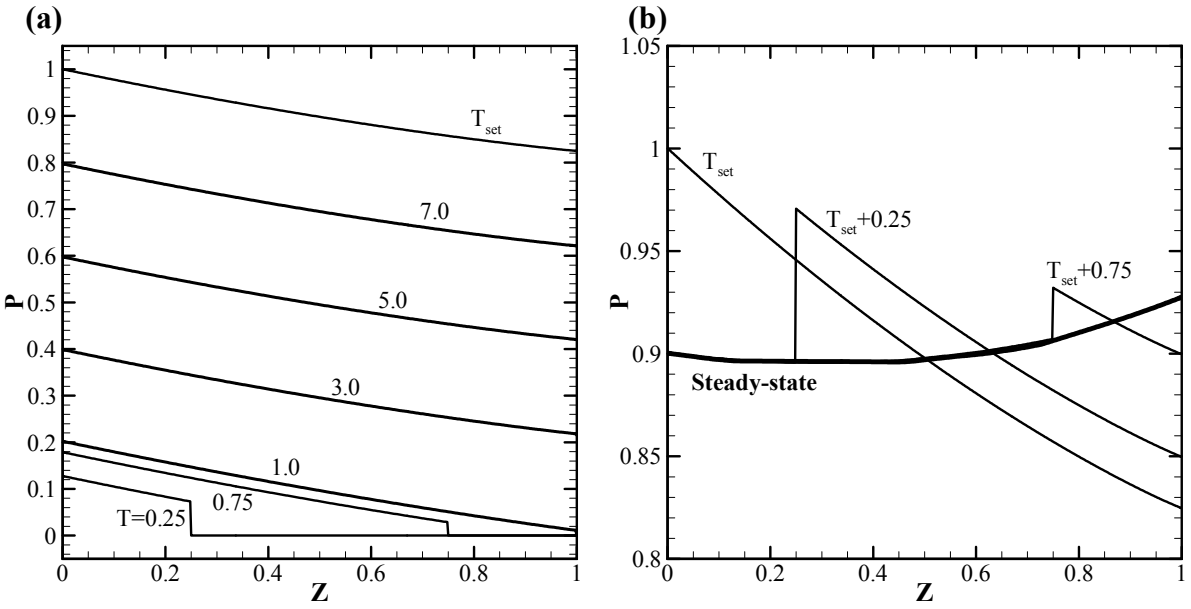

Figure 4.10 – Time evolution of the pressure field along the pipe length for β=0.1, λ=1 and B_R=0.1. (a) After the pump start-up ($T \leq T_{set}$) and (b) after the pump shut-down ($T \geq T_{set}$).

Figure 4.10 shows the pressure distribution throughout the pipe after the pump start-up (Figure 4.10a) and after the shutdown (Figure 4.10b), providing an explanation for the non-uniform pressure profile after stabilization. As noted in Figure 4.10a, the pressure takes approximately $T\approx1.0$ to reach the outlet and increases continuously with an almost constant gradient after that. When the pump is turned off at $T=T_{set}$, the inlet pressure reduces to its steady-state value creating a reverse wave that is transmitted to the outlet (see curve $T=T_{set}+0.25$ in Figure 4.10b). As the reverse wave is propagated to the outlet, the outlet pressure continues to increase because of the inertia. Nevertheless, when this wave reaches the outlet, the existing pressure gradient is not high enough anymore to overcome the fluid yield stress and then the pressure stabilizes. One can see that the final pressure distribution is not uniform along the pipe and that the outlet pressure is even larger than its inlet counterpart, as observed in the experiments described above.

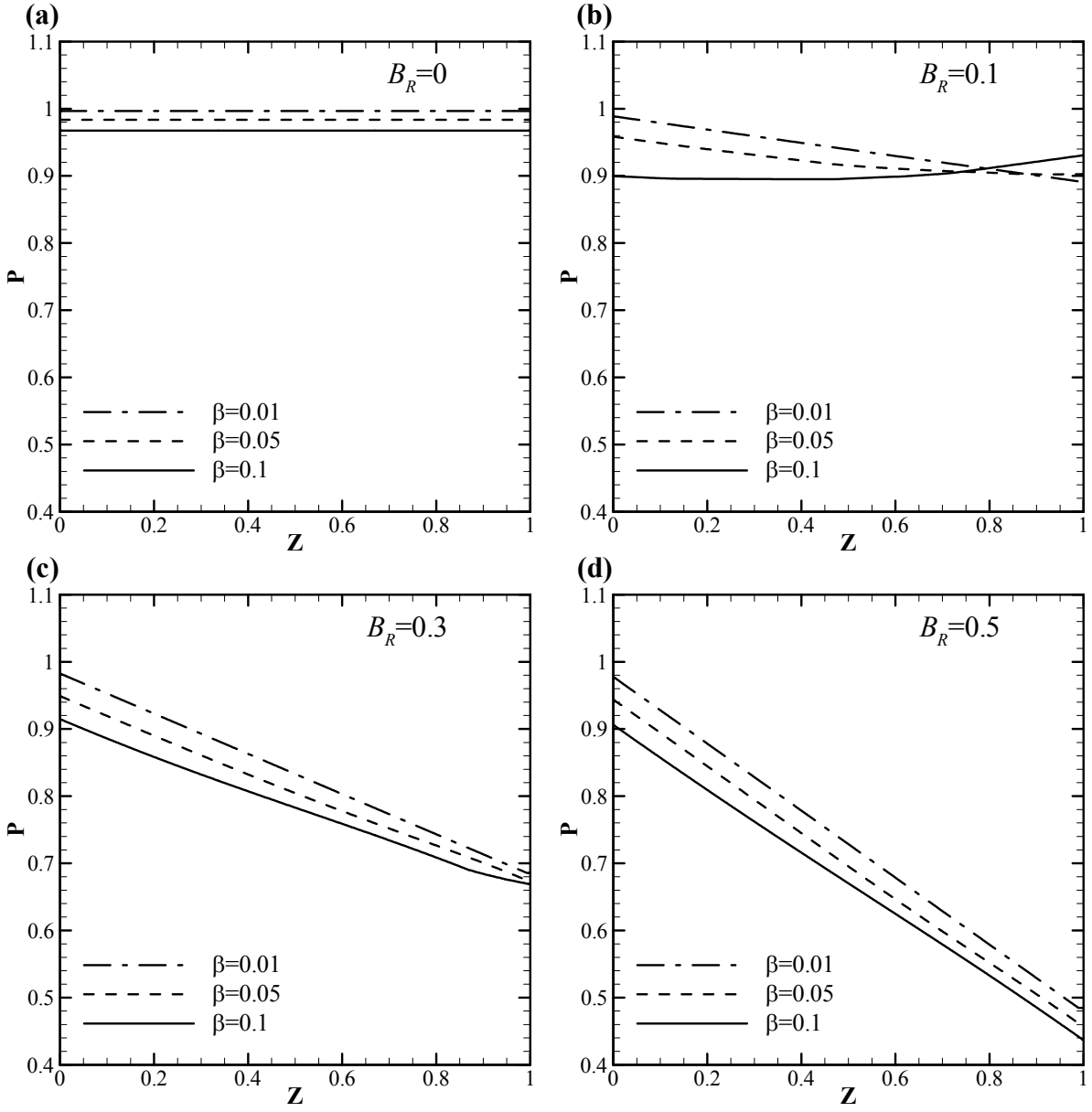

Figure 4.11 – Steady-state pressure distribution as a function of β for different values of Bingham number and λ=1.0. (a) B_R=0, (b) B_R =0.1, (c) B_R =0.3 and (d) B_R =0.5.

The sensitivity of the final pressure distribution along the pipe with respect to B_R, λ and β is now presented in Figure 4.11 and Figure 4.12. The effect of the Bingham number for different values of β is depicted in Figure 4.11. As expected, the Newtonian fluid pressure stabilizes uniformly along the pipe (B_R=0) whereas the final value reduces with β. Bingham fluids, however, present non-uniform final pressure distributions, as shown in Figure 4.11. This inlet-to-outlet pressure difference grows with the Bingham number. On the other hand, the increase of β reduces the final pressure gradient at the expense of a reduction in the inlet pressure. By comparing Figure 4.11b with Figure 4.12, one can see that the final pressure distribution is significantly affected by λ so that the inlet-to-outlet pressure difference can

even become negative. Nevertheless, the pressure gradient is insensitive to λ for small values of β.

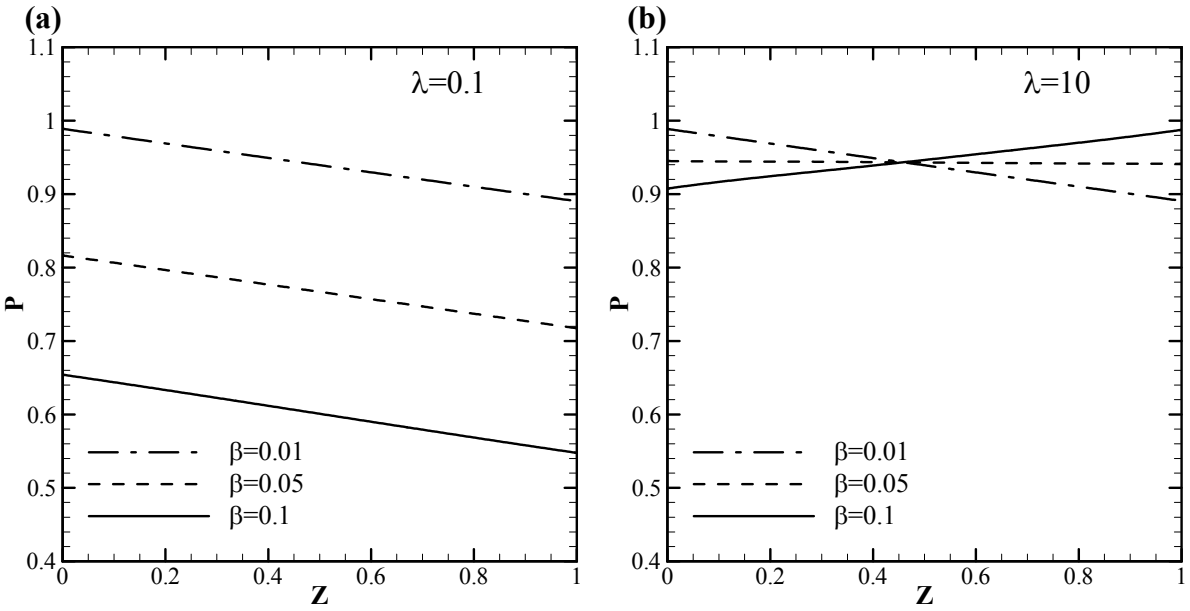

Figure 4.12 – Steady-state pressure distribution as a function of β for different values of λ and B_R=0.1. (a) λ = 0.1 and (b) λ =10.

4.7 Conclusions of Paper 2

The current work puts forward a mathematical model to predict pressure propagation when a drilling fluid, modeled as either Bingham or Newtonian fluid, is pumped into a closed well. Pressure values obtained from the model for water and two different drilling fluids are compared to measured data. The computed magnitudes and oscillation frequencies show reasonable fair matches with the measured counterparts for both kinds of fluid. In contrast with Newtonian fluids, oscillation is dissipated more quickly and pressure is not fully transmitted in Bingham fluids because of the yield stress. It was found that pressure propagation stops as soon as the pipe pressure gradient is insufficiently high to overcome the fluid yield stress.

Three dimensionless parameters were identified to govern pressure propagation: λ, β and the Bingham number. The first is the product of the aspect ratio and the Reynolds number divided by the Mach number and the second, the ratio of excessive pressure generated by the transient ($\rho c v_{in}$) and the maximum pressure applied at the pipe inlet. A sensitivity analysis was thus conducted to verify how these parameters affect pressure propagation in a closed

pipe. The main conclusion is that pressure propagation can be enhanced by reducing the Bingham number or enlarging β or λ. The model results are indeed insensitive to λ for small values of β (~0.01).

Finally, it is worth mentioning that this proposed model can be potentially applied to simulate pressure activated downhole completion equipment, such as pressure pulsation activated downhole valves/sliding sleeve. Nonetheless, the model is only valid for weakly compressible flows, viscoplastic fluids, but cannot be applied to high frequency oscillating flows, very deep wells and for gel breaking. In order to expand the model applicability, alternatives for the friction factor approach, weakly compressible flows and viscoplastic fluids need to be found.

5 THE EFFECT OF COMPRESSIBILITY ON FLOW START-UP OF WAXY CRUDE OILS

Gabriel M. Oliveira, Cezar O. R. Negrão

Journal of Non-Newtonian Fluid Mechanics 220 (2015) 137–147

The current work presents a mathematical model to simulate the flow start-up of gelled oils in pipelines. The model comprises the conservation equations of mass and momentum and an elasto-viscoplastic constitutive equation to account for thixotropy of the material. The flow is considered one-dimensional, laminar and compressible and the cross-section shear stress is admitted to vary linearly so that the constitutive equation can be integrated along the pipe radius. The balance equations are solved by the method of characteristics, the constitutive equation by the finite difference method and finally they are altogether integrated iteratively. Two kinds of boundary conditions are investigated: a constant inlet pressure and a constant inlet flow rate. Two time-scales are identified in the current study: the pressure wave propagation time and the material response time. It can be anticipated that the ratio of this two times are quite important on the restart time in case of a constant pressure boundary condition and on the magnitude of the maximum pressure for a constant flow rate boundary condition.

Keywords: Waxy Crude Oil. Structured Material. Compressible Flow. Transient Simulation.

5.1 Introduction

Oil fields such as those recently found along the Brazilian coast line can be as far as 300 km away from the seashore so as to convey oil from platforms to the land is a huge challenge. An alternative for the transport is to pump oil from the offshore production platform to the coast by using long pipelines. As the oil found in these oil fields is highly paraffinic, wax precipitation can take place at high temperatures in order that the oil can gel at the ambient temperature (~20^{o}C). Therefore, the sea bottom temperature (~4^{o}C), where the pipelines are placed, provide favorable conditions for oil gelation. Not only wax precipitation increases the oil viscosity but also impairs flow start-ups. High pump pressures may be required at the flow start-up in order to break-up the gel structure. Such high pressures lead to overestimation of pipeline resistance and/or pipe dimension, making the project unfeasible.

A reliable prediction of gelled fluid start-ups demands appropriate robust models for the transient phenomenon. Several works have been dedicated to model flow start-ups in pipelines, being most of them concerned specifically with waxy crude oils (Ritter and Batycky, 1967; Cawkwell and Charles, 1987; Sestak et al., 1987; Chang et al., 1999; Davidson et al., 2004; Vinay et al., 2006; Frigaard et al., 2007; Vinay et al., 2007; Wachs et al., 2009; Oliveira et al., 2010; Negrão et al., 2011; Souza Mendes et al., 2012). Despite the fluid being compressed at inlet in order to displace the material throughout the whole pipe, some works have considered the problem as incompressible (Ritter and Batycky, 1967; Sestak et al., 1987; Chang et al., 1999; Souza Mendes et al., 2012), as the liquid compressibility is usually very small. Whereas the incompressible fluid motion is usually considered quasi-steady so that the transient phenomenon depends only on the changes of fluid properties (thixotropy), the compressible flow analysis includes both the inertia and the transient terms.

The low temperature at the seabed shrinks the oil (Phillips et al., 2011) as an outcome of density reduction and of wax crystallization. The shrinkage may create spaces within the gelled material providing compressibility to the material. Therefore, fluid compressibility may play a role in flow start-ups of oils as a pressure variation, resulting from fluid compression at the pipeline inlet, takes some time to be sensed at the outlet. For instance, a pressure wave with a typical speed of 1000 m/s takes about 5 minutes to reach the other pipe end of a 300 km long pipeline.

Flow start-up problems can be viewed from two different perspectives: i) the determination of the minimum inlet pressure that overcomes the material yield stress and consequently, starts up the flow or; ii) the determination of the maximum pressure that results from a imposed inlet flow rate. Inasmuch as the first can be treated as quasi-steady incompressible, the second, which is the most common case in real applications, can only be dealt by using a transient compressible flow model as only one fluid velocity is admitted throughout the pipe in quasi-steady approaches.

Gel breaking is another important issue that must be addressed in flow start-ups. As reported by review papers of Mewis (1979), Barnes (1997) and Mewis and Wagner (2009), time dependent properties of gels have been studied for a long time. Although the material elasticity has been recognized as important in gel properties (Mujumdar et al., 2002; Dullaert and Mewis, 2006; Souza Mendes, 2009; Souza Mendes, 2011; Souza Mendes and Thompson, 2013), many thixotropy models used to approach flow start-ups oils (Ritter and Batycky, 1967; Cawkwell and Charles, 1987; Sestak et al., 1987; Chang et al., 1999; Davidson et al., 2004; Vinay et al., 2006; Frigaard et al., 2007; Vinay et al., 2007; Wachs et al., 2009; Oliveira

et al., 2010) have considered the gels as viscoplastic (Worrall and Tuliani, 1964; Cheng and Evans, 1965; Houska, 1980; Nguyen and Boger, 1985; Toorman, 1997). Few works such as those after Negrão et al. (2011) and Souza Mendes et al. (2012) have already dealt gel breaking as an elasto-viscoplastic phenomenon. The first employed the thixotropy model after Dullaert and Mewis (2006) whereas the second used his own model (Souza Mendes, 2009).

All thixotropic models are based on a structure parameter following Houska (1980) to represent the structuring level of the material. The structure parameter that usually varies from zero (unstructured) to one (fully structured) is governed by a kinetic equation composed of a build-up and break-down term. The first represents aggregation forces, such as the Brownian motion, and the latter is either shear rate (Dullaert and Mewis, 2006) or shear stress (Souza Mendes, 2009; Souza Mendes, 2011; Souza Mendes and Thompson, 2013) induced.

Whether the material flows or not and how long it takes to flow depends on the material structure strength and on the stress level the structure is submitted. The material time response is usually represented in the evolution equation of the structure parameter by a characteristic time, e.g., the equilibrium time, t_{eq}, defined by (Souza Mendes, 2009; Souza Mendes, 2011; Souza Mendes and Thompson, 2013). Considering the fluid motion as compressible, two characteristic times are important in flow start-up: the material time response and the time for the pressure wave to travel throughout the whole pipeline. Since the fluid is stressed as the pressure wave propagates, the material structure can only be broken during or after the pressure propagation. Therefore, the relative magnitude of these two characteristic times rules the time required for the flow start-up.

The current work proposes a different approach for the flow start-up of gelled oils in pipelines by considering that the time for the flow restart and the magnitude of pressures obtained within the pipe depend on both the material time response and on the fluid compressibility. The model is based on the conservation equation of mass and momentum assuming the fluid motion as weakly compressible and on a thixotropy model.

Despite the elasto-viscoplastic thixotropy model after Dullaert and Mewis (2006) being used in a previous work (Negrão et al., 2011) to deal with compressible flow start-ups in pipelines, the model does not clearly establish a material structure characteristic time that is required in the current analysis. In addition to that, the kinetic equation for the structure parameter and elastic deformation goes to infinity as time tends to zero which does not allow changes of the structure parameter and elastic deformation at time zero and makes the numerical solution quite sensitive to the time-step at the beginning of the simulation.

Therefore, the thixotropy model after Souza Mendes and Thompson (2013) is chosen instead of the Dullart and Mewis's model.

Two kinds of boundary conditions are considered: a constant inlet pressure and a constant inlet flow rate. In the first, the required time for starting-up the flow for a given pressure is determined whereas in the latter, the maximum pressure reached in the restart for an imposed flow rate is obtained. Considering the material as elasto-viscoplastic, the effect of the material elasticity is also investigated.

5.2 Mathematical Model

The problem was devised as a long horizontal pipeline in which the fluid is at rest (under no stress) at time zero, as shown in Figure 5.1. At the outlet, the pressure is considered to be zero and at the inlet, two types of boundary conditions are admitted: i) a constant inlet pressure and ii) a constant flow rate.

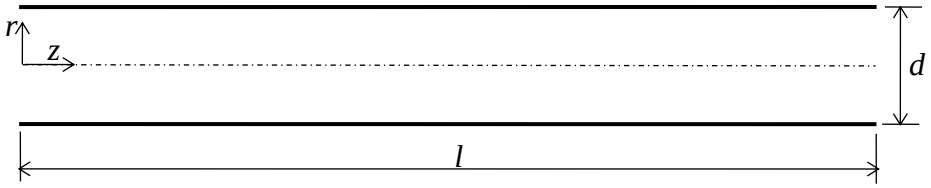

Figure 5.1 – Illustration of the Pipeline geometry

5.2.1 Governing Equations

By considering the flow as laminar, one-dimensional, the conservation equations of mass and momentum are thus written, respectively, as,

$$\frac{\partial \rho}{\partial t} + \rho \frac{\partial V}{\partial z} + V \frac{\partial \rho}{\partial z} = 0 \tag{5.1}$$

and,

$$\rho \frac{\partial V}{\partial t} + \rho V \frac{\partial V}{\partial z} + \frac{\partial p}{\partial z} = -\frac{4}{d} \tau_w \tag{5.2}$$

where ρ is the fluid density, V is the axial velocity, p is the pressure and τ_w shear stress at the pipe wall, d is the pipe diameter, t and z are the time and axial coordinates, respectively. All dependent variables are averaged throughout the pipe cross sectional area. By substituting the definition of isothermal compressibility, $\alpha = \frac{1}{\rho}\frac{\partial \rho}{\partial p}\bigg|_T = \frac{1}{\rho c^2}$, into Eq. (5.1), the mass balance equation is reduced to,

$$\frac{\partial p}{\partial t} + \frac{1}{\alpha}\frac{\partial V}{\partial z} + V\frac{\partial p}{\partial z} = 0 \tag{5.3}$$

where c is the pressure-wave speed and T is the temperature.

5.2.2 Constitutive Equation

The viscoelastic thixotropy model proposed by Souza Mendes and Thompson (2013) is used to account for gel-breaking and recovery. The model comprises a constitutive equation based on the Jeffrey´s model:

$$\dot{\gamma} + \theta_2(\lambda)\ddot{\gamma} = \frac{\theta_2(\lambda)}{\eta_\infty}\left(\frac{\tau}{\theta_1(\lambda)} + \dot{\tau}\right) \tag{5.4}$$

where $\dot{\gamma}$, $\ddot{\gamma}$, τ and $\dot{\tau}$ are, respectively, the shear rate, the rate of change of the shear rate, the shear stress and rate of change of the shear stress. θ_1 and θ_2 are the time-dependent relaxation and retardation times, respectively, which depend on a structure parameter (λ):

$$\theta_1(\lambda) = \left(1 - \frac{\eta_\infty}{\eta_v(\lambda)}\right)\frac{\eta_v(\lambda)}{G_s(\lambda)} \tag{5.5}$$

$$\theta_2(\lambda) = \left(1 - \frac{\eta_\infty}{\eta_v(\lambda)}\right)\frac{\eta_\infty}{G_s(\lambda)} \tag{5.6}$$

where η_∞ is the viscosity at infinite shear rate and η_v and G_s are the structure-dependent material viscosity and elastic modulus:

$$G_s(\lambda) = G_0 e^{m\left(\frac{1}{\lambda} - \frac{1}{\lambda_0}\right)} \tag{5.7}$$

$$\eta_v(\lambda) = \eta_\infty e^{\lambda} \tag{5.8}$$

where λ_0 and G_0 are the structure parameter and the elastic modulus for the fully structured material, respectively, and m is a constant value. This structure parameter is computed by using the following kinetic equation,

$$\frac{d\lambda}{dt} = \frac{1}{t_{eq}}\left[\left(\frac{1}{\lambda} - \frac{1}{\lambda_0}\right)^a - \left(\frac{\lambda}{\lambda_{eq}}\right)^b \left(\frac{1}{\lambda_{eq}} - \frac{1}{\lambda_0}\right)^a\right] \tag{5.9}$$

where t_{eq} is characteristic time for the structure recover or break-down for a given level of stress and λ_{eq} is the equilibrium structure parameter calculated as:

$$\lambda_{eq}(\tau) = \ln\left(\frac{\eta_{eq}(\tau)}{\eta_\infty}\right) \tag{5.10}$$

and η_{eq} is the equilibrium viscosity computed according to:

$$\eta_{eq}(\dot{\gamma}_{eq}) = \left(1 - e^{-\eta_0 \dot{\gamma}_{eq}/\tau_y}\right)\left[\frac{\tau_y - \tau_{yd}}{\dot{\gamma}_{eq}} e^{-\dot{\gamma}_{eq}/\dot{\gamma}_{yd}} + \frac{\tau_{yd}}{\dot{\gamma}_{eq}} + K\dot{\gamma}_{eq}^{n-1}\right] + \eta_\infty \tag{5.11}$$

where K and n are, respectively, the consistency index and power-law index, τ_y and τ_{yd} are, respectively, the static and dynamic yield stresses and $\dot{\gamma}_{yd}$, the shear rate that marks the transition in stress from τ_y to τ_{yd}. As the pipeline aspect ratio (d /l) is quite small, the pressure is admitted to be constant across the pipeline section, resulting in a linear shear stress distribution along the cross section:

$$\tau = \tau_w \frac{2r}{d} \tag{5.12}$$

where d is the inner pipe diameter, r is the radial position and τ_w is the shear stress on the pipe wall which depends on time and axial position, z. By substituting Eq. (5.12) into Eq. (5.4) and defining $-\partial v/\partial r$ as the shear rate, the following equation is found:

$$-\frac{\partial v}{\partial r} + \theta_2(\lambda)\frac{\partial}{\partial t}\left(-\frac{\partial v}{\partial r}\right) = \frac{2r}{d}\frac{\theta_2(\lambda)}{\eta_\infty}\left(\frac{\tau_w}{\theta_1(\lambda)} + \dot{\tau}_w\right) \tag{5.13}$$

where v is the axial velocity. Assuming τ_w as a known time-dependent value, Eq. (5.13) can be integrated to obtain the radial velocity profile along the time.

5.2.3 Dimensionless equations and scale analysis

In contrast to incompressible flows in which the pressure wave speed is infinite so that any pressure variation at one pipe end is immediately sensed at the other end, a pressure change in compressible flows travel at a finite wave speed. Therefore, the pressure wave takes a finite time to reach the pipe outlet after the fluid being compressed at the inlet. As a consequence, the material is only shear stressed at a certain pipe position when the pressure wave hits that position. However, the material structure may not change immediately after being stressed once the time for changing the structure depends on the initial strength of the material and on the level of stress. As defined by Souza Mendes and Thompson (2013), t_{eq} in Eq. (5.9) is a characteristic time for changing the structure parameter, λ, which can also be understood as a time scale for material break-down at a certain level of stress. The break-down time is in the order of magnitude of t_{eq} if the shearing time is smaller than the equilibrium time and the material breaks down as it is sheared when the shearing time is larger than t_{eq}. Since the material is stressed in flow start-ups as pressure propagates along the pipe, the relative order of magnitude between the start-up shearing time scale, l/c, and t_{eq} may play a significant hole in the material break-down and consequently, in the start-up time. The analysis here presented is based on the relative order of magnitude of these time scales as they not only affect the start-up time but also the magnitude of pressures throughout the pipeline.

The problem parameters are now scaled following the ideas of Souza Mendes and Thompson (2013). By choosing the characteristic shear rate to be c/d, the characteristic shear stress to be the dynamic yield stress, τ_{yd}, and the characteristic time to be the time for pressure propagation along the pipe length (l/c), the following dimensionless parameters for the constitutive model are obtained: $\tau_y^* = \tau_y / \tau_{yd}$, $t_{eq}^* = t_{eq}(c/l)$, $G_0^* = G_0 l/(\eta_\infty c)$, $\dot{\gamma}_{yd}^* = \dot{\gamma}_{yd}/(c/d)$, $\eta_\infty^* = \eta_\infty (c/d)/\tau_{yd}$, $\eta_0^* = \eta_0 (c/d)/\tau_{yd}$ and $K^* = K\tau_{yd}^{n-1}/\eta_\infty^n$. The pressure is scaled by the force that balances the dynamic yield stress in the pipe and the velocities by the wave speed so that the dimensionless counterparts are given by $p^*=p/(4\tau_{yd}l/d)$, $v^*=v/c$ and $V^*=V/c$, respectively. The dimensionless forms of time, axial and radial positions are defined, respectively, as $t^*=t(c/l)$, $z^*=z/l$ and $r^*=r/d$. By scaling the governing equations using these dimensionless parameters, the following equations are obtained:

$$\frac{\partial p^*}{\partial t^*} + \eta_\infty^* \phi \frac{\partial V^*}{\partial z^*} + V^* \frac{\partial p^*}{\partial z^*} = 0 \tag{5.14}$$

$$\eta_\infty^* \phi \rho^* \frac{\partial V^*}{\partial t^*} + \eta_\infty^* \phi \rho^* V^* \frac{\partial V^*}{\partial z^*} + \frac{\partial p^*}{\partial z^*} + \tau_w^* = 0 \tag{5.15}$$

where $\tau_w^* = \tau_w / \tau_{yd}$ and ϕ is equal to $¼(\rho cd/\eta_\infty)d/l$, which can be can be understood as the relationship between the inertia of the pressure wave and the viscous dissipation, as discussed elsewhere (Oliveira et al., 2012b). ϕ can also be expressed as a function of the Reynolds number ($Re=\rho Vd/\eta_\infty$), Mach number ($M=V/c$) and the pipe aspect ratio ($\delta=d/l$), resulting in $\phi = ¼\delta Re/M$. The product η_∞^* by ϕ can be understood as the inverse of a dimensionless compressibility:

$$\eta_\infty^* \phi = \frac{\rho c^2 d}{\tau_{yd} l} = \frac{1}{\alpha^*} \tag{5.16}$$

where $\alpha^* = \tau_{yd} l / (\rho c^2 d) = \alpha \tau_{yd} l / d$. Notably, the pressure wave only propagates at the speed of sound, *c*, when the problem is thermodynamic reversible whereas in a real situation, the pressure wave speed depends on the magnitude of the viscous dissipation. Therefore, the higher is α* the more dissipating is the flow.

The dimensionless form of Eq. (5.13) is thus given by,

$$-\frac{\partial v^*}{\partial r^*} + \theta_2^*(\lambda) \frac{\partial}{\partial t^*}\left(-\frac{\partial v^*}{\partial r^*}\right) = \frac{2}{\eta_\infty^*} r^* \theta_2^*(\lambda)\left(\frac{\tau_w^*}{\theta_1^*(\lambda)} + \dot{\tau}_W^*\right) \tag{5.17}$$

where $\dot{\tau}_w^* = \frac{\dot{\tau}_w c}{\tau_{yd} l}$, $\theta_1^*(\lambda) = \frac{\theta_1(\lambda) c}{l} = \frac{1}{G_0^*}(1-e^{-\lambda}) e^{\lambda - m\left(\frac{1}{\lambda}-\frac{1}{\lambda_0}\right)}$ and $\theta_2^*(\lambda) = \frac{1}{G_0^*}(1-e^{-\lambda}) e^{-m\left(\frac{1}{\lambda}-\frac{1}{\lambda_0}\right)}$.

A scale analysis of the terms of Eqs. (5.14) and (5.15), based on the methodology described by Bejan (2004), is now carried out in order to evaluate their relative order of magnitude during the flow start-up. For the weakly compressible flows considered here, the order of magnitude of the Mach number is assumed to be smaller than 0.1. In other words, the dimensionless velocity is in the order of the magnitude of the Mach number.

For the current analysis, it is now assumed that the pressure at *t=0* changes from zero to a maximum value within a time interval *l/c* and also that the pressure varies from a maximum value at the inlet to *p=0* at the outlet. Additionally, the dimensionless velocity is considered to change from zero to the maximum Mach number within the same time and length scales. Finally, the dimensionless density and shear stress at the wall take the order of magnitude of *1.0* and of the maximum pressure, respectively. The following dimensionless scales are thus identified for the changes,

$$p^* \sim p_{in}^*; \quad V^* \sim M; \quad \rho^* \sim 1; \quad \tau_w^* \sim p_{in}^*; \quad t^* \sim 1; \quad z^* \sim 1 \tag{5.18}$$

By assuming $p_{in}^* = 10$ and the maximum Mach number equal to *0.1* for a weakly compressible flow, the order of magnitude of the terms of Eqs. (5.14) and (5.15) will be,

$$10 \quad ; \quad 0.1\eta_\infty^*\phi \quad ; \quad 1 \tag{5.19}$$

$$0.1\eta_\infty^*\phi \quad ; \quad 0.1^2\eta_\infty^*\phi \quad ; \quad 10 \quad ; \quad 10 \tag{5.20}$$

Notably, if $\eta_\infty^*\phi \geq 10^2$, the third term of continuity equation and the second term of the momentum equation is at least one order of magnitude smaller than the other terms. In the current analysis, the product of ϕ by η_∞^* is considered to be at least equal to 100 so that the second and the third terms of Eqs. (5.14) and (5.15) can be disregarded. Additionally, the ρ^* in the momentum balance is considered to be constant and equal to 1 once the changes of density are computed by changes of pressure in both equations – mass and momentum. Therefore, the equations to be solved take the form:

$$\frac{\partial p^*}{\partial t^*} + \eta_\infty^*\phi\frac{\partial V^*}{\partial z^*} = 0 \tag{5.21}$$

$$\eta_\infty^*\phi\frac{\partial V^*}{\partial t^*} + \frac{\partial p^*}{\partial z^*} + \tau_w^* = 0 \tag{5.22}$$

5.3 Solution Algorithm

The governing equations are solved by the method of characteristics (MOC) that is typically used for solving hyperbolic partial differential equations (Wylie et al., 1993). The method consists in simplifying partial differential equations to a family of ordinary differential equations, along which the solution can be integrated from an initial condition. In the current case, Eqs. (5.21) and (5.22) are reduced to two total differential equations, which are valid over the characteristic lines *dz*/dt** = ± 1:

$$\left.\begin{aligned} &\frac{dp^*}{dt^*} + \eta_\infty^*\phi\frac{dV^*}{dt^*} + \tau_w^* = 0 \qquad (5.23)\\ &\frac{dz^*}{dt^*} = +1 \qquad (5.24)\end{aligned}\right\} \quad C^+$$

$$\left.\begin{aligned} -\frac{dp^*}{dt^*}+\eta_\infty^*\phi\frac{dV^*}{dt^*}+\tau_w^*=0 \quad &(5.25)\\ \frac{dz^*}{dt^*}=-1 \quad &(5.26)\end{aligned}\right\} \quad C^-$$

Notably, plots of Eqs. (5.24) and (5.26) provide straight lines on the *z-t* plane, as shown in Figure 5.2, which are named characteristic lines C^+ and C^-, respectively. It is worth noting that Eqs. (5.23) and (5.25) are valid only over the C^+ and C^- characteristic line, respectively.

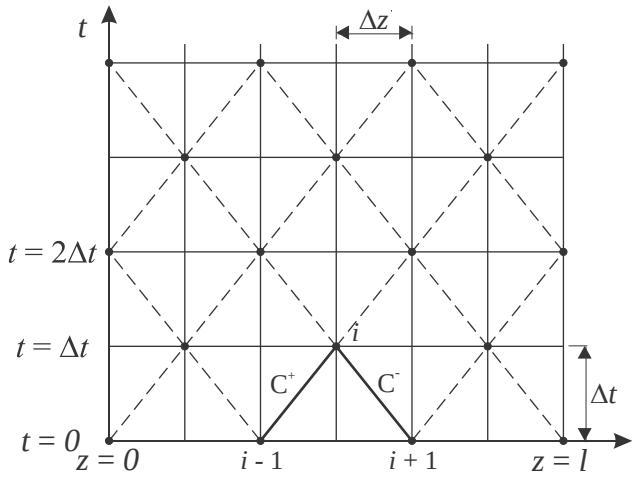

Figure 5.2 – *z-t* grid for solving the governing equations.

The pipeline is divided into N_z equal reaches, Δz^*, as shown in Figure 5.2. In order to satisfy both Eqs. (5.24) and (5.26), the time-step is computed according to $\Delta t^*=\Delta z^*$. If p^* and V^* are both known at position *i-1* and known values are assumed for τ_w^* at past and present times, Eq. (5.23) can be integrated over the characteristic line C^+ and therefore, be written in terms of unknown variables p^* and V^* at point *i*. Integration of Eq. (5.25) along line C^-, with p^*, V^* and τ_w^* known, leads to a second equation in terms of the same two unknown variables at *i*. By solving the two resulting algebraic equations, p^* and V^* can be obtained at point *i* as a function of known previous time-step values at points *i-1* and *i+1*:

$$\left(p^*\right)_i^{k+1}=\frac{F_+ + F_-}{2} \quad (5.27)$$

$$\left(V^*\right)_i^{k+1}=\frac{F_+ - F_- -\left(\tau_w^*\right)_i^{k+1}\Delta z^*}{2\eta_\infty^*\phi} \quad (5.28)$$

where,

$$F_{+} = \left(p^{*}\right)_{i-1}^{k} + \eta_{\infty}^{*}\phi\left(V^{*}\right)_{i-1}^{k} - \frac{1}{2}\left(\tau_{w}^{*}\right)_{i-1}^{k}\Delta z^{*} \tag{5.29}$$

$$F_{-} = \left(p^{*}\right)_{i+1}^{k} - \eta_{\infty}^{*}\phi\left(V^{*}\right)_{i+1}^{k} + \frac{1}{2}\left(\tau_{w}^{*}\right)_{i+1}^{k}\Delta z^{*} \tag{5.30}$$

By dividing the pipe radius in N_r points, the constitutive Eq. (5.17) can be discretized by using the implicit finite difference method and the following algebraic equation is found:

$$\begin{aligned}(1+e)\left(v^{*}\right)_{j,i}^{k+1} = (1+e)\left(v^{*}\right)_{j+1,i}^{k+1} + e\left(\left(v^{*}\right)_{j,i}^{k-1} - \left(v^{*}\right)_{j+1,i}^{k-1}\right) + \\ \frac{\left(\left(r^{*}\right)_{j+1}^{2} - \left(r^{*}\right)_{j}^{2}\right)}{\eta_{\infty}^{*}}\left[(e+f)\left(\tau_{w}^{*}\right)_{i}^{k+1} - e\left(\tau_{w}^{*}\right)_{i}^{k-1}\right]\end{aligned} \tag{5.31}$$

where $e = \dfrac{\left(\theta_{2}^{*}\right)_{j,i}^{k+1}}{\Delta t^{*}}$, $f = \dfrac{\left(\theta_{2}^{*}\right)_{j,i}^{k+1}}{\left(\theta_{1}^{*}\right)_{j,i}^{k+1}}$. Positions *j* and *j+1* mean two adjacent radial positions; an outer and an innermost, respectively, and *k*, *k-1* and *k+1* stand for the current, the past and the future time. By knowing all variables and parameters at the previous time-step, the wall shear stress at past and future times and the velocity at the outermost position at present time, the velocity $\left(v^{*}\right)_{j,i}^{k+1}$ can be determined. As θ_{1}^{*} and θ_{2}^{*} are functions of λ, the discrete values of λ are obtained from the explicit discretization of Eq. (5.9):

$$\lambda_{j,i}^{k+1} = \lambda_{j,i}^{k} + \frac{\Delta t^{*}}{t_{eq}^{*}}\left[\left(\frac{1}{\lambda_{j,i}^{k}} - \frac{1}{\lambda_{0}}\right)^{a} - \left(\frac{\lambda_{j,i}^{k}}{\lambda_{eq,j,i}^{k+1}}\right)^{b}\left(\frac{1}{\lambda_{eq,j,i}^{k+1}} - \frac{1}{\lambda_{0}}\right)^{a}\right] \tag{5.32}$$

where $\lambda_{eq,j,i}$ is obtained from Eq. (10) as a function of the local value of shear stress ($\tau_{w,i}$ *r/d*).

The integration of the radial velocity profile (Eq. (5.31)) along the pipe cross section results in the average velocity:

$$\left(\bar{V}^{*}\right)_{i}^{k+1} = 2\sum_{j=1}^{M}\left(\left(v^{*}\right)_{j+1,i}^{k+1} + \left(v^{*}\right)_{j,i}^{k+1}\right)\left(\left(r^{*}\right)_{j+1}^{2} - \left(r^{*}\right)_{j}^{2}\right) \tag{5.33}$$

As wall shear stress is not a known value at time *k+1*, an iterative solution must be carried out between Eqs. (5.27), (5.28), (5.31) and (5.33) to obtain τ_{w}^{*}. The problem solution begins with the fluid standing still unstressed at time zero, so that *p**, *V** and τ_{w}^{*} are all zero at each computing point *i*. The solution consists in finding *p** and *V** for each grid point along

$t^*=\Delta t^*$ by using Eqs. (5.27) and (5.28) and attributing a wall shear stress at *k+1*, $\left(\tau_w^*\right)_i^{k+1}$. Eq. (5.31) along with Eq. (5.32) is solved to provide the radial velocity profile by using the same attributed $\left(\tau_w^*\right)_i^{k+1}$ value. An average velocity can then be obtained from Eq. (5.33) and compared with the average counterpart given by Eq. (5.28). Inasmuch as the average velocity values are different, $\left(\tau_w^*\right)_i^{k+1}$ is corrected and $(\bar{V}^*)_i^{k+1}$ and $(V^*)_i^{k+1}$ are computed again. $\left(\tau_w^*\right)_i^{k+1}$ is corrected using an iterative procedure based on the root finding secant method until $(\bar{V}^*)_i^{k+1}$ and $(V^*)_i^{k+1}$ are very close. As soon as convergence has been reached, the solution evolves to the next time-step and then proceeds until the simulation time has been covered.

5.4 Results

As an initial condition, the fluid velocity and pressure are set to zero throughout the domain, $V^*(z^*,t^*=0)=0$ and $p^*(z^*,t^*=0)=0$. The pressure is assumed to be zero at the outlet throughout the whole simulation, $p^*(z^*=1,t^*)=0$, whereas two types of inlet boundary conditions are considered: $p^*(z^*=0,t^*)=p_0^*$ and $V^*(z^*=0,t^*)=V_0^*$, where p_0^* and V_0^* are constant values.

5.4.1 Model Validation

In order to validate the model, the numerical solution is compared with the analytical solution presented by Oliveira et al. (2010). As the analytical solution applies to a Newtonian fluid, the elastic terms of the constitutive equation were disregarded and the viscosity was set to a constant value. Only the constant pressure case was considered and p_0^* was fixed at 10. A grid size of 20 points was established in the radial direction and two grid sizes of 50 and 100 points were considered, respectively, in the axial direction. The numerical results, as displayed in Figure 5.3, agree quite well with the analytical solution for both axial grid sizes. Assuming that the 20×100 ($N_r \times N_z$) mesh size provides accurate enough results, this mesh was used for most simulations shown in the next section. However, some highly oscillating results required a more refined mesh and in these cases, a mesh size of 20x400 was used instead.

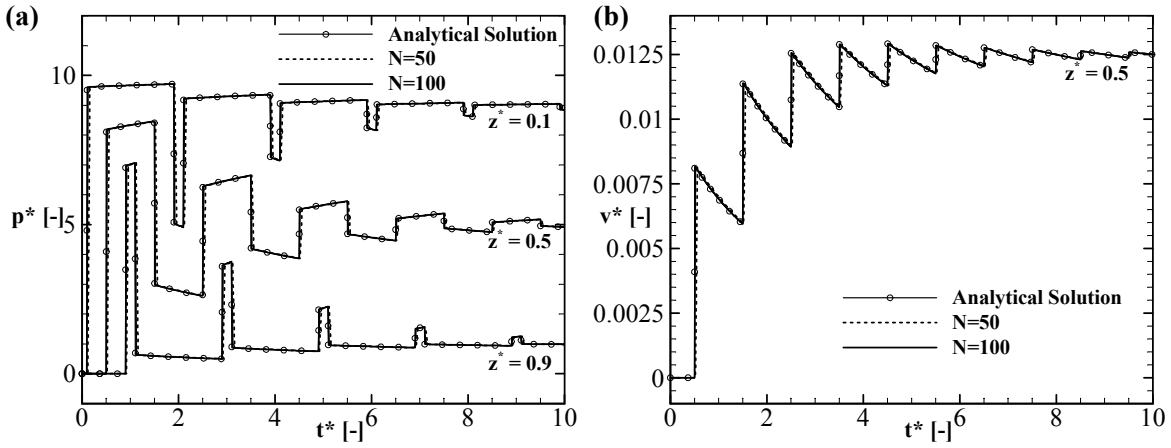

Figure 5.3 – Comparison between the numerical result and the analytical solution for a Newtonian fluid. (a) Time evolution of pressure at different axial positions and (b) Time evolution of the velocity at z*=0.5.

5.4.2 Case Studies

The purpose of the current section is mainly to evaluate how compressibility, by means of changing ϕ, and the equilibrium time, t_{eq}^*, affect the flow start-up in the pipeline. In addition to ϕ and t_{eq}^*, only the effect G_0^* is also investigated in the sensitivity analysis because of the large number of model parameters. The following parameters are then chosen: τ_y^*=1, $\dot{\gamma}_{yd}^*=10^{-8}$, $\eta_\infty^*=10^2$, $\eta_0^*=10^9$ and K^*=10, n= 0.5, m= 1.0, a= 1.0, b= 1.0.

5.4.2.1 *Inlet pressure case*

In this case, the dimensionless inlet pressure at time zero is set to 10.0 meaning that the inlet pressure is ten times larger than the pressure required to balance the dynamic yield stress, τ_{yd}. Figure 5.4(a) shows the time evolution of pressure for different axial positions, whereas Fig. 4(b) depicts the fluid average velocity at z^*=0.0, z^*=0.5, and at z^*=1.0, for ϕ=1.0, $t_{eq}^*=1.0$ and $G_0^*=10^2$. The high frequency pressure and velocity oscillations at early simulation times are the result of pressure wave propagation and reflection within the fully structured portion of the material that is highly elastic. The pressure fluctuations, however, are fast dissipated because the initially fully structured material is also highly viscous. After the high frequency oscillation being dissipated, the material remains stressed near the inlet by a high pressure gradient which gradually breaks down the gel from the inlet to the outlet propagating the pressure in a low frequency. A comparison of Figs. 5.4(a) and 5.4(b) shows that this low frequency pressure wave propagates at the same speed the fluid starts moving

throughout the pipe, indicating the continuous material break-down. After about 50 units of time, the fluid starts exiting the pipe and the outlet pressure reaches its maximum value. From this time on, the pressure within the whole pipe and the outlet velocity are reduced to reach the equilibrium and the flow in fact starts up.

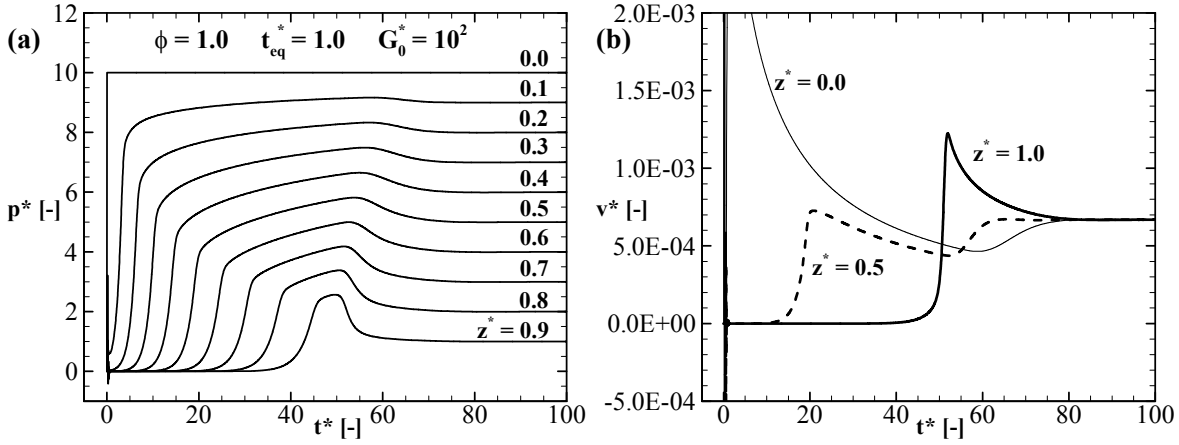

Figure 5.4 – Time variation of (a) pressure and (b) average velocity at different axial positions. Inlet pressure case with ϕ=1.0, $t_{eq}^{*}=1.0$ and $G_0^{*}=10^2$.

Figure 5.5 presents the time change of the structure parameter for different axial and radial positions. As noted, the variation of the structure parameter is not only faster but also higher at the pipe wall in comparison with the other radial positions. Additionally, the closer to the inlet the faster is the variation of the structure parameter. The speed in which the structure parameter changes in the axial direction is in agreement with low frequency wave speed described in the previous paragraph. In other words, the flow only starts up when the pressure wave reaches the pipe outlet changing the material structure throughout the whole pipe. As expected, the steady-state structure parameter depends on the radius but not on the axial position. Although not shown in Figure 5.5 the structure parameter at pipe centerline remains unchanged at its initial value because the material is not sheared at that position.

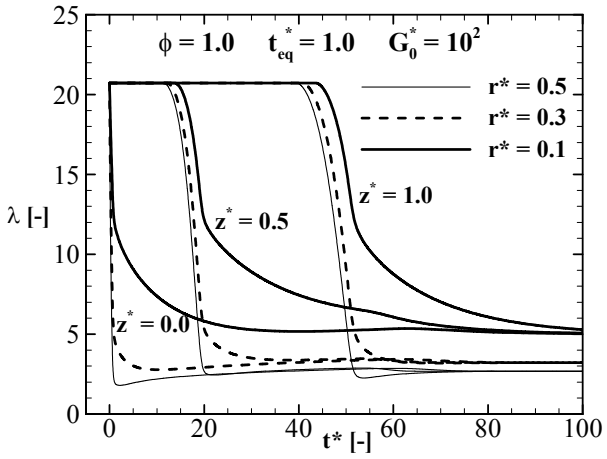

Figure 5.5 – Time variation of the structure parameter for different radial and axial positions. Inlet pressure case with ϕ=1.0, $t_{eq}^{*}=1.0$ and $G_0^{*}=10^2$.

Figure 5.6(a) and Figure 5.6(b) show the pressure at the middle of the pipe, z^{*}= 0.5, as a function of time for ϕ=1.0 and ϕ=100, respectively, and different values of t_{eq}^{*}. As shown, the higher the ϕ the less dissipative is the system so that the steady-state is reached faster and the result is more oscillating in comparison with the lower ϕ case. Figure 5.6 also shows that the time for the system to reach the steady-state increases with t_{eq}^{*}. For the less dissipative case and t_{eq}^{*}=1.0 (Figure 5.6(b)), the material breaks down as the pressure wave propagates, and the flow stabilizes as soon as the pressure oscillation dissipates. As t_{eq}^{*} increases to 10, the pressure also oscillates but the flow does not start up because the material does not break down immediately. It means that the material is shaken within the material elastic regime, as a result of pressure propagation, but does not change its initial structure instantly. Similarly to the less dissipative case, the material also breaks down as soon as the pressure wave propagates throughout the pipe for the more viscous case (ϕ=1.0 in Fig. 6(a)) and $t_{eq}^{*}=0.1$, but the pressure does not oscillate because of the higher dissipation. Nevertheless, the pressure propagation along the pipe is delayed with the augmentation of the equilibrium time so that the material begins to break down only when the pressure starts changing at a certain axial position. It is worth noting that the required time for the pressure to start changing is in the order of 10 times t_{eq}^{*}. Excepting the high frequency oscillations, the maximum pressure in both high and low dissipative cases takes place when the material breaks down and consequently, starts flowing throughout the whole pipe.

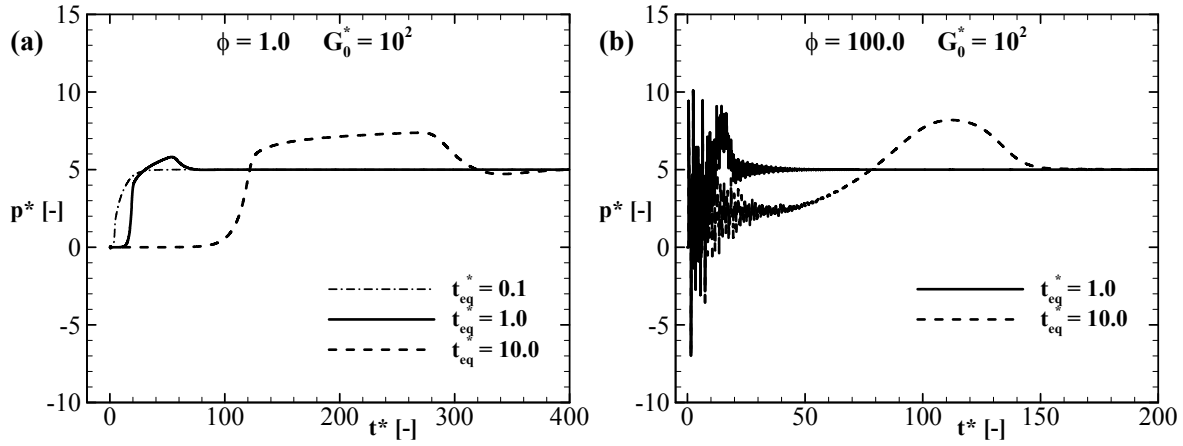

Figure 5.6 – Time variation of pressure at z^*=0.5 for different equilibrium times. a) ϕ=1.0 and b) ϕ=100.0. Inlet pressure case with $G_0^* = 10^2$.

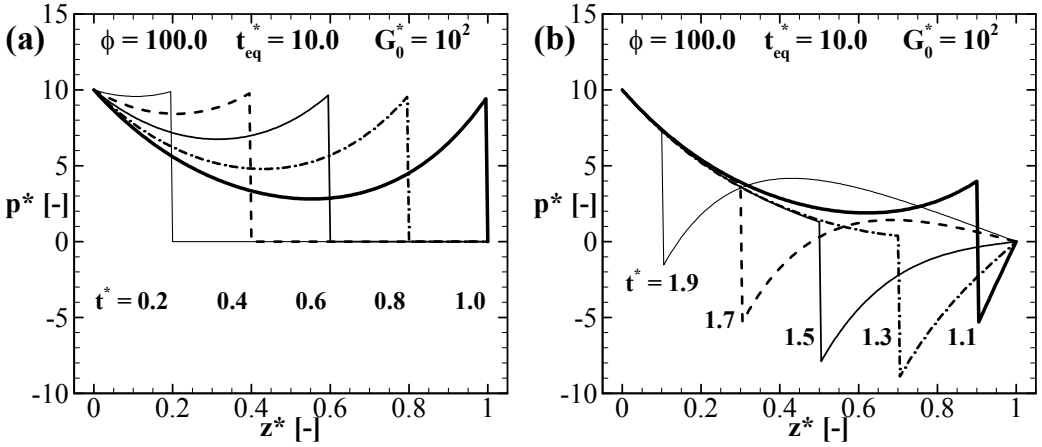

Figure 5.7 – Axial pressure distribution for different simulation times. (a) t^*=0.2, 0.4, 0.6, 0.8 and 1.0 and (b) t^*=1.1, 1.3, 1.5, 1.7 and 1.9. Inlet pressure case with $\phi = 100$, $t_{eq}^* = 10^2$ and $G_0^* = 10^2$

Despite the abnormal aspect of the oscillations in Figure 5.6(b) that reach negative pressures and also values as high as the inlet pressure, the oscillations are caused by pressure propagation within the fully structured material that is significantly elastic and not by numerical instability. Figure 5.7 displays the axial pressure distribution for different times in order to explain that. As exhibited in Figure 5.7(a), the pressure propagates at sound speed similarly to an inviscid inelastic case but differently from a low viscous Newtonian fluid case that presents an almost linear pressure distribution upwind the wave front. Additionally, the axial distribution presents an adverse gradient with pressures lower than the wave front values. This nonlinear pressure distribution results from the material elastic stretch. Differently from an inviscid model that reduces the pressure to zero after being reflected at the pipe outlet, the current case pressure is reduced to negative values after the wave

reflection, as shown in Figure 5.7(b). The reason for that are the lower pressure values found upwind the wave crest before the wave reflection.

Although the inlet pressure has being imposed as a step function this is improbable to take place in a real situation because of pumping system inertia. This unlikely fast pressure change at the pipe inlet may be, therefore, the cause of the exaggerated pressure oscillations observed at early simulation times. In order to evaluate the effect of the step change, the inlet pressure was gradually imposed by using a ramp function combined with a step function:

$$p^*(0,t) = \begin{cases} p_0^* \dfrac{t^*}{t_r^*}, & 0 \le t^* < t_r^* \\ p_0^*, & t^* \ge t_r^* \end{cases} \tag{5.34}$$

and p_0^* is the final value of the ramp function and t_r^* is the dimensionless time (=$t_r\, c/l$) for p_0^* to be established. In this case, p_0^* was made equal to 10.0 and the results are shown in Figure 5.8(a). In comparison with Figure 5.6(b), the magnitude of the oscillation has reduced significantly without showing negative values.

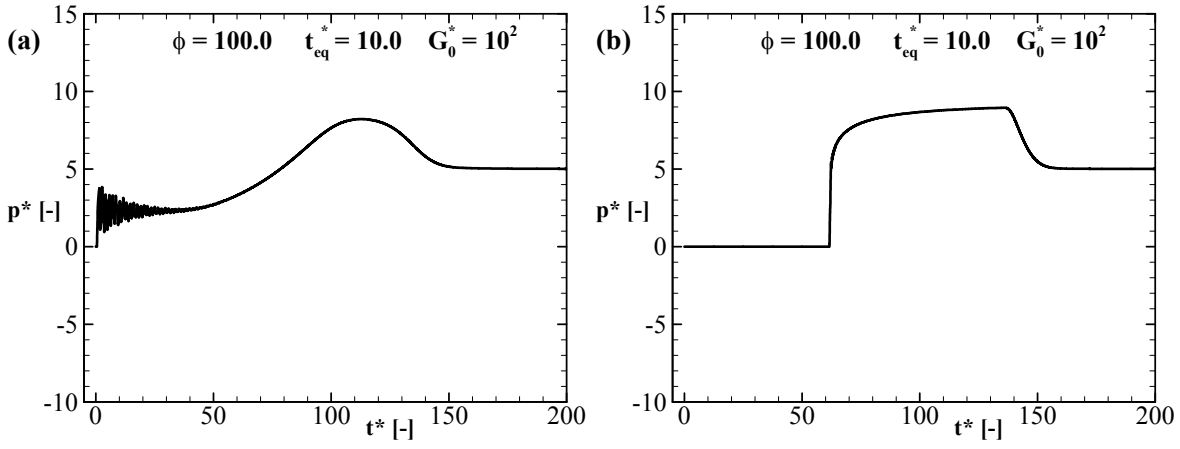

Figure 5.8 – Time variation of pressure at z^*=0.5 for $\phi = 100$, $t_{eq}^* = 10^2$ and $G_0^* = 10^2$. a) inlet pressure applied with ramp duration of $t_r^* = 1$ and b) inelastic model. Inlet pressure case.

To investigate the effect of the material elasticity on the pressure propagation for ϕ = 100 case, the elastic effects were removed from the constitutive equation. Fig. 8(b) shows the results for this exclusively viscous model. A comparison of Figure 5.8(b) with Figure 5.8(a) and Figure 5.6(b) shows that the pressure oscillations have completely disappeared and also that the pressure propagation has significantly being delayed. The elimination of the elastic effect made the problem highly dissipative because of the high viscosity of the fully

structured material. It can be concluded that the elastic effect is the reason for the pressure propagation in this low ϕ value case. Notably, the removal of the elastic effect of the ϕ=100 case made the pressure response quite similar to the quite dissipative ϕ=1 case of Figure 5.6 (a) for $t_{eq}^{*}=10$. Nevertheless, the exclusively viscous problem responds faster than the visco-elastic model.

Figure 5.9 shows the axial distributions of pressure and of the structure parameter at the wall for three ϕ values and $t_{eq}^{*}=100$, after a period of t^{*}=50. Whereas the pressure wave has reached the pipe outlet for the less dissipative case (ϕ = 100) establishing a pressure gradient throughout the whole pipe, the pressure has only propagated near the pipe inlet for ϕ = 1. In other words, the material is stressed differently along the axial position depending on the ϕ value so that the high ϕ value case is firstly affected throughout the whole pipe in comparison to the others. According to Figure 5.9(b), only the less dissipative flow has started after 50 time unit, once the structure parameter at the wall has changed throughout the whole pipe.

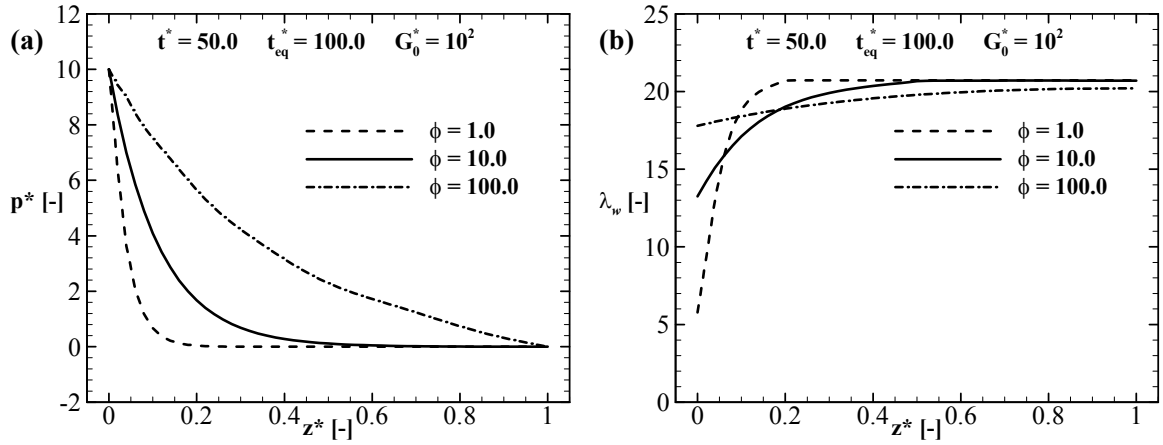

Figure 5.9 – Axial distribution of (a) pressure and of the (b) structure parameter at the wall after a period of t^{*}=50 for different values of ϕ. Inlet pressure case with $t_{eq}^{*}=100$ and $G_0^{*}=10^2$.

Figure 5.10 depicts the time variation of pressure in different axial positions, for two different ϕ values and $t_{eq}^{*}=100$. In the less dissipative case found in Figure 5.10(b), the pressure wave propagates fast, oscillates in high frequency throughout the whole pipe and the oscillation is also rapidly dissipated. Despite the fluid being stressed in all axial positions, the material structure has not been fully broken after the dissipation of the high frequency oscillation. The material structure starts breaking down throughout the whole pipe almost simultaneously as the pressure in all axial positions increases (t*~250) and drops (t*~1000)

almost at the same time. On the contrary, the pressure does not oscillate and does not propagate immediately throughout the whole pipe in the higher dissipative case, as shown in Figure 5.10(a). In fact, the material structure starts changing from inlet to the outlet delaying the complete break-down. Whereas in the less dissipative case of Figure 5.10(b) the flow takes about 1000 time units to start up, in the higher dissipative case of Figure 5.10(a) the flow starts after 2000 time units. It is worth mentioning that in both cases the flow only starts up when the pressure begins to drop throughout the whole pipe to reach the steady-state.

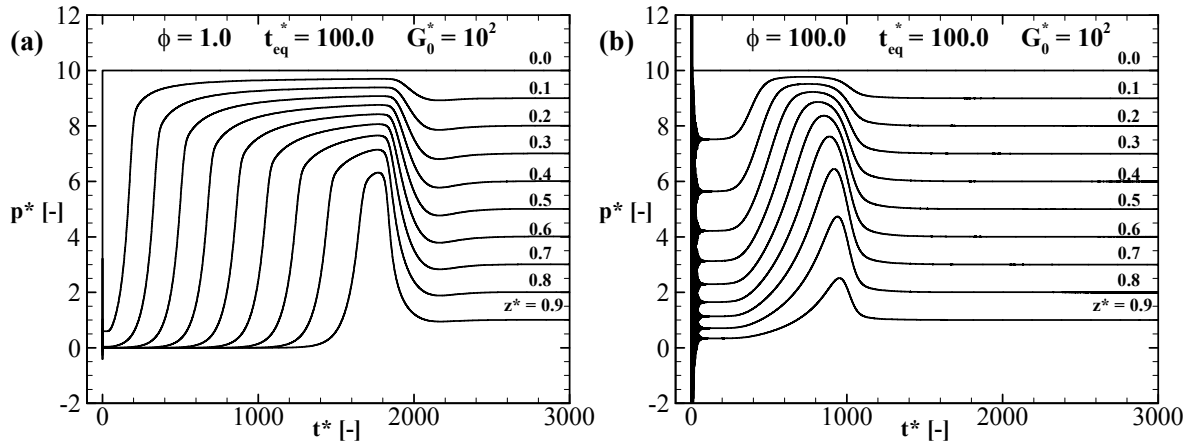

Figure 5.10 – Time variation of pressure at different axial positions for $t_{eq}^{*} = 100$ and two ϕ values: a) ϕ=1 and b) ϕ=100.0. Inlet pressure case with $G_0^{*} = 10^2$.

The effect of the material elasticity is now investigated by changing the values of G_0^{*}. Notably, the lower the G_0^{*} the more elastic is the material and the higher the G_0^{*} the more rigid is the fluid. Figure 5.11 shows the effect of elasticity on the pressure variation at the middle of the pipe. In spite of the high value of t_{eq}^{*} in the more dissipative case (ϕ=1.0), the reduction of G_0^{*} enlarges the portion of the fully structured material that is stressed within the pipe, reducing the pressure peaks at the flow start-up. For the less dissipative case (ϕ=100), on the other hand, the reduction of G_0^{*} not only increases the pressure oscillation because of the higher elasticity but also reduces the level of the material structure at the start-up so that the material breaks down as the pressure propagates.

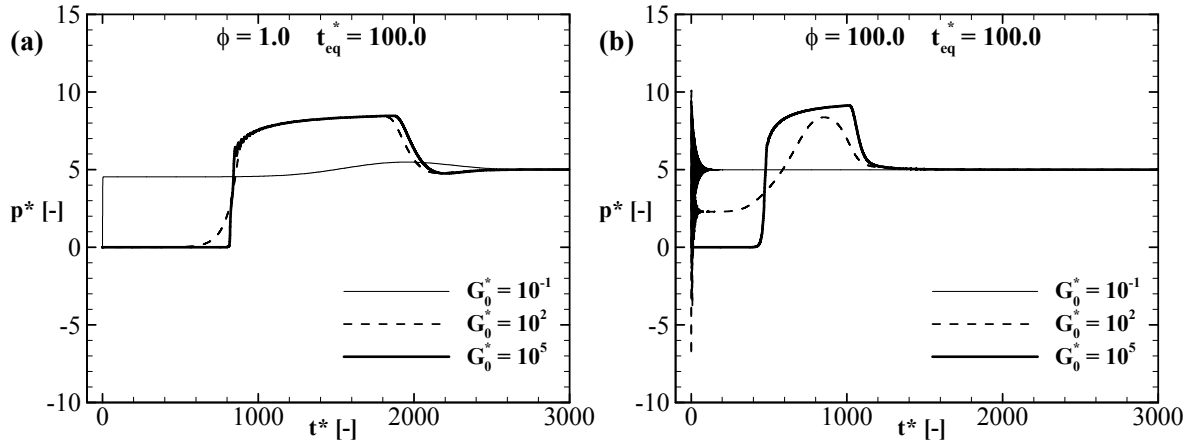

Figure 5.11 – Time variation of pressure at z*=0.5 for different three G_0^* values and two ϕ values: a) ϕ = 1 and b) ϕ = 100.0. Inlet pressure case with $t_{eq}^* = 100$.

5.4.2.2 *Inlet flow rate case*

The inlet flow rates set in this section are chosen to provide the same steady-state pressure obtained in the constant inlet pressure cases. Figure 5.12 presents the time variation of pressure and average velocity for different axial positions, ϕ=10.0, $t_{eq}^* = 1.0$ and $G_0^* = 10^2$. As noted, the pressure increases up to the time the fluid starts flowing at the pipe outlet and then is relieved. The fast pressure increase at the inlet takes place to overcome the elastic yield of the structured material and the first relief of the inlet pressure at t^*=2.9 is caused by the partial material break-down near the pipe inlet. After that, the pressure wave progresses breaking down the material structure throughout the pipe up to t^*=20 when the pipe is finally relieved and the flow starts up.

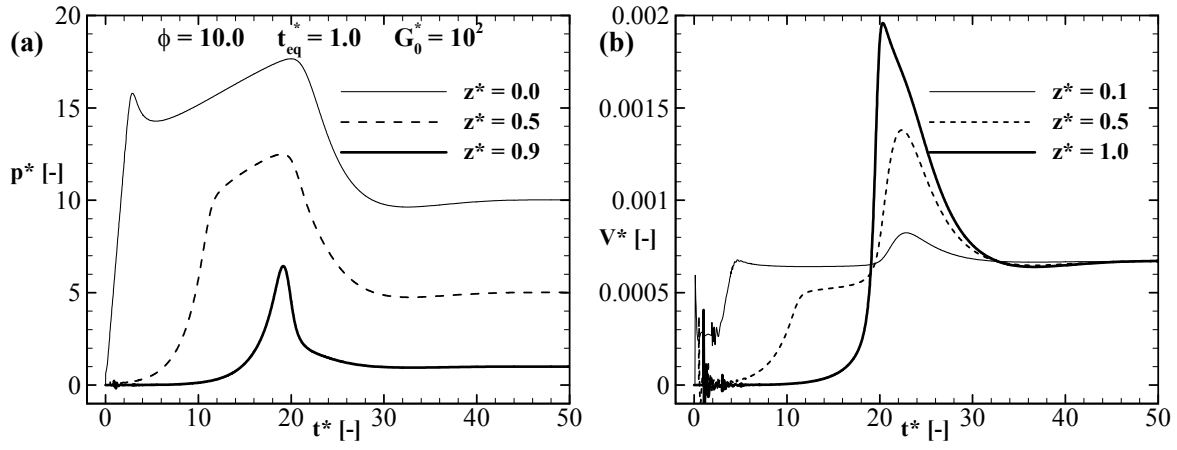

Figure 5.12 – Time variation of (a) pressure and of (b) average velocity for different axial positions. Inlet flow rate case with ϕ=10.0, $t_{eq}^* = 1.0$ and $G_0^* = 10^2$.

Figure 5.13 presents the time variation of the inlet pressure for three different equilibrium times and two ϕ values. As noted, the higher the equilibrium time the higher is the pressure magnitude and the time for breaking down the material structure. Additionally, the pressure peaks increase and the breaking down time diminishes with the reduction of dissipation (increase of ϕ). The results for Newtonian fluid with the same viscous dissipation in steady-state are also shown in Figure 5.13. Whereas the pressure the Newtonian fluid does not fluctuate for the high dissipative case (ϕ=1), the pressure for ϕ=10 oscillates at *c/l* frequency for a short period of time so as to double the inlet pressure at t^*=2.0. The Newtonian fluid starts flowing much faster than the structured fluids, regardless the ϕ value or the equilibrium time. The maximum inlet pressure for the Newtonian fluid can be larger or smaller than those for the structured fluid depending on the magnitude of the equilibrium time.

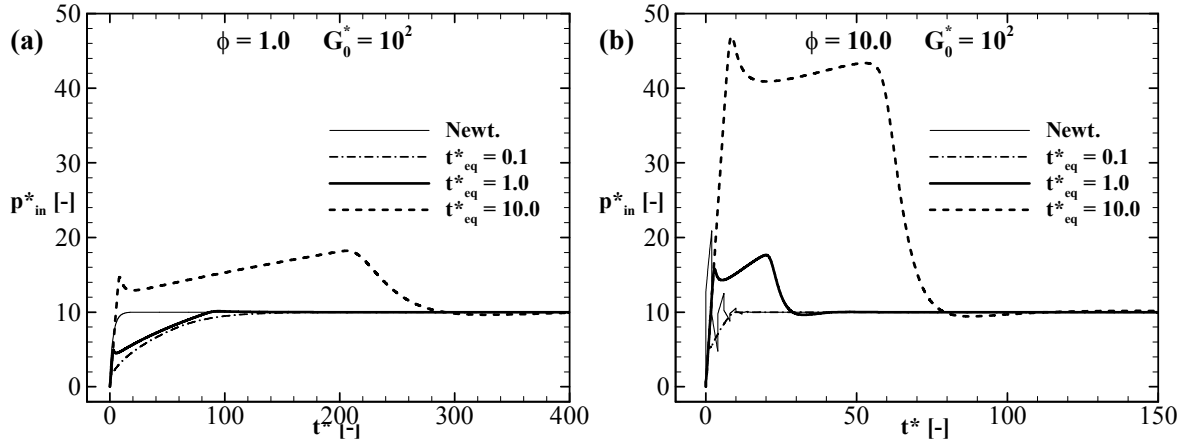

Figure 5.13 – Time variation of the inlet pressure for different t_{eq}^* and two ϕ values: a) ϕ=1.0 and b) ϕ=10.0. Inlet flow rate case with $G_0^* = 10^2$.

In order to check if the magnitudes of the start-up pressures are affected by the speed in which the material is stressed, the inlet flow rate is imposed from zero to its steady-state value based on a ramp function combined with a step function:

$$Q^*(0,t) = \begin{cases} Q_0^* \dfrac{t^*}{t_r^*}, & 0 \le t^* < t_r^* \\ Q_0^*, & t^* \ge t_r^* \end{cases} \tag{5.35}$$

where Q_0^* is the dimensionless flow rate that provides the same steady-state result as the constant inlet pressure case. Figure 5.14 presents the time variation of the inlet pressure for

different values of t_r^*, $t_{eq}^* = 10$ and ϕ=10.0. In spite of the pressure peak being reduced and the pressure time response being increased with t_r^*, the pressure magnitude is only slightly affected for $t_r^* = t_{eq}^*$. The pressure peaks are diminished because the increase of t_r^* renders time for the material to break down so that the flow resistance is reduced as the stress is increased. Notably, the time for the material break-down depends is larger, equal and smaller than t_r^* for t_r^* smaller, equal and larger than 100, respectively.

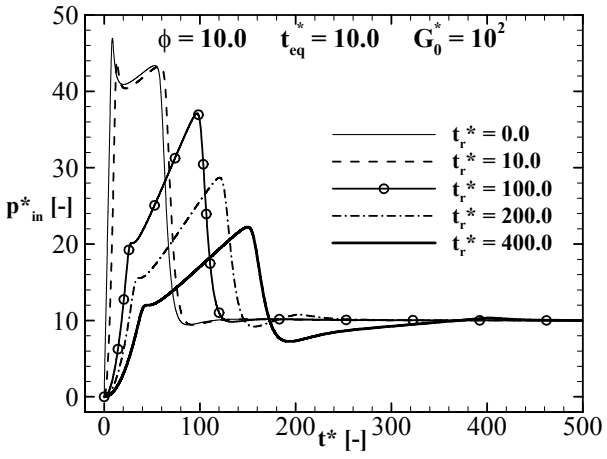

Figure 5.14 – Time variation of the inlet pressure for different values of equilibrium time and two elasticity values. a) $G_0^* = 10^{-1}$ and b) $G_0^* = 10^5$. Inlet flow rate case with ϕ=10.0.Time variation of the inlet pressure for different changes of the inlet flow rate. Inlet flow rate case with ϕ=10.0, $t_{eq}^* = 10.0$ and $G_0^* = 10^2$.

The effect of the material elasticity on the start-up pressure is now investigated for a constant inlet flow rate. As shown in Figure 5.15, the less elastic (high G_0^*) is the material the higher is the pressure needed for the material break-down and the faster is the material response. In spite of the pressure change being independent on t_{eq}^* up to material initial break-down, the smaller the equilibrium time the faster is the material break-down and the smaller the pressure required for break-down. Both Figs. 5.15(a) and (b) show an amplification of the region where the high frequency pressure oscillations take place. For the more elastic case ($G_0^* = 10^{-1}$), the frequency of oscillation coincides with the pressure wave frequency (*c/l*) and by enlarging G_0^* to 10^5, the oscillations take place because of material break-down at the inlet.

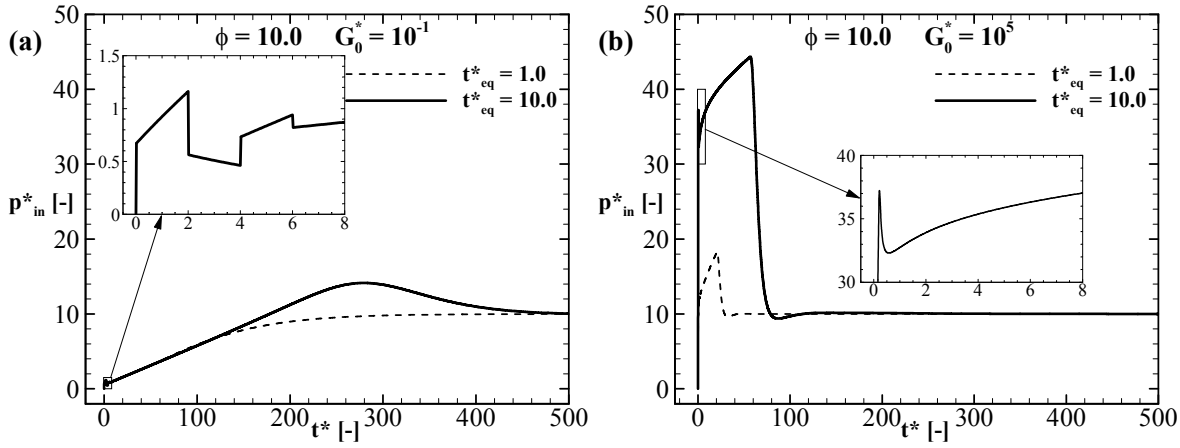

Figure 5.15 – Time variation of the inlet pressure for different values of equilibrium time and two elasticity values. a) $G_0^* = 10^{-1}$ and b) $G_0^* = 10^5$. Inlet flow rate case with ϕ=10.0.

5.5 Conclusions of Paper 3

The current work puts forward a mathematical model to predict pressure changes during the flow start-up of structured fluids in pipelines. The flow is considered weakly compressible whereas the structured fluid is modeled by using the Souza Mendes and Thompson (2013) constitutive equations. Two time scales were identified as important parameters for gel breaking: the shearing time and the time for material break-down. The first was defined as the pressure wave propagation time and the second as the equilibrium time defined in the structure parameter model of Souza Mendes and (2013). Two types of inlet boundary conditions were considered: constant pressure and constant flow rate. Whereas in the first, the required time for the flow start-up for a given pressure is determined, in the latter, the maximum pressure reached in the restart for an imposed flow rate is obtained.

The conclusions can thus be summarized as follow:

i) If the equilibrium time is smaller than the pressure propagation time, the flow starts up as soon as the pressure wave reaches the pipe outlet;

ii) An avalanche effect is observed for equilibrium time higher than the pressure propagation time;

iii) The lower the viscous dissipation in comparison to the fluid compressibility the faster is the flow start-up;

iv) The reduction of the elastic modulus reduces the pressure peaks for high dissipative material and reduces the start-up time for less dissipative materials;

v) For a constant inlet flow rate boundary condition, the higher the equilibrium time or the higher the dissipation the larger is the pressure peak necessary for the flow start-up;

vi) By slowing down the variation of the inlet flow rate, the inlet pressure peaks are reduced.

6 CONCLUSÕES E SUGESTÕES PARA TRABALHOS FUTUROS

6.1 Conclusões Gerais

No presente trabalho foi apresentada a coletânea de artigos que discutem modelos matemáticos desenvolvidos para prever a propagação de pressão durante fenômenos transientes em fluidos não newtonianos. O escoamento do fluido é considerado unidimensional, fracamente compressível e isotérmico. O modelo baseia-se nas equações diferencias parciais de balanço da massa e de quantidade de movimento, que são convertidas em equações diferenciais totais através do método das características. As equações diferenciais ordinárias resultantes são então integradas pelo método das diferenças finitas a partir de uma condição inicial. A compressibilidade do fluido é modelada através da utilização de equação de estado que relaciona a massa específica com a pressão. Diferentes comportamentos reológicos são considerados no modelo através de equações constitutivas que representam o fluido não newtoniano. Em cada artigo apresentado na coletânea uma situação transitória diferente foi explorada. De forma geral, deve-se destacar que o problema é intrinsicamente transiente e não pode ser tratado como estacionário.

No primeiro artigo tratou-se da sobrepressão gerada devido à desaceleração do fluido pelo fechamento brusco de válvula. No segundo explorou-se a transmissão de pressão em poço de petróleo, enquanto no terceiro estudou-se os efeitos da compressibilidade na quebra da estrutura de fluido gelificado durante o reinício do escoamento.

Basicamente, como síntese geral de todos os eventos analisados tem-se:

i. O comportamento viscoplástico do fluido de Bingham proporciona atenuação da pressão ao longo da geometria que está diretamente ligada à tensão limite de escoamento do fluido, à dissipação viscosa, à compressibilidade do fluido e também à condição de contorno. Quando mais rápida a variação da condição de contorno e menor a dissipação viscosa em relação à inércia de propagação, maior a não linearidade na distribuição da pressão.

ii. O estudo da quebra do gel mostrou a importância de duas escalas de tempo: tempo de propagação da onda de pressão e tempo característico de reestruturação. Se o tempo de reestruturação é menor que o tempo de propagação da pressão, o escoamento se iniciará assim que a onda de pressão chegar à saída do tubo. Em contrapartida, se o tempo de restruturação for maior que o tempo de propagação, efeito avalanche pode ser observado.

iii. A elasticidade do fluido pode atuar favorecendo a propagação da pressão e reduzir as pressões necessárias para o reinício do escoamento

6.2 Sugestões para Trabalhos Futuros

Visando a continuidade da pesquisa, e tendo em vista as lacunas observadas, considera-se fundamental em trabalhos futuros:

- Modelar os efeitos da temperatura e da transferência de calor;
- Avaliar o efeito do histórico térmico e de cisalhamento na propagação da pressão;
- Incluir os efeitos da temperatura e da pressão nas propriedades do fluido;
- Avaliar, validar e caracterizar de forma experimental o problema utilizando fluidos com variados comportamentos reológicos.

REFERÊNCIAS

Anderson JD (1990) Modern compressible flow: with historical perspective, 2nd ed. McGraw-Hill Inc., New York, United States.

Barnes HA (1997) Thixotropy—a review. J Nonnewton Fluid Mech 70:1–33.

Bejan A (2004) Convection Heat Transfer, 3rd ed. John Wiley & Sons

Bergant A, Simpson AR, Tijsseling AS (2006) Water hammer with column separation: A historical review. J Fluids Struct 22:135–171.

Bergant A, Simpson AR, Vítkovský JP (2001) Developments in unsteady pipe flow friction modelling. J Hydraul Res 39:249–257.

Bird RB, Armstrong RC, Hassager O (1987) Dynamics of Polymeric Liquids - Vol. 1. In: 2nd Editio. John Wiley & Sons, New York, United States.

Brunone B, Ferrante M, Cacciamani M (2004) Decay of Pressure and Energy Dissipation in Laminar Transient Flow. J Fluids Eng 126:928.

Brunone B, Golia UM, Greco M (1995) Effects of Two-Dimensionality on Pipe Transients Modeling. J Hydraul Eng 121:906–912.

Brunone B, Karney BW, Mecarelli M, Ferrante M (2000) Velocity Profiles and Unsteady Pipe Friction in Transient Flow. J Water Resour Plan Manag 126:236–244.

Cawkwell MG, Charles ME (1987) An improved model for start-up of pipelines containing gelled crude oil. J. Pipelines 7:41–52.

Chang C, Nguyen QD, Rønningsen HP (1999) Isothermal start-up of pipeline transporting waxy crude oil. J Nonnewton Fluid Mech 87:127–154.

Cheng DC-H, Evans IF (1965) Phenomenological characterization of the rheological behaviour of inelastic reversible thixotropic an antithixotropic fluids. Br J Appl Phys 16:1599–1617.

Davidson MR, Nguyen QD, Chang C, Rønningsen HP (2004) A model for restart of a pipeline with compressible gelled waxy crude oil. J Nonnewton Fluid Mech 123:269–280.

Duan H-F, Ghidaoui MS, Lee PJ, Tung YK (2012) Relevance of Unsteady Friction to Pipe Size and Length in Pipe Fluid Transients. J Hydraul Eng 138:154–166.

Dullaert K, Mewis J (2006) A structural kinetics model for thixotropy. J Nonnewton Fluid Mech 139:21–30.

El-Gendy H, Alcoutlabi M, Jemmett M, Deo M, Magda J, Venkatesan R, Montesi A (2012)

The propagation of pressure in a gelled waxy oil pipeline as studied by particle imaging velocimetry. AIChE J 58:302–311.

Frigaard I, Vinay G, Wachs A (2007) Compressible displacement of waxy crude oils in long pipeline startup flows. J Nonnewton Fluid Mech 147:45–64.

Ghidaoui MS, Zhao M, McInnis DA, Axworthy DH (2005) A Review of Water Hammer Theory and Practice. Appl Mech Rev 58:49–76.

Holmboe EL, Rouleau WT (1967) The Effect of Viscous Shear on Transients in Liquid Lines. J Basic Eng 89:174–180.

Houska M (1980) Inzenyrske aspekty reologie tixotropnich kapalin. PhD Thesis, Techn. Univ. Prague, Prague.

Melrose JC, Savins JG, Foster WR, Parish ER (1958) A Practical Utilization of the Theory of Bingham Plastic Flow in Stationary Pipes and Annuli. Pet Trans 213:316–324.

Mewis J (1979) Thixotropy - a general review. J Nonnewton Fluid Mech 6:1–20.

Mewis J, Wagner NJ (2009) Thixotropy. Adv Colloid Interface Sci 147–148:214–227.

Mitsoulis E (2007) Flows of Viscoplastic Materials: Models and Computations. In: Binding DM, Hudson NE, Keunings R (eds) Rheology Reviews 2007. The British Society of Rheology, London, UK.pp 135–178

Mujumdar A, Beris AN, Metzner AB (2002) Transient phenomena in thixotropic systems. J Nonnewton Fluid Mech 102:157–178.

Negrão COR, Franco AT, Rocha LLV (2011) A weakly compressible flow model for the restart of thixotropic drilling fluids. J Nonnewton Fluid Mech 166:1369–1381.

Nguyen QD, Boger D V. (1985) Thixotropic behaviour of concentrated bauxite residue suspensions. Rheol Acta 24:427–437.

Oliveira GM de, Franco AT, Negrão COR, Martins AL, Silva RA (2013) Modeling and validation of pressure propagation in drilling fluids pumped into a closed well. J Pet Sci Eng 103:61–71.

Oliveira GM, Franco AT, Negrão COR (2015) Mathematical Model for Viscoplastic Fluid Hammer. J Fluids Eng 138:011301.

Oliveira GM, Negrão COR (2015) The effect of compressibility on flow start-up of waxy crude oils. J Nonnewton Fluid Mech 220:137–147.

Oliveira GM, Negrão COR, Franco AT, Silva RA, Martins AL (2012a) Mathematical Model for Pressure Transmission in Drilling Fluids. In: Proceedings of the 2012 AADE National Technical Conference and Exhibition, April 10-11 2012. American Association of Drilling Engineers, Houston, Texas.

Oliveira GM, Negrão COR, Franco AT (2012b) Pressure transmission in Bingham fluids compressed within a closed pipe. J Nonnewton Fluid Mech 169–170:121–125.

Oliveira GM, Rocha LLV, Franco AT, Negrão COR (2010) Numerical simulation of the start-up of Bingham fluid flows in pipelines. J Nonnewton Fluid Mech 165:1114–1128.

Owayed JF, Tiab D (2008) Transient pressure behavior of Bingham non-Newtonian fluids for horizontal wells. J Pet Sci Eng 61:21–32.

Phillips DA, Forsdyke IN, McCracken IR, Ravenscroft PD (2011) Novel approaches to waxy crude restart: Part 1: Thermal shrinkage of waxy crude oil and the impact for pipeline restart. J Pet Sci Eng 77:237–253.

Ritter RA, Batycky JP (1967) Numerical Prediction of the Pipeline Flow Characteristics of Thixotropic Liquids. Soc Pet Eng J 7:369–376.

Sestak J, Charles ME, Cawkwell MG, Houska M (1987) Start-up of gelled crude oil pipeline. J. Pipelines 6:15–24.

Sobey RJ (2004) Analytical solutions for unsteady pipe flow. J Hydroinformatics 6:187–207.

Souza Mendes PR (2009) Modeling the thixotropic behavior of structured fluids. J Nonnewton Fluid Mech 164:66–75.

Souza Mendes PR (2011) Thixotropic elasto-viscoplastic model for structured fluids. Soft Matter 7:2471–2483.

Souza Mendes PR, Abreu Soares FSM, Ziglio CM, Gonçalves M (2012) Startup flow of gelled crudes in pipelines. J Nonnewton Fluid Mech 179–180:23–31.

Souza Mendes PR, Thompson RL (2013) A unified approach to model elasto-viscoplastic thixotropic yield-stress materials and apparent yield-stress fluids. Rheol Acta 52:673–694.

Streeter VL, Wylie EB (1974) Waterhammer and Surge Control. Annu Rev Fluid Mech 6:57–73.

Swamee PK, Aggarwal N (2011) Explicit equations for laminar flow of Bingham plastic fluids. J Pet Sci Eng 76:178–184.

Thorley ARD (2004) Fluid Transients in Pipelines Systems, 2nd Editio. The American Society of Mechanical Engineers, New York, United States.

Toorman EA (1997) Modelling the thixotropic behaviour of dense cohesive sediment suspensions. Rheol Acta 36:56–65.

Vinay G, Wachs A, Agassant JF (2006) Numerical simulation of weakly compressible Bingham flows: The restart of pipeline flows of waxy crude oils. J Nonnewton Fluid Mech 136:93–105.

Vinay G, Wachs A, Frigaard I (2007) Start-up transients and efficient computation of isothermal waxy crude oil flows. J Nonnewton Fluid Mech 143:141–156.

Wachs A, Vinay G, Frigaard I (2009) A 1.5D numerical model for the start up of weakly compressible flow of a viscoplastic and thixotropic fluid in pipelines. J Nonnewton Fluid Mech 159:81–94.

Wahba EM (2008) Modelling the attenuation of laminar fluid transients in piping systems. Appl Math Model 32:2863–2871.

Wahba EM (2013) Non-Newtonian fluid hammer in elastic circular pipes: Shear-thinning and shear-thickening effects. J Nonnewton Fluid Mech 198:24–30.

White FM (2003) Fluid Mechanics, 5 th Editi. McGraw-Hill Inc., New York, United States.

Worrall WE, Tuliani S (1964) Viscosity changes during the ageing of clay-water suspensions. Trans Br Ceram Soc 63:167–185.

Wylie EB, Streeter VL, Suo L (1993) Fluid transients in systems. Prentice Hall, New Jersey - United States.

APÊNDICE A – PROGRAMA COMPUTACIONAL WELLPRESS

O modelo matemático apresentado nos artigos da coletânea foi e continua sendo aprimorado para representar cada vez melhor os problemas transitórios verificados em operações de perfuração de poços de petróleo. Para tornar possível a utilização do modelo matemático desenvolvido, foi criado um programa computacional com interface gráfica para avaliação de pressões em operações de perfuração de poços de petróleo. Denominou-se o programa computacional de WellPress – Well Pressure Simutation (v. 3.1.2014). O pedido de registro de propriedade intelectual encontra-se em andamento. Com este programa é possível simular uma série de fenômenos transitórios que ocorrem no ambiente de perfuração de poços de petróleo. Na Figura A.1 apresenta-se a tela principal do programa desenvolvido com destaque para a evolução temporal da variação da pressão ao longo da geometria.

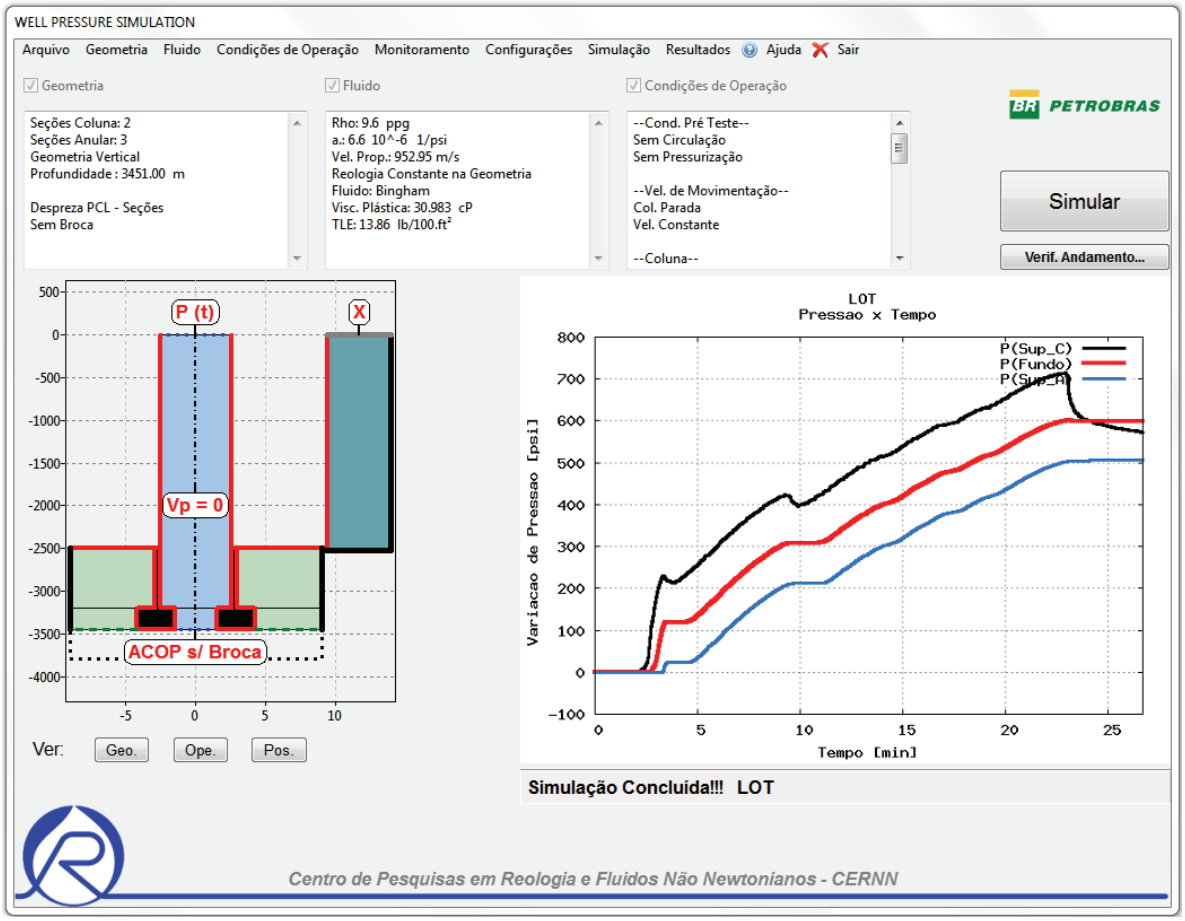

Figura A.1. – Interface Gráfica do Programa Computacional WellPress para um teste de campo.

APÊNDICE B – PRÊMIO ANP DE INOVAÇÃO TECNOLÓGICA 2016

Parte dos estudos realizados neste doutorado está vinculado com o projeto de pesquisa realizado com a Petrobras e intitulado: Avaliação Numérico-Experimental de Escoamentos em Hidráulica de Poços. Com esta parceria, e com os interesses da Petrobras, o modelo matemático desenvolvido foi incluído no "Programa de Diagnóstico de Problemas de Perfuração em Tempo Real (PWDa)".

Este projeto PWDa, coordenado pela empresa Engineering Simulation and Scientific Software Ltda (ESSS) em parceria com as universidades UCL, UFRRJ, UTFPR e com a Petrobras, tem por objetivo o desenvolvimento de programa de interpretação automatizada de dados provenientes de sensores instalados em sistemas de perfuração, buscando detecção imediata de sinais indicativos de situações indesejadas, a fim de que ações corretivas ou preventivas possam ser tomadas. Este é o primeiro software desenvolvido no País com modelos de cálculos transientes para interpretações em tempo real de possíveis problemas operacionais durante a perfuração de poços, auxiliando o processo de tomada de decisão, por meio de metodologia automatizada de análise de dados com critérios quantitativos, retirando a parte subjetiva da interpretação e identificação de eventos.

Ao submeter o PWDa para o Prêmio ANP de Inovação Tecnológica no ano de 2016, da Agência Nacional do Petróleo e Gás Natural e Biocombustíveis, o projeto venceu na categoria II: Inovação Tecnológica desenvolvida no Brasil por micro, pequena ou média empresa do segmento de petróleo, gás natural e biocombustíveis em colaboração com empresa petrolífera.

APÊNDICE C – OUTRAS PUBLICAÇÕES

Publicação em Revista

MITISHITA, RODRIGO S.; **OLIVEIRA, GABRIEL M**.; SANTOS, TAINAN G.M.; NEGRÃO, CEZAR O.R.. Pressure Transmission in Yield Stress Fluids - an Experimental Analysis. JOURNAL OF NON-NEWTONIAN FLUID MECHANICS, v. 261, p. 50-59, 2018.

Publicações em Congressos

MITISHITA, RODRIGO S.; **OLIVEIRA, GABRIEL M**.; NEGRÃO, C. O. R.. A Numerical and Experimental Study of the Pressure Transmission in Viscoplastic Fluids Confined In Pipelines. In: 24th ABCM International Congress of Mechanical Engineering, 2017, Curitiba. Proceedings of the 24th ABCM International Congress of Mechanical Engineering, 2017.

GALDINO, J. F.; **OLIVEIRA, G. M.**; FRANCO, A. T.; NEGRÃO, C. O. R.. Transient Mathematical Model for Kick Detection. In: 24th ABCM International Congress of Mechanical Engineering, 2017, Curitiba. Proceedings of the 24th ABCM International Congress of Mechanical Engineering, 2017.

GALDINO, J. F.; **OLIVEIRA, G. M.;** FRANCO, A. T.; NEGRÃO, C. O. R.. Modeling of Pressure Transmission in Gas Kicks. In: ENAHPE 2017 - Encontro Nacional de Hidráulica de Perfuração de Poços de Petróleo, 2017, Domingos Martins. Proceedings of the ENAHPE 2017 ? Encontro Nacional de Hidráulica de Perfuração de Poços de Petróleo, 2017.

SANTOS, T. G. M.; **OLIVEIRA, G. M**.; Gleber Tacio TEIXEIRA, GLEBER T.; MARTINS, ANDRÉ L.; NEGRÃO, CEZAR O. R.. Avaliação de testes de BOP através da simulação numérica. In: VII Encontro Nacional de Hidráulica de Perfuração e Completação de Poços de Petróleo e Gás, 2017, Vitória. Anais do VII Encontro Nacional de Hidráulica de Perfuração e Completação de Poços de Petróleo e Gás, 2017.

SANTOS, T. G. M.; **OLIVEIRA, G. M.**; NEGRÃO, C. O. R.. Numerical Comparison of one and two-Dimensional Models for Non-Newtonian Fluid Hammer. In: 16th Brazilian Congress on Thermal Sciences and Engineering, 2016, Vitoria. Proceedings of the 16th Brazilian Congress on Thermal Sciences and Engineering, 2016.

SANTOS, T. G. M. ; **OLIVEIRA, G. M**. ; NEGRÃO, C. O. R. . Numerical Study and Validation of Non-Newtonian Fluid Hammer in Circular Pipes. In: 23rd ABCM International Congress on Mechanical Engineering, 2015, Rio de Janeiro. Proeceedings of the 23rd ABCM International Congress of Mechanical Engineering, 2015.

OLIVEIRA, G. M.; FRANCO, A. T.; NEGRÃO, C. O. R.; MARTINS, A. L.. Efeito da Reologia na Modelagem da Transmissão de Pressão em Testes de Absorção. In: VI Encontro Nacional de Hidráulica de Poços de Petróleo e Gás, 2015, Caldas Novas - GO. Anais do VI Encontro Nacional de Hidráulica de Poços de Petróleo e Gás, 2015.

GALDINO, J. F.; **OLIVEIRA, G. M.**; FRANCO, A. T. ; NEGRÃO, C. O.R. Análise da Propagação de Pressão em Fluidos de Perfuração Durante Kick de Gás. In: VI Encontro Nacional de Hidráulica de Poços de Petróleo e Gás, 2015, Caldas Novas - GO. Anais do VI Encontro Nacional de Hidráulica de Poços de Petróleo e Gás, 2015.

OLIVEIRA, G. M.; FRANCO, A. T.; NEGRÃO, C. O. R.; VADINAL, R. B.; LOMBA, B. S.; FONSECA, T. U.; MARTINS, A.L.. Pressure Transmission in Gelled Drilling Fluids. In: SPE/IADC Drilling Conference and Exhibition, 2015, London. SPE/IADC Drilling Conference and Exhibition.

OLIVEIRA, G. M.; SANTOS, T. G. M.; FRANCO, A. T.; NEGRÃO, C. O.R.. Pressure Transmission in Visco and Pseudoplastic Fluids During Closed Well Operations. In: VII Brazilian Conference on Rheology, BCR 2015, Curitiba.

OLIVEIRA, G. M.; SANTOS, T. G. M.; FRANCO, A. T. ; NEGRÃO, C. O. R. . Numerical Investigation of Start-up of Structured Fluid Flows in Pipelines. In: 15th Brazilian Congress of Thermal Sciences and Engineering - ENCIT, 2014, Belém - PA. Proceedings of 15th ENCIT, 2014.

OLIVEIRA, G. M.; GALDINO, J. F. ; FRANCO, A. T.; NEGRÃO, C. O. R.; MARTINS, A. L.. Pressure Propagation in Drilling Fluids During a Kick of Gas. In: V Encontro Nacional de Hidráulica de Poços de Petróleo e Gás - ENAHPE 2013, 2013, Teresópolis - RJ. Anais do V ENAHPE, 2013.

GALDINO, J. F.; **OLIVEIRA, G. M.**; FRANCO, A. T.; NEGRÃO, C. O. R. Transient Mathematical Model for Well Kick During Drilling Operations. In: 22nd International Congress of Mechanical Engineering - COBEM, 2013, Ribeirão Preto - SP. Proceedings of 22nd COBEM, 2013.

NEGRÃO, C. O. R.; **OLIVEIRA, G. M.**; Cogo, T. J. ; Franco, A. T.. Numerical and Experimental Investigation of Drilling Fluid Flow Start-up. In: 5th Workshop on Viscoplastic Fluids: From Theory to Application, 2013, Rueil-Malmaison – França.

OLIVEIRA, G. M.; GALDINO, J. F.; Franco, A.T.; Negrão, Cezar O.R.. Prediction of Pressure Transmission During a Kick of Gas in Well Drilling Operations. In: 5th Workshop on Viscoplastic Fluids: From Theory to Application, 2013, Rueil-Malmaison – França.